

1 **What controls fire size in the South American Gran Chaco?**
2 **Exploring atmospheric and landscape drivers through Remote**
3 **Sensing.**

4 Rodrigo San Martín¹, Catherine Ottlé¹, Anna Sorensön^{2,3,4}, Pradeebane Vaittinada Ayar¹,
5 Florent Mouillot⁵, Marielle Malfante⁶

6
7 ¹Laboratoire des Sciences du Climat et de l'Environnement, LSCE/IPSL, CEA-CNRS-UVSQ, Université Paris-
8 Saclay, Gif-sur-Yvette, France;

9 ²Centro de Investigaciones del Mar y la Atmósfera (CIMA), CONICET – Universidad de Buenos Aires, Buenos
10 Aires, Argentina;

11 ³CNRS, CNRS – IRD – CONICET – UBA, Instituto Franco-Argentino para el Estudio del Clima y sus Impactos
12 (IRL 3351 IFAECI), Argentina;

13 ⁴Facultad de Ciencias Exactas y Naturales, Universidad de Buenos Aires, Buenos Aires, Argentina;

14 ⁵UMR CEFE, University of Montpellier, CNRS, EPHE, IRD, Montpellier, France;

15 ⁶Univ. Grenoble Alpes, CEA, List, Grenoble, France;

16 *Correspondence to:* Rodrigo San Martin (rodrigo.sanmartin@lsce.ipsl.fr)

17

18 **Abstract.** Wildfires are key ecological agents in the Gran Chaco, one of the world's largest tropical dry
19 forest systems. We analyzed more than 100,000 fire patches across the Wet, Dry and Very Dry Chaco
20 between 2001 and 2022, to quantify environmental and anthropogenic controls on fire size. Fire sizes
21 were strongly right-skewed: more than 80 % were smaller than 5 km², yet large and extreme fires
22 dominated total burned area. Megafires (> 100 km²) occurred in all subregions, while gigafires (> 1000
23 km²) were rare but concentrated in the Dry Chaco. Fire Weather Index–burned area correlations
24 exhibited strong spatial contrasts, reaching values of up to $r = 0.7$ in the Wet Chaco and showing weaker,
25 more heterogeneous relationships in drier regions. Meteorological conditions during fires, particularly
26 persistent strong winds, were associated with larger and more elongated patches. Random Forest models
27 showed that topography and land cover composition together accounted for about 60 % of total SHAP
28 importance, whereas demographic variables had very low SHAP contributions in the models. Human
29 pressures shape ignition timing but showed limited direct influence on fire size once landscape structure
30 was included in the models. These results provide a quantitative basis for improving regional fire danger
31 assessments in the Gran Chaco.

32 1 INTRODUCTION

33 Wildfires shape global ecosystems by influencing vegetation structure, biodiversity, and landscape
34 composition (Bowman et al., 2009; Archibald et al., 2013; Chuvieco et al., 2020). The Gran Chaco,
35 spanning around 1.1 million km² across Argentina, Bolivia, Paraguay, and Brazil, is one of the largest
36 remaining dry forest ecosystems, with marked variation in precipitation, vegetation, and human land use
37 (Morello and Adámoli, 1968; Olson et al., 2001; Ginzburg et al., 2005; Torrella and Adámoli, 2005).
38 Fire has long modulated its vegetation structure and driven transitions between forests, shrublands, and
39 grasslands (Bucher, 1982; Kunst et al., 2003; Vidal-Riveros et al., 2023).

40 In recent decades, fire regimes in the Gran Chaco have shifted under the combined influence of land-
41 use intensification, changes in fire use and suppression practices, and increasing climatic variability
42 (Gasparri et al., 2008; De Marzo et al., 2021; Baumann et al., 2022; Marengo et al., 2022; Vidal-Riveros
43 et al., 2023; San Martín et al., 2023; San Martín, 2024).

44 Fuel characteristics and availability play a central role (Bravo et al., 2014; Argañaraz et al., 2016, 2018;
45 Vidal-Riveros et al., 2023). In native grasslands and savannas of the Gran Chaco, fine fuels typically
46 reach 4,000 to 5,000 kg of dry biomass per hectare per year, supporting medium to high intensity surface
47 fires (Bravo et al., 2025). In productive systems such as silvopastoral areas or improved pastures,
48 implanted tropical forage grasses can increase fine-fuel loads substantially (up to double the biomass),
49 locally enhancing fire intensity (Kunst et al., 2016).

50 Landscape heterogeneity further controls fire propagation, as the juxtaposition of rivers, wetlands,
51 shrublands, forests and grasslands in the Gran Chaco, together with traditional firebreak construction
52 and other local management practices, often restricts fire spread and creates natural or managed barriers
53 to fire (Kunst et al., 2003; San Martín et al., 2023; Vidal-Riveros et al., 2023; Bravo et al., 2025). These
54 interacting landscape controls challenge the idea of uniform and spatially consistent anthropogenic
55 effects on fire regimes across global dry ecosystems (Bistinas et al., 2014; Andela et al., 2017; Archibald
56 et al., 2018; Kelley et al., 2019; Jones et al., 2022).

57 Human activity is also a central component of fire regimes in the Gran Chaco. Across the region, most
58 ignitions originate from rural land management practices, including pasture renewal burns, garbage
59 burning, intentional clearing for agriculture or real-estate conversion, and opportunistic burning
60 associated with hunting (Naval Fernández et al., 2023; Vidal-Riveros et al., 2023; San Martín et al.,
61 2023; San Martín, 2024; Bravo et al., 2025). In the wetlands and floodplain grasslands of the Wet Chaco,
62 intentional burning for pasture renovation or vegetation clearing typically occurs towards the end of
63 winter and beginning of spring (end of the cold dry season) and, to a lesser extent, in late summer
64 (towards the end of the wet season) (San Martín et al., 2023). Winter burns are usually controlled and
65 produce small, patchy scars, whereas late-summer fires are more prone to escape and become larger,
66 particularly in anomalous dry years (Saucedo and Kurtz, 2025). Despite these differences in fire

67 behavior, vegetation often shows rapid post-fire recovery in the Wet Chaco (Bravo et al., 2025; Saucedo
68 and Kurtz, 2025). In contrast, the central and western Dry Chaco show a higher prevalence of land-
69 management fires linked to deforestation, rangeland conversion, and dry-season vegetation clearing
70 (Baumann et al., 2022; Gasparri et al., 2008; Naval Fernández et al., 2023; San Martín et al., 2023).
71 Between 2001 and 2019, nearly 40% of the 51.000 km² of deforested area in the Argentine Dry Chaco
72 was associated with burned surfaces (San Martín et al., 2023).

73 Cultural dimensions further shape ignition patterns: indigenous and rural communities in the Dry Chaco
74 use fire for subsistence activities and landscape maintenance, balancing risks and ecological benefits
75 (Sugiyama et al., 2025).

76 In this context, the 2020 fire season illustrated how socio-environmental factors interact under
77 exceptional circumstances. The COVID-19 pandemic altered mobility, enforcement capacity and on-
78 the-ground fire management across many regions worldwide. As discussed by Naval Fernández et al.
79 (2023), in several fire-prone landscapes, such as the Brazilian Pantanal and other tropical savannas, the
80 reduction or suspension of field surveillance and firefighting activities during lockdowns led to
81 increased fire activity (Garcia et al., 2021; Kumar et al., 2022; Eklund et al., 2022). In contrast, in other
82 regions, strict mobility restrictions reduced human-caused ignitions, highlighting the strong coupling
83 between human presence and fire occurrence, as reported for regions in Asia and North America
84 (Paudel, 2021; Poulter et al., 2021). In the Gran Chaco and adjacent drylands of central Argentina,
85 mobility also declined sharply during the peak fire months, yet suppression capacity remained relatively
86 stable due to the continued availability of volunteer brigades (Naval Fernández et al., 2023). Recent
87 socio-anthropological work further shows that the lockdown period through 2020 overlapped with
88 ongoing agrarian expansion and land-clearing dynamics, with deforestation, burning and road-
89 infrastructure projects proceeding despite mobility restrictions, reinforcing long-standing territorial
90 inequalities and weak institutional fire governance (Castilla, 2021; Schmidt and Castilla, 2023). This
91 combination indicates that many ignitions were not accidental or urban in origin, but instead linked to
92 rural land-clearing practices, pasture renewal and other management activities, underscoring the central
93 role of human agency even under atypical social conditions (Naval Fernández et al., 2023; San Martín,
94 2024).

95 At broader temporal and spatial scales, climatic variability, especially the occurrence of prolonged
96 droughts related to the intensification of episodes of multi-year strong El Niño–Southern Oscillation
97 (ENSO) negative phases (La Niña), has been associated with large fire seasons in the Chaco and
98 neighboring biomes (Alencar et al., 2015; Naumann et al., 2023). These climate anomalies reduce fuel
99 moisture and extend the window for fire spread (Doblas-Reyes et al., 2021; De Marzo et al., 2023; Arias
100 et al., 2024). In particular, several recent extreme fire seasons coincided with the 2020–2023 La Niña,
101 which strongly affected moisture availability and fire activity throughout the Gran Chaco and its
102 surroundings (Kumar et al., 2022; Naval Fernández et al., 2023; San Martín, 2024).

103 Although individual drivers of fire occurrence are increasingly well understood, the way these factors
104 interact to determine the final size of fires in the Gran Chaco remains poorly quantified. Existing studies
105 highlight the importance of drought, fuel moisture deficits and human land use in shaping ignition
106 patterns and BA totals, yet the mechanisms that control how far fires spread under contrasting
107 environmental and land-use contexts remain unresolved (San Martín et al., 2023; Vidal-Riveros et al.,
108 2023, 2024; Bravo et al., 2025). Baumann et al. (2022) showed that deforestation pathways vary by actor
109 and context, altering fuel configurations and fire–landscape interactions, San Martín et al. (2023)
110 demonstrated that precipitation–BA relationships differ markedly across land-cover types, and Levers
111 et al. (2024) projected that continuing agribusiness expansion could intensify fire impacts on
112 ecologically and socially sensitive areas. Together, these studies reveal substantial spatial heterogeneity
113 in fire dynamics, but none explicitly evaluate how meteorological variability interacts with landscape
114 structure and human pressures to shape final fire size.

115 Some classification efforts have begun to map regional fire diversity but still overlook key atmospheric
116 determinants. Vidal-Riveros et al. (2024) grouped Paraguayan Chaco fire regimes by severity, frequency
117 and extent, while Naval-Fernández et al. (2025) used multivariate clustering of landscape attributes to
118 delineate pyroregions in the Argentine Chaco. These approaches captured meaningful spatial patterns,
119 yet they did not incorporate high-resolution meteorological conditions, limiting their ability to identify
120 the atmospheric processes that influence fire expansion.

121 In summary, no study has yet combined meteorological anomalies, fire morphology metrics, and
122 landscape context to assess how short-term weather and long-term environmental gradients determine
123 fire size in the Gran Chaco. This gap is critical given the biome's diverse ignition sources, propagation
124 through heterogeneous fuels, and sharp transitions in hydrology, vegetation structure, and land-use
125 intensity.

126 Advances in satellite Earth Observation now allow for such integration. Global burned area (BA)
127 products such as FireCCI51 offer consistent daily burned surface estimates at moderate spatial resolution
128 (Chuvieco et al., 2020). Event-based datasets including FRY (Laurent et al., 2018; Mouillot et al., 2023)
129 and the Global Fire Atlas (Andela et al., 2019) reconstruct individual fires and enable the analysis of
130 attributes such as ignition date, duration, size and morphology (Moreno et al., 2021; Takacs et al., 2021;
131 García et al., 2022). In this study, we use FRYv2.0, which integrates the FRYv1.0 pixel aggregation
132 method with the latest version of FireCCI51 BA mapping (Lizundia-Loiola et al., 2020), and we
133 combine it with environmental and meteorological datasets to quantify how different drivers influence
134 fire size across the Gran Chaco.

135 Specifically, we aim to answer the following scientific questions:

136 (1) What are the primary fire-size characteristics and their frequency across the Gran Chaco between
137 2001 and 2022? (2) To what extent do meteorological conditions influence the size and expansion of
138 individual fires? (3) Beyond weather, what roles do vegetation type, topography and human activity

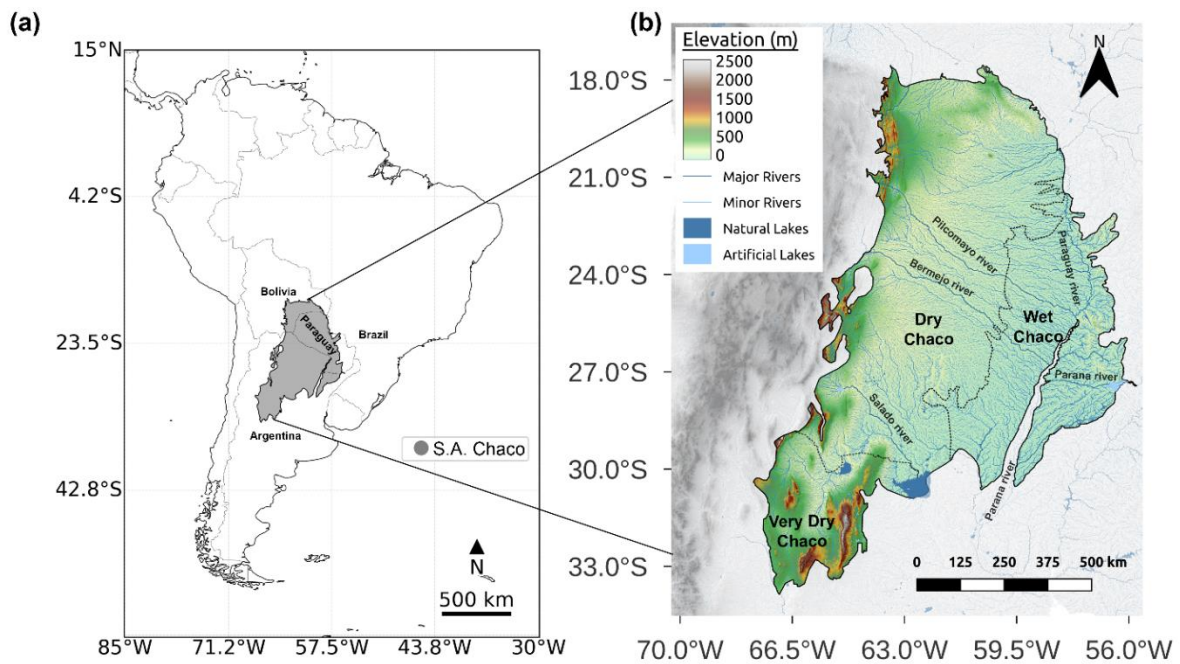
139 play in shaping fire size and fire occurrence across the region? (4) Which of these drivers best explain
140 the spatial and temporal variability of fire size among the different subregions of the Gran Chaco?

141 **2 METHODS**

142 **2.1. Study area**

143 The Gran Chaco is an extensive tropical and subtropical region of South America, covering
144 approximately 1,100,000 km² (**Fig. 1**). It contains the world’s largest continuous dry tropical forest and
145 extensive wetland systems (Bucher, 1982; Olson et al., 2001). In the literature, terminology varies with
146 references to the South American Chaco, the Gran Chaco, or just Chaco. To avoid confusion, we only
147 use Gran Chaco in this work.

148



149 **Fig. 1.** The Gran Chaco location in South America (a) and its topography (b) with its different subregions, main rivers, and lakes. Based on
150 Shuttle Radar Topography Mission (SRTM) at 90m (SRTM | NASA Earthdata, 2024) and HydroSHEDS (Lehner et al., 2008).
151

152
153 The region is mostly flat and low (<200 m.), with higher and undulating terrain towards the northeast
154 limit (~500 m), the western Andean foothills (~2,000 m), and the southwestern Sierras de Córdoba
155 (~2,900 m). Following Olson et al. (2001), we distinguish a humid eastern Wet Chaco from a drier
156 western Dry Chaco, shaped by west–east gradients in precipitation, vegetation, and hydrology (Morello
157 and Adámoli, 1968; Bucher, 1982; Ginzburg et al., 2005; Torrella and Adámoli, 2005). The Wet Chaco
158 receives up to 1,800 mm/year and supports wetlands and palm savannas, while the Dry Chaco gets 300–
159 800 mm/year and is dominated by drought-adapted forests and shrublands. Following Baumann et al.
160 (2018), we identify a drier subregion in the southwest called the Very Dry Chaco, characterized by lower
161 biomass, greater aridity, higher elevations, and distinct fire regimes. Its area is delimited using the
162 borders of the Argentine provinces of Mendoza, San Luis, Córdoba, San Juan, and La Rioja.

163 The Gran Chaco forms part of the La Plata basin (Musser, 2024). Rivers such as the Pilcomayo, Bermejo,
164 and Salado originate in the Andes, cross the Dry Chaco, and disperse into alluvial megafans, streams,
165 and wetlands in the eastern Wet Chaco. This west–east hydrological gradient drives seasonal contrasts:
166 in dry months, the Dry Chaco faces water scarcity, whereas the Wet Chaco retains permanent wetlands
167 that sustain ecological processes and fauna (Naumann et al., 2023).
168 The region harbors exceptional biodiversity, with over 3,400 plant species and hundreds of vertebrates,
169 many endemic (Redford et al., 1990; Bucher and Huszar, 1999; Nori et al., 2016).
170 Fire activity shows pronounced subregional contrasts across the Gran Chaco. The Wet Chaco presents
171 a bimodal fire season, with peaks at the end of the warm wet season (late summer–autumn) and again at
172 the end of the cold dry season (late winter–spring), while the Dry Chaco exhibits a unimodal pattern
173 restricted to the end of the cold dry season, towards late winter–spring (San Martín et al., 2023). Mean
174 annual BA is about 15,000 km²/yr in the Wet Chaco and roughly 8,500 km²/yr in the Dry and Very Dry
175 Chaco together, based on annual BA totals for 2001–2019. Despite its higher annual BA, the Wet Chaco
176 burns repeatedly on much of the same land; about 57% of its burned surface experienced at least two
177 fire events between 2001 and 2019, indicating high recurrence rather than continuous spatial expansion.
178 In contrast, about 66% of the burned surface in the Dry Chaco represents one-time fires, with burns
179 advancing over previously unburned forests. In this western subregion, fires typically follow
180 deforestation rather than acting as the primary clearing mechanism (San Martín et al., 2023). These
181 contrasts reflect the greater continuity of fine fuels and higher fire recurrence in the eastern Wet Chaco,
182 compared with the more intermittent and fuel limited conditions characterizing the Dry and Very Dry
183 Chaco.

184

185 **2.2 Datasets**

186 2.2.1 Fire patches

187 In this study, we used FRYv2.0, a recent global database of fire patch (FP) functional traits (morphology,
188 fire spread, and timing) to investigate fire dynamics and their underlying drivers in the Gran Chaco
189 (Laurent et al., 2018; Mouillot et al., 2023). FRYv2.0 is an updated, second-generation version of the
190 original FRY database that aggregates burned area (BA) pixels from the latest FireCCI51 dataset and
191 from the MODIS MCD64A1 product into individual FPs using fixed temporal cut-offs of 6, 12, or 24
192 days to delimit the extent of a fire event or the onset of a new one. Compared with the original release,
193 it provides extended patch-level information, including morphology (for example area, perimeter, shape
194 index, core area), temporal traits such as burn dates and duration, dynamic traits such as rate of spread,
195 fire radiative power (FRP) and severity indicators, and associated land cover. The FRYv2.0
196 morphological metrics describe the geometry and structure of each FP: *n_{cell}* quantifies the number of
197 burned pixels from the input BA product that form the fire patch; *area* represents the total burned surface;
198 the *shape index* captures deviations from a compact circular shape; the *core-area index* indicates the

199 proportion of interior, non-edge area; *eccentricity* measures patch elongation; and the *perimeter-to-area*
200 *ratio* characterizes boundary complexity and compactness.

201 Patch-level functional traits are computed only for patches composed of at least five burned pixels, to
202 avoid geometric and orientational instability in very small patches. FRP-based diagnostics, including
203 ignition timing derived from active-fire detections, are assigned only to patches larger than 100 ha
204 (approximately sixteen FireCCI51 pixels). This ignition dating offers a more accurate estimate of fire
205 onset than the default burn-date information in FireCCI51 or MODIS MCD64A1, which relies on the
206 day of first BA detection.

207 For this work, we selected the FRYv2.0 version based on FireCCI51 rather than the version based on
208 the MODIS MCD64A1 BA product, because the FireCCI51 input has higher spatial resolution (250 m
209 compared to 500 m), provides better spatial detail for the heterogeneous landscapes of the Gran Chaco,
210 and ensures consistency with our previous FireCCI51 based analysis (San Martín et al., 2023), thus
211 avoiding additional uncertainty from mixing BA products. The FRYv2.0 FireCCI51-based dataset used
212 here is publicly available at <https://osf.io/rjvz5/files/osfstorage> (last accessed on 10 June 2025).

213 2.2.2 Meteorological Data

214 To study meteorological and climate time series in the region, we used the ERA5-Land global reanalysis
215 dataset focused on land surface variables, developed by the European Centre for Medium-Range
216 Weather Forecasts (ECMWF) (Muñoz-Sabater et al., 2021). It provides high-resolution data for land–
217 atmosphere interactions, designed to improve the ERA5 dataset by offering finer detail (0.1° instead of
218 0.25° spatial resolution) for variables affecting the land surface.

219 The product is available in the Copernicus Data Store (CDS) in NetCDF at
220 <https://cds.climate.copernicus.eu/cdsapp#!/dataset/reanalysis-era5-land> (last accessed on 30 May 2024).

221 We downloaded hourly data arrays covering January 2001 through January 2023.

222

223 2.2.3 Environmental and Anthropogenic Data

224 We compiled several spatial datasets that represent biophysical conditions and human-related drivers
225 relevant to fire activity in the Gran Chaco.

226 *Topography* was obtained from the NASA SRTM v3 product (<https://srtm.csi.cgiar.org>, accessed 26
227 May 2025). This product provides a 3 arc-second (approximately 90 m) digital elevation model (DEM)
228 in WGS84 geographic coordinates. Slope and aspect were calculated from this DEM using the Horn
229 algorithm as implemented in the *richdem TerrainAttribute* function, which estimates local gradients
230 over 3 by 3 cells (Horn, 1981).

231 *Land cover* (LC) was obtained from the ESA Climate Change Initiative Moderate Resolution Land
232 Cover product (CCI MRLC; <https://cds.climate.copernicus.eu/datasets/satellite-land-cover>, accessed 26
233 May 2025). This product provides annual maps at 300 m spatial resolution for the period 1992 to 2022.

234 We selected CCI MRLC because its resolution is appropriate for the regional extent of this study, which
235 covers more than 1,100,000 km². The product has undergone extensive validation, is widely used in
236 regional land surface studies, and ensures consistency with our previous analyses in the Gran Chaco
237 (Defourny et al., 2023; Harper et al., 2023; San Martín et al., 2023). Using MapBiomass Chaco would
238 have required a dedicated comparison and validation exercise that was beyond the scope of this fire size
239 study.

240 *Fuel accumulation* before each fire was characterized using MODIS LAI at 500 m resolution and 8-day
241 intervals. We used MOD15A2H (Terra) for 2001 to 2002 and MCD15A2H (Terra and Aqua combined)
242 for 2002 to 2023. Only observations with quality level 0 were retained. For each fire, we extracted all
243 LAI values from MODIS pixels that overlapped the fire patch. To represent the accumulated biomass
244 that could contribute to fire spread, we defined the pre-fire period as the interval between 1 August of
245 the year before the fire and the ignition date. This window captures the seasonal minimum at the end of
246 the winter dry season and the entire subsequent growing season. A 4-step rolling mean with a minimum
247 of one valid value was applied to reduce high frequency noise. The final pre-fire LAI value for each fire
248 patch was the mean LAI across this August to ignition interval. This variable, which we refer to as the
249 mean LAI of the previous growing season, served as a proxy for the biomass accumulated before the
250 fire.

251 *Soil properties* were obtained from the SoilGrids250m database. The variables used were soil organic
252 carbon at 0 to 5 cm depth, sand fraction, and bulk density. We used the one-kilometer aggregated layers
253 provided by *SoilGrids* and computed means for each fire patch.

254 *Population density* was taken from the Gridded Population of the World version 4 (GPWv4) (CIESIN,
255 2017; <https://www.earthdata.nasa.gov/data/projects/gpw>, accessed November 25, 2025). The native
256 resolution of this product is approximately 30 km. Since the dataset was not modified, population values
257 were assigned to each fire patch using nearest neighbor extraction.

258 *Livestock density* was obtained from the Gridded Livestock of the World version 4 (GLWv4;
259 https://dataverse.harvard.edu/dataverse/glw_4, accessed November 25, 2025). This dataset is available
260 at roughly 10 km resolution. The original values were used as provided. For each fire patch, livestock
261 density (number of cattle / km²) was summarized using zonal means.

262 *Road density* was derived from two global road network datasets to account for uncertainties in road
263 mapping, particularly the incomplete representation of informal, unpaved or irregular roads in some
264 regions of the Gran Chaco. We used two independent sources: OpenStreetMap (OSM;
265 <https://www.openstreetmap.org>, accessed November 25, 2025), which is community-curated and
266 generally more complete in populated areas, and the Microsoft Bing AI Global Roads dataset (MS;
267 <https://github.com/microsoft/RoadDetections>, accessed November 25, 2025), which is algorithmically
268 extracted from high-resolution satellite imagery and tends to provide broader coverage in rural and
269 sparsely populated landscapes. For all main analyses, road density was computed from the OSM dataset,

270 while the MS product was used only in a sensitivity experiment to evaluate the robustness of road-
271 related effects (see *Section 2.3.9*).

272 Roads were maintained in vector format and intersected with a regular 0.03° grid (~3 km), projected
273 onto an equal-area coordinate system for accurate calculations of road length and cell area. Road density
274 (km km⁻²) was computed for each grid cell, and fire patches were assigned an area-weighted mean value
275 based on all overlapping cells. The 0.03° resolution was selected after testing coarser and finer grids,
276 providing the best trade-off between capturing road density within each patch and preserving the
277 surrounding spatial context while maintaining consistency across both road datasets. Using both
278 products in this way ensured that the inferred influence of human accessibility on fire behavior was not
279 dependent on a single mapping dataset, while keeping OSM as the reference road layer for the core RF
280 configurations.

281 2.2.3 Climate Oscillations

282 To account for the influence of large-scale climate variability, we included the Multivariate El Niño–
283 Southern Oscillation (ENSO) Index version 2 (MEI.v2), developed by NOAA's Physical Sciences
284 Laboratory. The MEI.v2 time series was obtained from NOAA PSL at <https://psl.noaa.gov/enso/mei/>
285 (last accessed 26 May 2025).

286

287 **2.3 Data processing and analysis methods**

288 2.3.1 Fire Weather Index (FWI)

289 We built an ERA5-Land-based Canadian Fire Weather Index (FWI; Van Wagner, 1987) dataset for the
290 Gran Chaco at 0.1° resolution and daily time steps. We converted hourly accumulated precipitation to
291 hourly rainfall by differencing successive steps and summing totals from 15 UTC (day D-1) to 15 UTC
292 (day D), matching the FWI daily window and corresponding to local noon in most of the Gran Chaco.
293 We applied this fixed 15 UTC cutoff to the full region to avoid inconsistencies caused by varying
294 national time zones and daylight-saving changes.

295 We extracted daily meteorological inputs (i.e., air temperature, relative humidity, wind speed at local
296 noon, and 24-h precipitation) to compute the six FWI sub-indices: Fine Fuel Moisture Code (FFMC),
297 Duff Moisture Code (DMC), Drought Code (DC), Initial Spread Index (ISI), Build-Up Index (BUI), and
298 FWI. We performed calculations with an adapted version of the *FireDanger* Python package
299 (<https://github.com/steidani/FireDanger>) compatible with *xarray* and *NetCDF*, including pixel-level day
300 length for DMC and hemisphere-specific drying factors for DC. We initialized the system on 1 January
301 1981 using Copernicus ERA5–FWI moisture codes at 0.25° (Vitolo et al., 2020) interpolated to 0.1°.

302 2.3.2 Land Cover processing

303 For this work, the original classes of CCIMRLC were grouped into eight categories relevant to the Gran
304 Chaco fire regime. These categories included tree cover, shrublands, grasslands, seasonally flooded
305 herbaceous vegetation, croplands, two mixed mosaics containing combinations of herbaceous and
306 woody vegetation, and an extra class we called “Others”, grouping the remaining underrepresented
307 classes in the Gran Chaco. For each FP we extracted the fractions of LC at the year of fire ignition, and
308 these fractions were used to calculate the following landscape heterogeneity indices:

309 In order to quantify the landscape heterogeneity within each FP and assess how the mix and spatial
310 balance of LC types influence fire outcomes, we calculated the Shannon diversity index (H) and Pielou's
311 evenness (E). They were computed as follows:

312

313 **(Eq. 1)** Shannon Diversity Index (Shannon, 1948):

314
$$H = - \sum_{i=1}^m p_i \log(p_i)$$

315 Where m is the number of land cover classes present in the fire patch, p_i is the proportion of land cover
316 type i , and the sum includes all classes with $p_i > 0$.

317

318 **(Eq. 2)** Pielou's evenness (Pielou, 1966):

319
$$E = \frac{H}{\log(m)}$$

320 Where H is the Shannon Diversity Index and m is the number of land cover classes present in the fire
321 patch.

322

323 2.3.3 Wind indices

324 Using ERA5-Land data, we calculated for each FP a metric specifically designed to capture the role of
325 strong, persistent winds in shaping fire behavior: the Extreme Wind Directionality Index
326 (EW_dir_index). This index measures both how often extreme winds occurred and how steady their
327 direction was.

328 The first component, fraction of extreme-wind days (EW_frac), is the proportion of burning days when
329 the daily maximum wind speed exceeded 25 km h^{-1} :

330 **(Eq. 3)** Extreme Wind Fraction Index:

331
$$EW_frac = \frac{EW}{N}$$

332 where EW is the number of days with extreme winds and N is the total fire duration (days). High values
333 indicate that strong winds occurred on many burning days.

334 The second component, wind direction steadiness (*wind_dir_R*), reflects how consistent the wind
335 direction was across the fire’s duration (N). Each day’s mean wind direction (θ_i , in radians) is
336 represented as a unit vector, summed across all days, and normalized by the fire duration:

337 **(Eq. 4)** *Wind Directionality Index*:

$$338 \quad \text{wind_dir_R} = \frac{\sqrt{(\sum_{i=1}^N \cos \theta_i)^2 + (\sum_{i=1}^N \sin \theta_i)^2}}{N}$$

339 Values near 1 mean that winds blew in a stable direction throughout the event, while values near 0 mean
340 that wind directions shifted substantially from day to day.

341 The *EW_dir_index* is the product of *EW_frac* and *wind_dir_R*:

342 **(Eq. 5)** *Extreme Wind Directionality Index*:

$$343 \quad \text{EW_dir_index} = \text{EW_frac} \times \text{wind_dir_R}$$

344 It reaches high values only when strong winds occur on many burning days and blow consistently from
345 the same direction, identifying fires likely driven by sustained, unidirectional wind conditions.

346 2.3.4 Burned Area vs Fire Counts

347 To examine the interannual relationship between fire counts and total BA, we compared annual BA and
348 annual fire counts for each of the three Gran Chaco subregions using FRYv2.0. For every year in 2001–
349 2022, total BA was computed as the sum of the burned surface of all fire patches within each subregion,
350 while fire counts were obtained as the number of individual patches whose ignition date fell within that
351 year. We then fitted simple linear regressions between annual BA and annual fire counts for each
352 subregion to quantify how ignition frequency explains interannual variability in BA and to assess
353 whether this relationship differs among the subregions and between the wet and dry seasons.

354 2.3.5 Fire size classification

355 To characterize how fires of different magnitudes contribute to overall fire activity in the Gran Chaco,
356 we classified all FPs from FRYv2.0 into six size categories. Fire events can be classified according to
357 multiple criteria, including behavior (rate of spread, intensity), ecological impact (severity), structure
358 (number of ignition points), or final extent. Because this study focuses specifically on the determinants
359 of final fire size, we adopted a size-based classification system. This choice allows us to map directly
360 the response variable of interest and to interpret the climatic, landscape, and anthropogenic factors that
361 control it.

362 To avoid ad-hoc or region-specific thresholds, we followed the standardized fire-size typology proposed
363 by Linley et al. (2022), who conducted the first global assessment aimed at harmonizing terminology
364 for large fires. They argue that terms such as “*megafire*” or “*large wildfire*” had been used inconsistently
365 across disciplines and agencies, often referring to different orders of magnitude depending on national
366 contexts or management traditions. They show that this lack of standardization complicates cross-
367 regional comparison and the interpretation of extreme events. To resolve this, they propose clear, size-

368 based definitions applicable worldwide: megafires as events with BA > 10,000 ha (100 km²), gigafires
369 > 100,000 ha (1000 km²), and terafires > 1,000,000 ha (10,000 km²). Their framework is explicitly
370 designed for satellite-derived BA products, including those used to build FRY, and provides a consistent
371 basis for global and regional analyses.

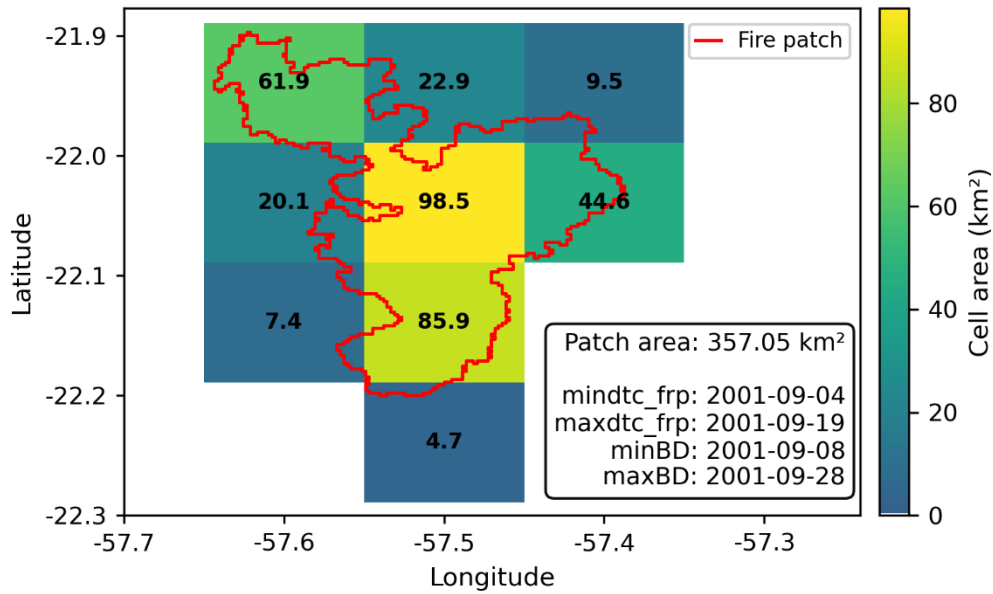
372 Using Linley's typology ensures that extreme fire classes in the Gran Chaco are comparable to global
373 assessments and avoids relying on operational thresholds used in some countries (e.g., 40,000 ha) that
374 lack a physical or ecological rationale. At the same time, the empirical distribution of FRYv2.0 patch
375 sizes in the Chaco is strongly right-skewed, with most events being small and only a few exceeding the
376 megafire threshold. For this reason, and to retain regional relevance, we adapted Linley's standardized
377 thresholds into operational size classes suitable for the Gran Chaco, while preserving the key Linley cut-
378 offs at 100 km² and 1000 km². FRYv2.0 imposes a practical lower limit on measurable patch size:
379 functional traits are computed only for patches composed of at least five FireCCI51 pixels (~0.3 km²),
380 and FRP-based diagnostics, including ignition dating, are provided only for patches larger than 100 ha
381 (1 km²; see *Section 2.2.1*). This naturally defines the smallest reliable category in our system.

382 The resulting scheme spans from a "very small" class (0–1 km²), which is more uncertain because FRY
383 patches in this range often lack complete geometric or FRP-based diagnostics, through small (1–5 km²),
384 medium (5–10 km²), and large (10–100 km²) events, up to megafires (100–1000 km²) and gigafires
385 (>1000 km²). No fire in the Gran Chaco exceeded 10,000 km², and therefore the terafire class defined
386 by Linley et al. is not used in this work.

387 2.3.6 Gridded burned area

388 To enable a spatiotemporal comparison between fire activity from FRYv2.0 fire patches and
389 meteorology, we developed a pipeline to transform the FP-based data into a monthly gridded product at
390 0.1°, matching the ERA5-Land grid (**Fig. 2**).

391



392

393 **Fig. 2.** Example of one FRY fire patch (red line) over the gridded FRY dataset. Each grid cell at 0.1° is assigned the burned area corresponding
 394 to the total fraction of the patch that overlaps it. The values printed over each grid cell correspond to these values.
 395

396 The temporal assignment of fires to months followed a hybrid strategy: where MODIS-derived hotspot
 397 detection dates (*mindtc_frp* and *maxdtc_frp*) were available in a given FP (typically absent in very small
 398 FPs) they were used. Both FireCCI51- and MODIS-based versions of FRYv2.0 include these hotspot
 399 date variables when available for the FP. When hotspot dates were missing, we used the FireCCI51-
 400 derived burn dates (*minBD* and *maxBD*), which are based on surface reflectance changes and are
 401 available for all FPs. For FPs spanning multiple months, we assigned the fire to the month in which it
 402 started, unless its duration in a subsequent month exceeded that of the starting month by more than two
 403 days.

404 Each FP was rasterized on a 0.01° grid by intersecting it with individual cells. The intersected area in
 405 square kilometers was computed using the WGS84 ellipsoid model. These contributions were
 406 aggregated per cell and per assigned month to build a three-dimensional array of monthly BA (*lat x lon*
 407 *x time*). A similar procedure was implemented for fire counts, using ignition (first detection) coordinates
 408 and dates. Each FP's fire ignition coordinate was allocated to the closest cell in the 0.1° grid. The
 409 resulting monthly gridded dataset included two variables: BA and counts.

410 To compute monthly BA anomalies, we derived pixel-level monthly climatologies for the period 2001–
 411 2020 from the gridded BA dataset. Anomalies were defined as the difference between each monthly BA
 412 value and the corresponding monthly climatological mean, following the same temporal normalization
 413 applied to meteorological variables.

414

415 2.3.7 Anomalies and climatologies

416 For all ERA5-Land variables, as well as the FWI index and its sub-indices, we computed pixel-level
417 daily climatologies using the 2001–2020 mean as the baseline. Meteorological anomalies were then
418 defined as the daily deviation from this climatology and subsequently aggregated to monthly values to
419 match the temporal scale of the BA analysis.

420 To compute monthly BA anomalies, we derived pixel-level monthly climatologies for the period 2001–
421 2020 from the gridded BA dataset. Anomalies were defined as the difference between each monthly BA
422 value and the corresponding monthly climatological mean, following the same temporal normalization
423 applied to meteorological variables. This anomaly-based formulation was used only for the correlation
424 analysis with FWI anomalies and not for any other statistical or spatial analyses in the manuscript.

425 For the specific analysis comparing monthly BA anomalies with monthly FWI anomalies, only pixels
426 with at least four fire-active months ($BA > 0$) during 2001–2022 were retained to avoid artefacts from
427 sparsely populated or highly skewed anomaly series. Correlations were computed using both Pearson’s
428 coefficient and Spearman’s rank coefficient.

429 We did not apply an FWI95-based threshold or similar fixed-percentile metrics, as these are less
430 comparable across the strong climatic gradient of the Gran Chaco and may artificially amplify or
431 dampen fire–weather relationships depending on local baseline conditions. Using pixel-level anomalies
432 instead allows each location to be evaluated relative to its own climatology, yielding a spatially
433 consistent and locally meaningful basis for comparison.

434

435 2.3.8 Fire-weather types

436 We classified fire patches (FPs) into three groups based on associated atmospheric conditions using the
437 K-means clustering algorithm (MacQueen, 1967) in *Python’s scikit-learn v1.3*. This approach follows
438 prior applications in fire studies (Ruffault et al., 2016, 2020; Vidal-Riveros et al., 2024) and aimed to
439 identify distinct fire-weather types (FWTs) and assess their influence on fire size and shape.

440 For this clustering analysis, we retained only fire patches between 1 and 100 km² ($N = 78,052$). At the
441 lower end, this choice is consistent with the construction of the FRYv2.0 database, where the FP
442 functional traits are computed only for patches composed of at least five burned pixels and smaller
443 patches are filtered out because their geometry and orientation are considered unreliable (see *Section*
444 *2.2.1*). In addition, FRP based diagnostics, including ignition timing derived from active fire detections,
445 are only provided for FPs larger than 1 km² (approximately 16 FireCCI51 pixels), so the smallest events
446 lack both robust geometric traits and FRP timing information. At the upper end, fires larger than 100
447 km² were excluded from the K-means analysis. In addition to their low frequency, these very large, long
448 duration patches often span heterogeneous landscapes and experience several distinct weather situations
449 over their burning period, so the associated ERA5-Land and FWI time series mix conditions from distant
450 locations and different days. This mixing makes the patch-averaged meteorological descriptors difficult

451 to interpret as a single coherent FWT and would likely introduce substantial biases in the clustering and
452 in the Random Forest (RF) models used later to analyze fire size drivers (see *Section 2.3.9*).
453 For each FP within the 1–100 km² range, we extracted daily ERA5-Land meteorological data and the
454 computed FWI time series from 7 months before ignition to 7 months after, and then built two feature
455 sets, one representing pre-fire conditions and one representing conditions during the fire.
456 For the *Pre-Fire* set, we used normalized anomalies of 2-m air temperature, 10-m wind speed, relative
457 humidity (RH), drought code (DC), and duff moisture code (DMC) (Ruffault et al., 2020). Pre-fire
458 values were calculated as the 3-day mean from ignition day (D) to D-2 to limit detection-date bias
459 (Lizundia-Loiola et al., 2020; Pettinari et al., 2021) while avoiding noise from longer lags.
460 For the *During-Fire* set, we computed the same variables averaged over the fire’s duration and added
461 the *Extreme Wind Fraction Index* and the *Extreme Wind Directionality Index*, described in *Section 2.3.3*.
462 All variables in both sets were standardized before clustering (mean = 0, $\sigma = 1$). The resulting data
463 matrix was clustered with $k = 3$, squared Euclidean distance, *k-means++* initialization, 50 random
464 restarts, and a convergence tolerance of 10^{-4} . We retained three clusters based on a prior hypothesis
465 (wind-driven, drought-driven, and neutral), an elbow in the within-cluster sum-of-squares curve, and a
466 peak in the silhouette coefficient at $k = 3$.
467 Cluster labels were assigned by interpreting centroid positions in principal component space and
468 examining the temporal evolution of variables (**Fig. S1**). Robustness was assessed using mean silhouette
469 coefficients and their distribution across clusters. The first two principal components explained more
470 than 60 % of the variance and clearly separated cluster centroids.

471

472 2.3.9 Fire size drivers

473 To investigate the role of environmental and anthropogenic variables in determining fire size, we
474 extracted a diverse set of FP-level potential predictors encompassing topographic, climatic,
475 anthropogenic, vegetation, and landscape heterogeneity dimensions. These variables, listed in **Table 1**,
476 were used as inputs in the RF models to assess their relative importance in explaining fire size.

477 Once all potential predictor variables were derived, we trained RF models using a set of 17 explanatory
478 variables to analyze the drivers of fire behavior, using the variable *n_cell* from the FRY dataset as the
479 response variable. This variable represents the number of FireCCI51 pixels within each FP and was
480 preferred over patch-based *area* due to the latter’s dependency on latitude, which introduced artificial
481 discontinuities. In contrast, *n_cell* provided a discrete and spatially consistent proxy for BA, improving
482 model stability and interpretability.

483 We implemented 12 primary RF models across five configurations: (i) a global model using all the
484 78,052 fire patches used for the clustering analysis (patches with area between 1 and 100 km²), (ii) three
485 subregion-specific models for the Wet, Dry, and Very Dry Chaco, (iii) two seasonal models based on

486 ignition season (wet vs dry), and (iv) two sets of three cluster-based models (pre-fire and during-fire
 487 conditions) derived from the FWT classification (see *Section 2.3.8*).

488

489 **Table 1.** Target and potential predictor features extracted from each FRY fire patch within the Gran Chaco region, grouped by variable types.
 490 These features were used for the Random Forest models trained in this work.

Category	Variables
Fire Size (target feature)	Number of pixels within the fire patch (250 m pixels from FireCCI51)
Topography	Mean Slope (%) Mean Elevation (m)
Meteorology (during fire mean)	Precipitation (mm) Maximum Wind Speed (km/h) Extreme Wind and Direction Index (EW_dir_index) Extreme Wind Days Fraction (EW_frac)
Anthropogenic proxies (year of fire ignition)	Cattle Density (heads/km ²) Road Density (km/km ²) Population Density (p/km ²)
Vegetation productivity (previous growing season)	LAI for previous growing season (MODIS-derived)
Land Cover Composition (year of fire ignition)	Flooded Herbaceous vegetation (%) Tree Cover (%) Shrublands (%) Trees/Shrubs/Herbs Mosaics (%) Natural/Croplands Herbaceous Mosaics (%)
Landscape Heterogeneity (year of fire ignition)	Land Cover Diversity (Shannon Index, H) Land Cover Evenness (Pielou Index, E)

491

492 All models were trained using the *ranger* R package (Wright and Ziegler, 2017) with quantile regression
 493 forests (Meinshausen, 2006). We used 500 trees, a minimum node size of 5, variance-based importance,
 494 and the Poisson split rule, with 4 variables considered at each split. Feature selection included correlation
 495 filtering ($r > 0.8$ threshold) and preliminary importance scores. Each model was trained on 75% of the
 496 data and validated on the remaining 25%. We evaluated feature contributions using SHAP (SHapley
 497 Additive exPlanations) values.

498 In addition to these primary configurations, we trained two diagnostic RF models to assess the
 499 robustness of our results. First, a “No Topography” model was built by removing elevation and slope
 500 from the predictor set while keeping all other variables and settings identical to the Full Chaco
 501 configuration. Second, an “MS Roads” model replaced the OSM-based road-density layer with the MS-
 502 based road density, again using the same sample of fire patches, hyperparameters, and training / test
 503 split as the Full Chaco RF. These sensitivity experiments were analyzed with the same SHAP-based
 504 diagnostics as the primary models and were used to evaluate whether the RF results were robust to
 505 changes in the predictor set and road-data source.

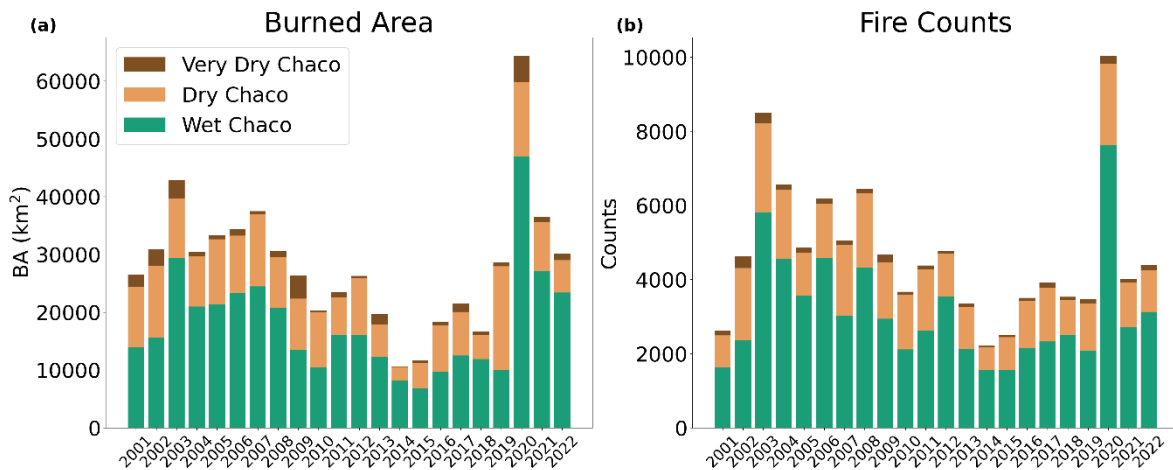
506 **3 RESULTS**

507 **3.1 Burned area and ignitions**

508 We examined the interannual variability of burned area (BA), fire counts, and mean fire duration across
509 the Gran Chaco between 2001 and 2022 (**Fig. 3; Fig. S3**). To complement these indicators, we quantified
510 the relationship between total BA and annual fire counts for each subregion and season, using linear
511 correlations (**Fig. S2**).

512 The time series reveals a sustained decrease in annual fire counts and BA from the early 2000s to the
513 late 2010s, followed by a pronounced peak in 2020–2021. Because the observational window begins in
514 2001, it is difficult to determine whether the downward phase reflects a longer-term trend or a segment
515 of decadal variability. These two peak years also show the largest BA of the record, particularly in the
516 Wet and Dry Chaco, and stand out clearly relative to the preceding trajectory.

517



518

519 **Fig. 3.** Interannual evolution of fire activity in the Gran Chaco from 2001 to 2022, derived from FRYv2.0 fire patches. (a) Total annual burned
520 area and (b) total annual fire counts, with stacked bars showing the contributions of the Wet, Dry, and Very Dry Chaco subregions.

521

522 BA and fire counts showed a broadly positive relationship, but with substantial regional and seasonal
523 differences. In the Wet Chaco, BA and fire counts were strongly correlated in both wet and dry seasons
524 ($R^2 = 0.96$ and 0.91 ; **Fig. S2**), indicating that interannual BA variability is largely explained by the
525 annual number of fire patches rather than by individual fire sizes. Mean fire duration remained stable
526 (approximately 10–12 days; **Fig. S3**).

527 The Dry Chaco exhibited a high wet-season correlation between BA and fire counts ($R^2 = 0.87$; **Fig.**
528 **S2**), but a much weaker dry-season relationship ($R^2 = 0.45$). This implies that, during the dry season,
529 fluctuations in BA are not tightly linked to fire counts, consistent with a larger contribution of size
530 extremes. Fire duration was also stable through the period (**Fig. S3**).

531 In the Very Dry Chaco, wet-season fires were infrequent and showed almost no relationship between
532 BA and fire counts ($R^2 = 0.11$; **Fig. S2**). In contrast, dry-season BA correlated strongly with the number
533 of fires ($R^2 = 0.78$). Mean fire duration was relatively constant, with no clear interannual trend (**Fig. S3**).
534 Overall, fire duration exhibited limited variation across subregions (**Fig. S3**), reinforcing that BA
535 fluctuations were controlled primarily by changes in fire counts and the distribution of fire sizes, rather
536 than by changes in the duration of individual fires.

537

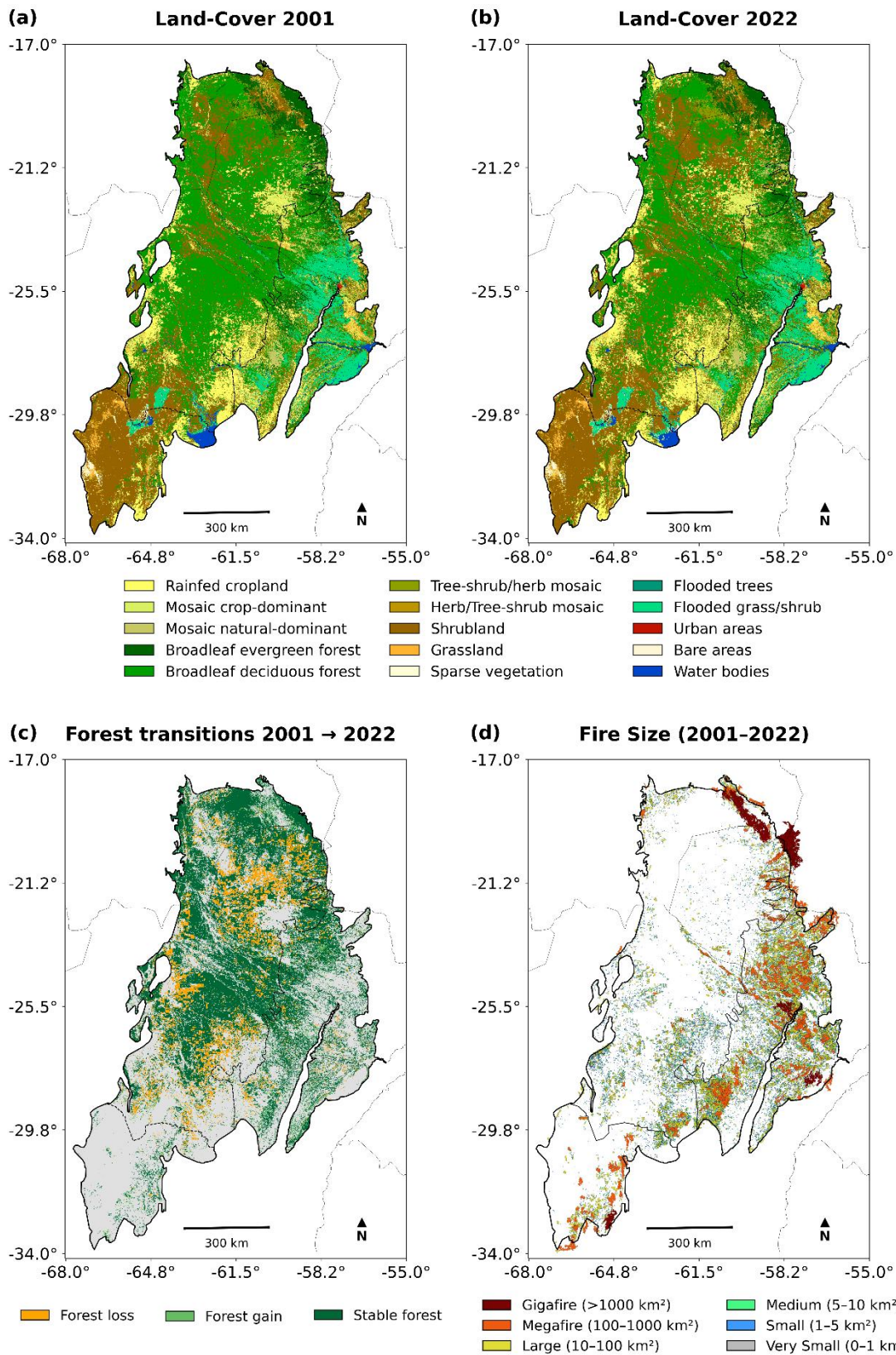
538 **3.2 Land Cover and Fire size distribution**

539 **Fig. 4** shows the land-cover distribution, forest transition patterns, and spatial distribution of fire events
540 categorized by size between 2001 and 2022. The Wet Chaco is dominated by seasonally flooded
541 herbaceous vegetation, forest mosaics, productive grasslands, and croplands, and it exhibits the highest
542 fire frequency. In contrast, the Dry and Very Dry Chaco regions show increasing proportions of
543 shrublands, fragmented forests, and agricultural frontiers. These long-term LC shifts are summarized in
544 **Fig. S4**, which illustrates the main transitions between 2001 and 2022 and highlights the substantial
545 expansion of shrublands and mosaic vegetation, together with a marked reduction in tree cover.

546 Fire size distribution is strongly right-skewed across all subregions: over 80 % of events fall within the
547 Very Small ($< 1 \text{ km}^2$) and Small ($1\text{--}5 \text{ km}^2$) categories (**Table S1**; **Fig. S6**). Larger fires, although less
548 frequent, account for a disproportionate share of total BA. While Very Small to Large ($10\text{--}100 \text{ km}^2$)
549 fires are widespread, Megafires ($100\text{--}1000 \text{ km}^2$) are most common in the Wet Chaco, likely due to
550 continuous fuel beds in grasslands and wetlands. These large fires often occur in areas dominated by
551 seasonally flooded herbaceous vegetation, which can generate high flammability during dry periods.
552 Gigafires ($> 1000 \text{ km}^2$), although rare, are almost exclusively observed in the Dry Chaco.

553 Forest loss is widespread across the Chaco in all three countries, with extensive deforestation frontiers
554 in both Argentina and Paraguay. However, the association between fires and these frontiers differs
555 regionally. In Argentina, deforestation zones often coincide with clusters of small and medium fires,
556 whereas in Paraguay and Bolivia fire activity is less evident along recent forest loss edges. In all regions,
557 most large fires occurred in non-forest areas. Shrublands were excluded from the forest class definition,
558 which here only includes tree-cover categories. The Sankey diagram in **Fig. S3** also shows that much of
559 the increase in shrublands and mixed vegetation mosaics originates from former tree-cover classes,
560 reinforcing the link between vegetation degradation and the fuel complexes that support the largest fires.
561 Across the full Chaco, BA were dominated by open formations: seasonally flooded grasses and herbs
562 account for more than 26% of the total, shrublands for 23% and mosaic vegetation for roughly 12%.
563 Tree cover represents about 24% of all BA, indicating that fires also affect forested and semi-forested
564 landscapes, particularly in the wetter and transitional subregions.

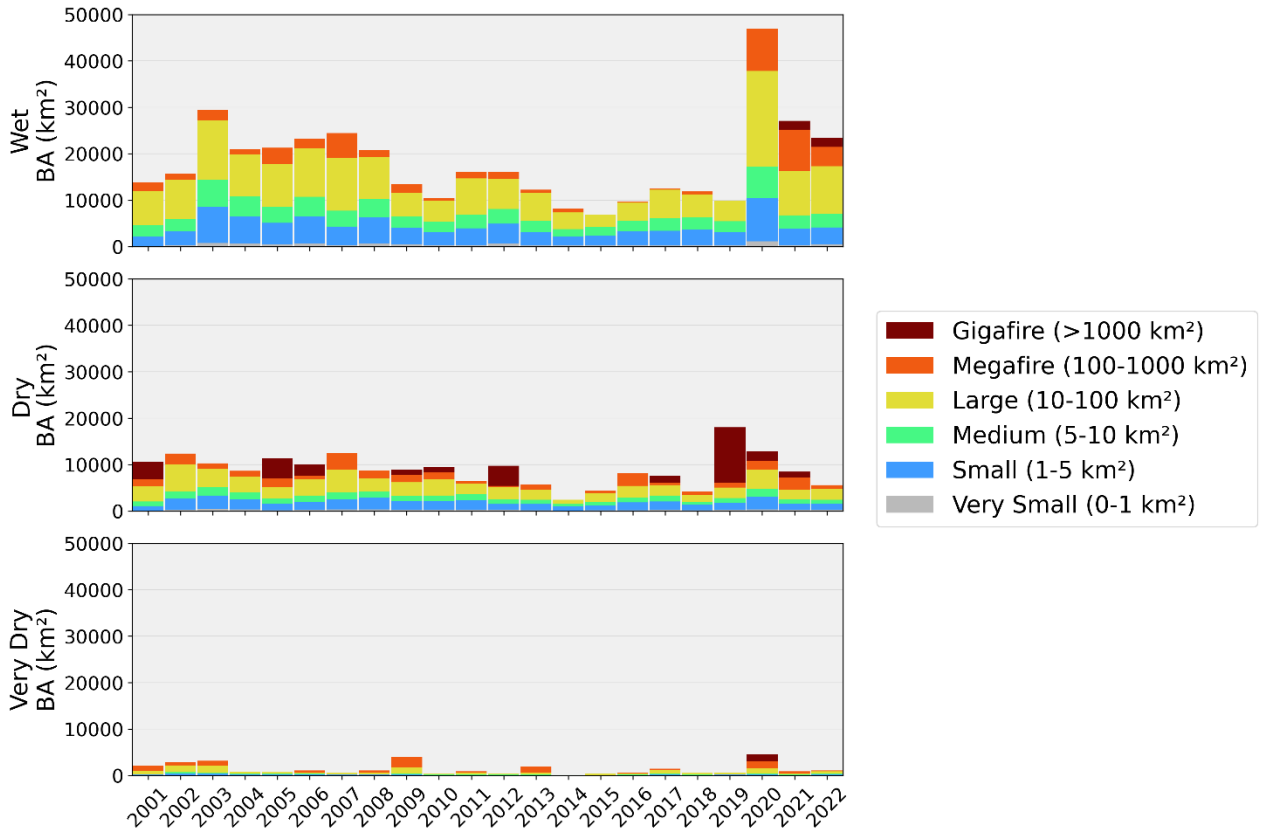
565



566
567
568
569
570
571

Fig. 4. (a) and (b) Land-cover distribution in the Gran Chaco based on ESA-CCI MRLC for 2001 and 2022, respectively. (c) Forest transition classes between 2001 and 2022, showing forest loss (forest to non-forest), forest gain (non-forest to forest), and stable forest. Forests include all tree cover classes (shrubs not included); non-forest pixels appear in grey. (d) Spatial distribution of fire events (2001–2022) categorized by fire size using FRYv2.0 data. Fire-size classes range from Very Small (< 1 km²) to Gigafires (> 1000 km²). Fires patches overlapping the Chaco boundary are retained.

572 Subregional patterns reveal strong gradients. In the Wet Chaco, flooded grasses and herbaceous
 573 vegetation together contribute more than 36% of the BA, followed by tree cover (24%), showing that
 574 fires extend beyond the floodplain system into forest–savanna transitions. In the Dry Chaco, shrublands
 575 dominate the burned LC composition (almost 39%), accompanied by substantial fractions of mosaic
 576 vegetation and tree cover, consistent with the vegetation degradation and forest-to-shrub transitions
 577 shown in **Fig. S3**. In the Very Dry Chaco, fires overwhelmingly affect shrublands, which represent more
 578 than 75% of all BA.
 579



580
 581 **Fig. 5.** Cumulative burned area(2001–2022) by fire-size class across the Wet, Dry, and Very Dry Chaco subregions.
 582

583 According to **Fig. 5**, the Wet Chaco registers the highest total burned area, nearly double that of the Dry
 584 and Very Dry regions. In this subregion, large fires contribute ~40% of annual BA, and small fires ~20%
 585 (**Fig. S5**). Despite their modest size, small fires contribute substantially to BA in the Wet Chaco due to
 586 their high frequency between 2001 and 2022 (>36,000). Extreme years such as 2003 and 2020 were
 587 marked by widespread outbreaks.

588 In the Dry Chaco, fire count is lower, but large fires play a more prominent role. Large fires account for
 589 about 25% of the annual BA, and gigafires can dominate totals in some years. For example, in 2019,
 590 just three gigafires in the Dry Chaco burned approximately 10,000 km², which corresponds to the
 591 region’s mean annual BA and represented more than 50% of the total for that year.

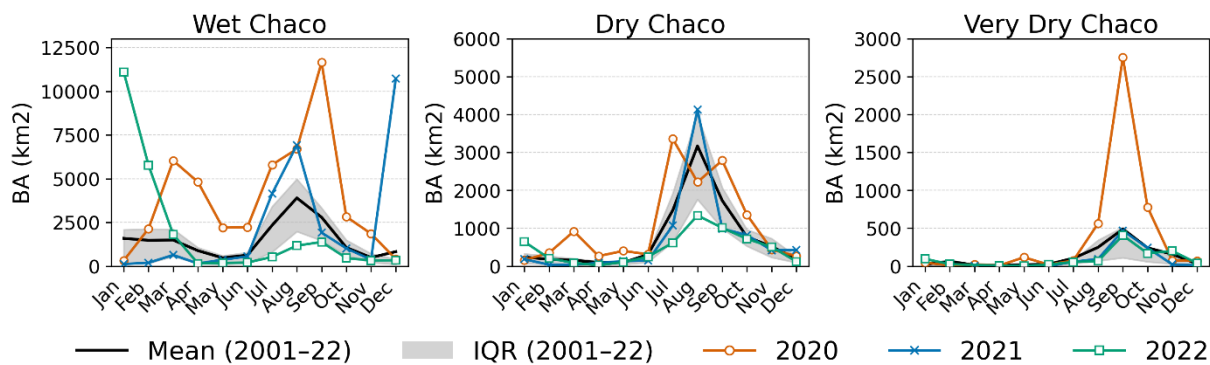
592 The Very Dry Chaco, while recording the lowest overall BA, exhibits abrupt interannual peaks driven
 593 by isolated megafires and gigafires, pointing to a more stochastic fire regime.

594 Between 2020 and 2022, the Wet Chaco experienced an unprecedented number of megafires and
 595 gigafires, both in terms of event counts and their contribution to total BA. These patterns align with the
 596 extreme fire weather anomalies described in *Section 3.3*.

597

598 3.3 Fire–weather relationship

599



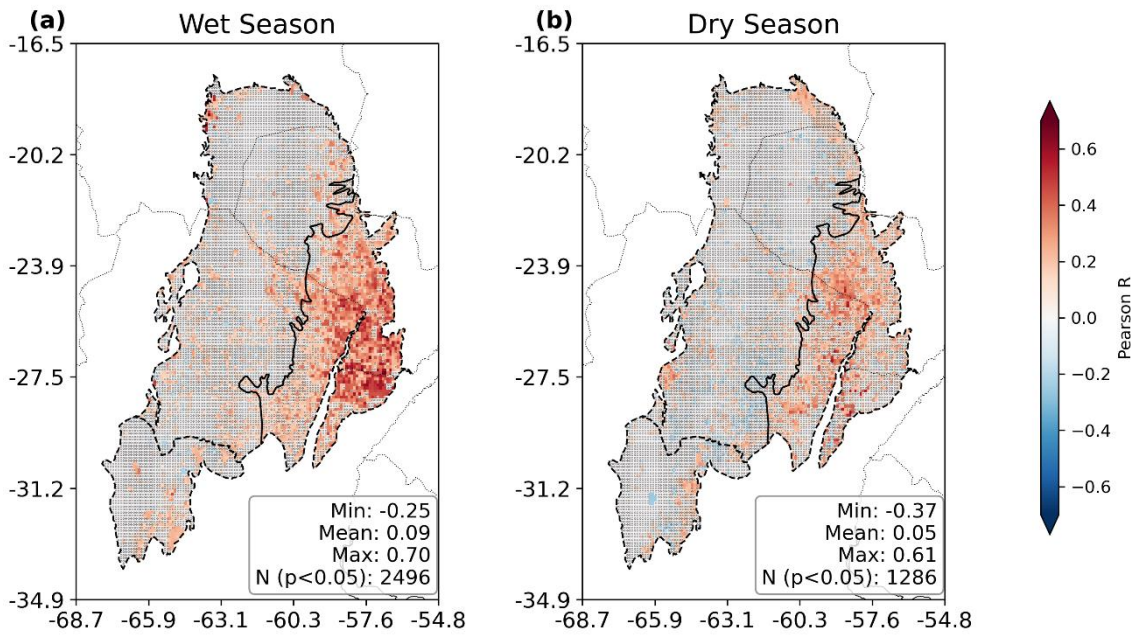
600 — Mean (2001–22) IQR (2001–22) ○ 2020 × 2021 □ 2022
 601 **Fig. 6.** Seasonality of burned area (BA, km²) in the Wet, Dry, and Very Dry Chaco. The black curve is the 2001–2022 monthly BA mean and
 602 the grey band shows the interquartile range (25–75%). Colored curves overlay monthly BA for 2020 (orange circles), 2021 (blue crosses), and
 603 2022 (green squares), highlighting differences from the climatological envelope. Y-axis limits differ by panel.

604

605 **Fig. 6** presents the monthly BA climatology (2001–2022) with 2020–2022 overlaid for the Wet, Dry,
 606 and Very Dry Chaco. In the Wet Chaco, BA in 2020 is above average for most months, with a secondary
 607 pulse in March–April (late wet season) preceding pronounced peaks in August–September (winter/dry
 608 season). In contrast, anomalies in 2021–2022 are concentrated in the summer/wet season (December–
 609 March), reaching levels similar to the typical late-winter/early-spring maximum, while post-winter
 610 months in 2022 remain mostly below average. In the Dry Chaco, 2020 stands out as extreme, particularly
 611 in July and September, whereas 2021 records an exceptional August at or above historical maxima and
 612 2022 stays near or below the mean. In the Very Dry Chaco, positive anomalies are dominated by 2020,
 613 with a sharp September maximum; 2021 shows only minor increases, and 2022 remains subdued.
 614 Overall, 2020 shows widespread positive anomalies lasting several months across all subregions. In
 615 contrast, 2021 and 2022 generally feature shorter peaks, often concentrated in summer, although 2021
 616 also records exceptional winter fires in the Dry Chaco. Activity during the canonical late-winter fire
 617 season is otherwise limited, particularly in 2022.

618 The spatial patterns of fire–weather coupling shown in Fig. 7 depict the per-pixel Pearson correlation
 619 between monthly Fire Weather Index (FWI) anomalies from ERA5-Land and BA anomalies derived
 620 from the gridded FRY dataset, both at 0.1° resolution, during the wet and dry seasons. FWI anomalies
 621 exhibit an approximately normal distribution, and after filtering pixels with fewer than four fire-active

622 months, most BA anomaly series are quasi-normal, justifying the use of Pearson correlation as described
 623 in *Section 2.3.7*. Significant positive correlations ($p < 0.05$) are concentrated in the Wet Chaco, where R
 624 coefficients reach up to 0.7 during the wet season. In contrast, the Dry and Very Dry Chaco show weaker
 625 and more spatially scattered relationships, partly due to lower fire frequency. Spearman correlations
 626 were also calculated, resulting in similar patterns with lower coefficients (maximum R of 0.52; **Fig. S7**)
 627
 628



629 **Fig. 7.** Spatial distribution of pixel-wise Pearson correlation coefficients between monthly Fire Weather Index (FWI) anomalies and monthly
 630 burned area (BA) for the period 2001–2022: (a) Wet Season and (b) Dry Season. The color bar indicates the strength and direction of the
 631 correlation (from negative in blue to positive in red). Inset statistics summarize the distribution of coefficients (Min, Mean, Max). Pixels marked
 632 with small black circles represent non-significant correlations (p -value > 0.05), while unmarked pixels indicate significant correlations (p -
 633 value < 0.05). Only pixels with more than 3-time steps with burned area > 0 were kept to avoid biased correlations related to very few or no
 634 fires.
 635
 636

637 To further explore the spatial sensitivity of fire activity to fire weather, **Fig. 8** compares per-pixel
 638 correlations between monthly FWI anomalies (see *Section 2.3.7*) and two metrics: fire counts and BA.
 639 Each dot represents a 0.1° grid cell, and quadrants classify response types. In the Wet Chaco, 93% of
 640 cells fall in Q1, where both metrics show positive correlations with FWI, with moderate mean values
 641 (0.17 ± 0.12 for ignitions, 0.19 ± 0.13 for BA) and strong inter-metric correlation ($r = 0.76$). The Dry and
 642 Very Dry Chaco show more heterogeneous patterns, with Q1 proportions of 59% and 61%, and weaker
 643 mean correlations (~ 0.04 – 0.06). Still, inter-metric spatial correlations remain high ($r = 0.81$ and
 644 $r = 0.72$), indicating that regions more sensitive to fire weather in terms of ignitions also tend to be more
 645 sensitive in terms of fire extent.
 646

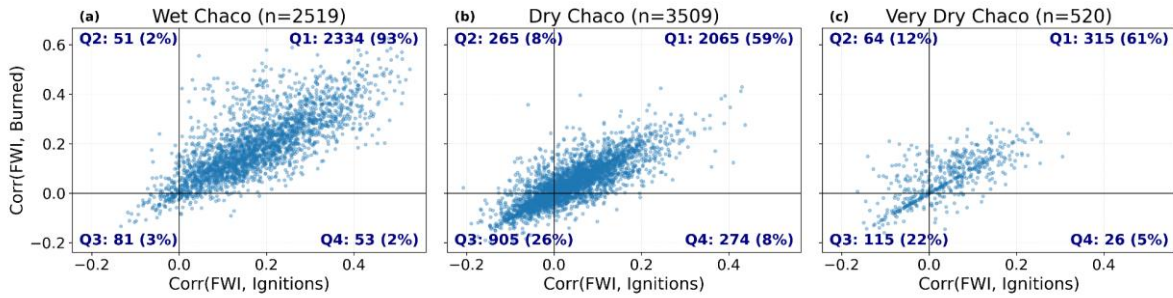


Fig. 8. Each panel shows a scatterplot of per-pixel Pearson correlation coefficients between the Fire Weather Index (FWI) and two fire activity metrics—ignition frequency (x-axis) and burned area (y-axis)—over the period 2001–2022. The panels correspond to the Wet, Dry, and Very Dry Chaco subregions, and each dot represents a $0.1^\circ \times 0.1^\circ$ grid cell. Quadrants are defined by the sign of each correlation coefficient to classify spatial patterns of fire–weather association: Q1 (top-right) includes pixels with positive correlations for both ignitions and burned area; Q3 (bottom-left) includes negative correlations for both; Q2 and Q4 represent divergent cases. For each subregion, quadrant counts, percentages, and summary statistics (mean \pm standard deviation of each correlation axis and Pearson r between them) are annotated.

Finally, the temporal co-evolution of annual BA and FWI anomalies is illustrated in the appendix (Figs. S9–S10). Several years, especially in the Wet Chaco, show strong spatial correspondence between extensive fire activity and positive FWI anomalies (e.g. 2012, 2020–2022). However, other years (e.g. 2003) reveal extensive BA without matching FWI extremes, underscoring that weather is not the sole driver of interannual variability.

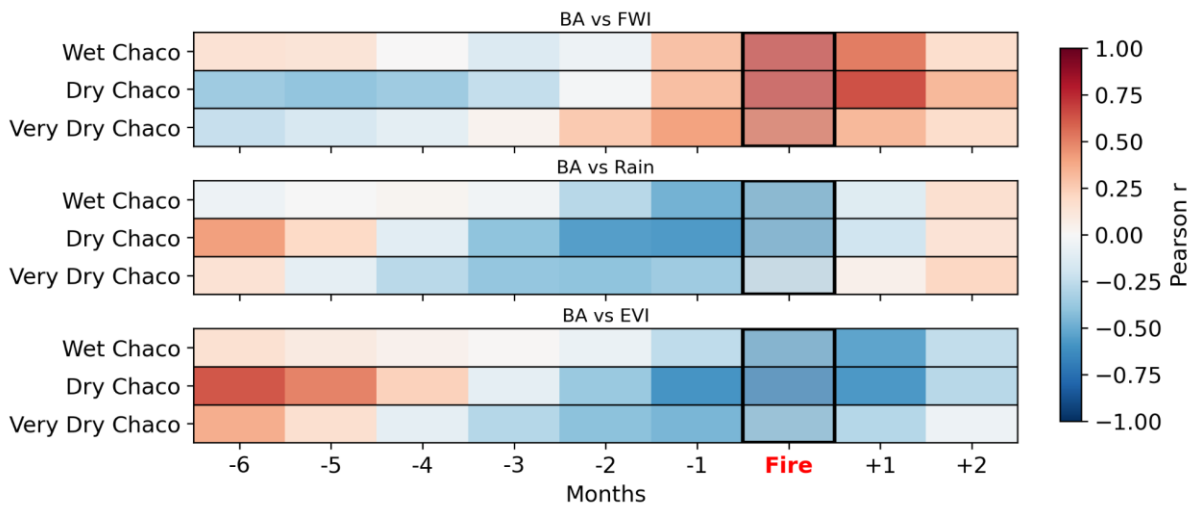
3.4 Temporal dynamics of fire–environment interactions

To explore how conditions evolve before and after fire events, we analyzed both regional time series and lagged correlations between BA anomalies and three key drivers: FWI, rainfall, and vegetation greenness (EVI), over the period 2001–2022.

The time series analysis (Fig. S10) reveals a coherent pattern in all subregions. Typically, positive rainfall anomalies (which automatically decrease FWI) are followed by increased EVI, indicating vegetation growth and fuel accumulation. When this is then followed by elevated FWI values (due to negative rain and humidity anomalies, extreme heat and/or strong winds), peaks in BA are frequently observed. This pattern supports the interpretation of a fire-favoring sequence: moisture enables biomass build-up, which is later dried and made flammable under high fire-weather conditions, culminating in fire activity. This cycle is particularly evident in major fire years such as 2020 and 2022, especially in the Wet Chaco, where the alignment between environmental anomalies and BA peaks is striking. In the Dry and Very Dry Chaco, the sequence is also well defined, although slightly more variable probably due to limited fuel accumulation.

The influence of large-scale climate variability, particularly the El Niño–Southern Oscillation (ENSO), is also reflected in the fire–environment dynamics. During La Niña phases (negative ENSO), we observe reduced rainfall and elevated FWI values, often coinciding with increased BA. Conversely, El Niño

678 episodes (positive ENSO) are associated with wetter conditions, lower fire-weather pressure, and
 679 reduced fire activity (**Fig. S10** and **Fig. S11**).
 680



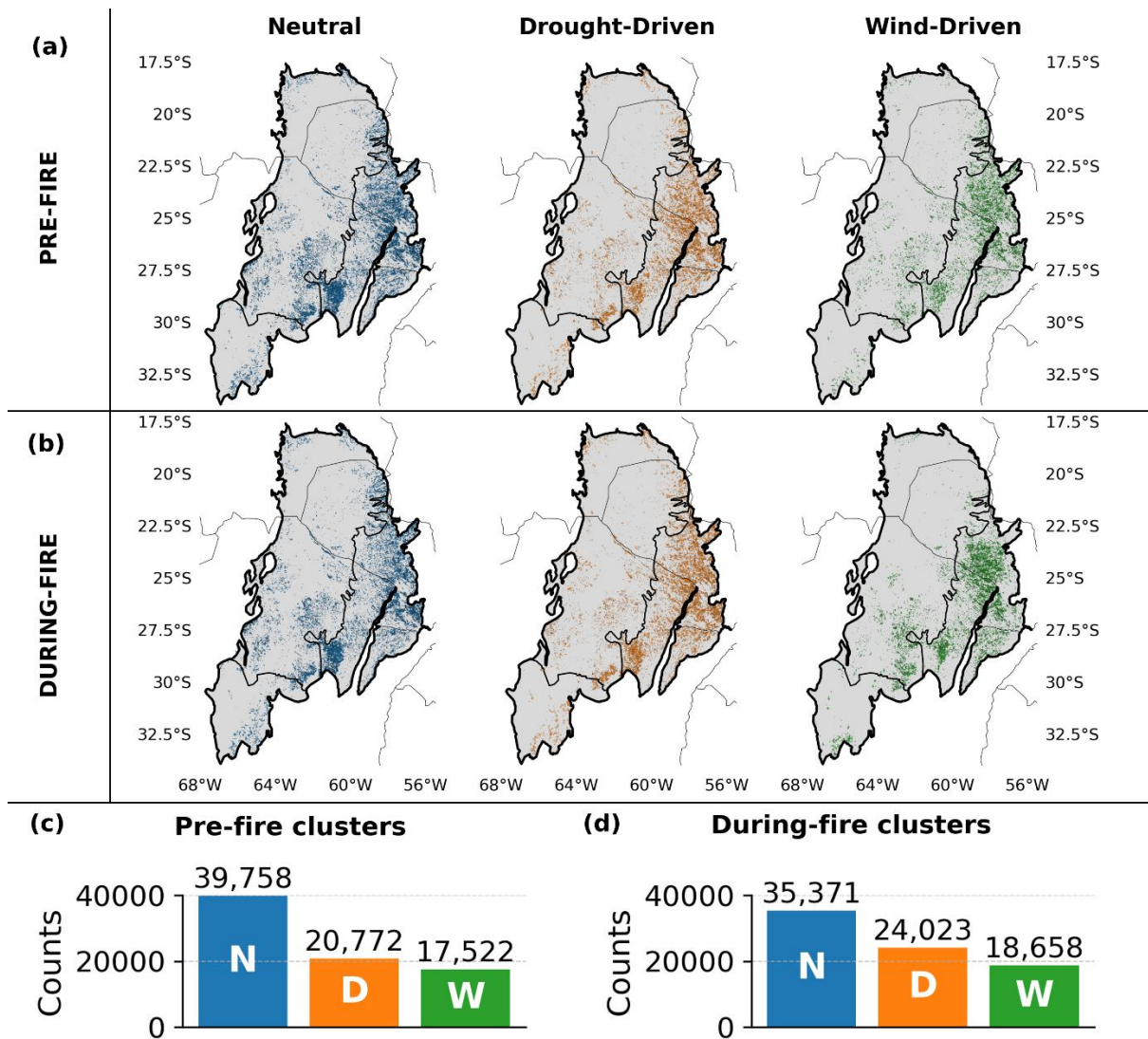
681
 682 **Fig. 9.** Lagged correlations between monthly anomalies of FWI, rainfall, and EVI with burned area in the Chaco. Each heatmap shows the
 683 Pearson correlation coefficient between the anomaly of a given variable (FWI, rainfall, or EVI) at different time lags and the burned area
 684 anomaly, for each Chaco subregion. Negative lags indicate the variable leads burned area; positive lags indicate it follows. Correlations are
 685 computed from pixel-based, region-averaged monthly time series for 2001–2022.

686
 687 **Fig. 9** shows lagged Pearson correlations between monthly anomalies of BA and FWI, rainfall, and EVI
 688 for the three Chaco subregions. Positive correlations between BA and FWI at lags 0 to +1 months,
 689 indicate that peak fire activity coincides with high fire-weather conditions. Rainfall and EVI display
 690 negative correlations with BA at short negative lags (–1 to –3 months), consistent with dry, senescent
 691 vegetation promoting flammability. At longer negative lags (–5 to –6 months), especially in the Dry and
 692 Very Dry Chaco, both variables correlate positively with BA, suggesting that wetter, greener periods
 693 months earlier promote fuel build-up. In the Wet Chaco, lag correlations are weaker and less structured,
 694 likely due to consistently moist conditions that buffer fire–environment coupling.

695
 696
 697
 698
 699
 700
 701
 702
 703

704 **3.5 Fire-weather types**

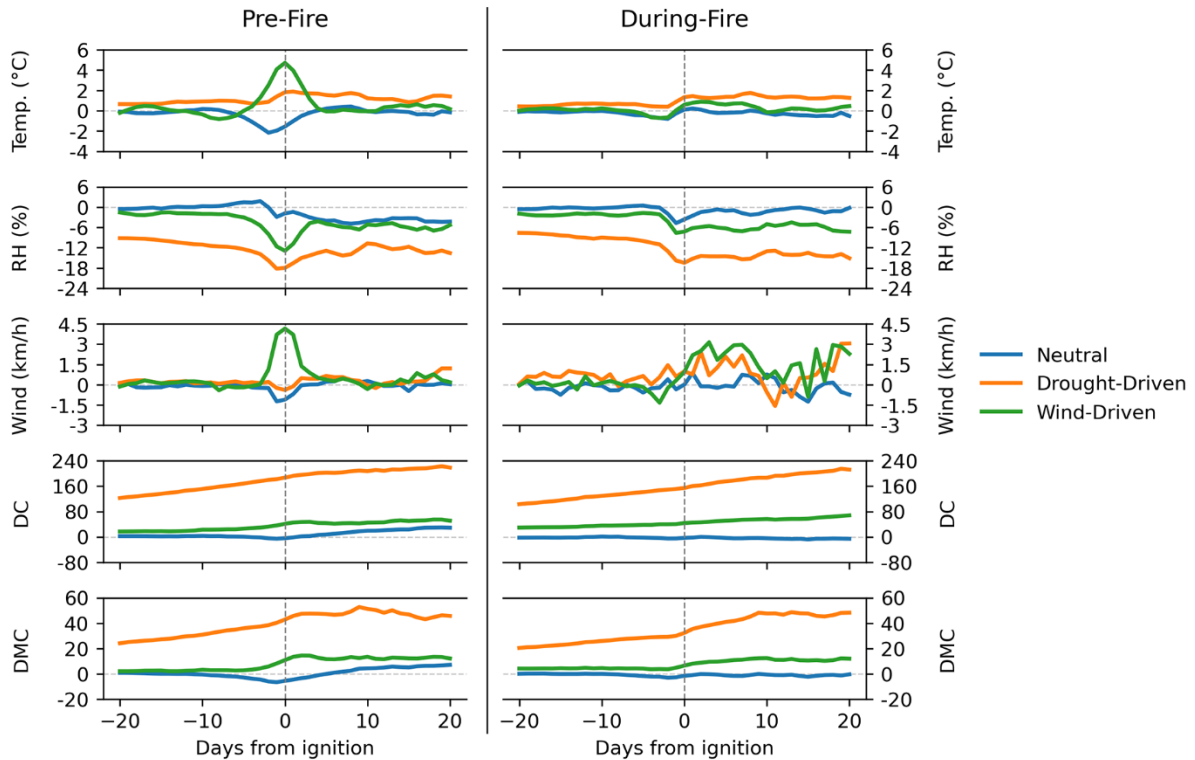
705 To characterize the atmospheric conditions associated with fire occurrence and fire growth, we analyzed
 706 the Fire-Weather Types (FWTs) assigned to each fire patch during the days preceding ignition (*Pre-
 707 Fire* clusters) and during the active burning period (*During-Fire* clusters). **Figure 10** presents the spatial
 708 distribution and frequency of the three FWT categories (Neutral, Drought Driven and Wind Driven) for
 709 both clustering types.
 710



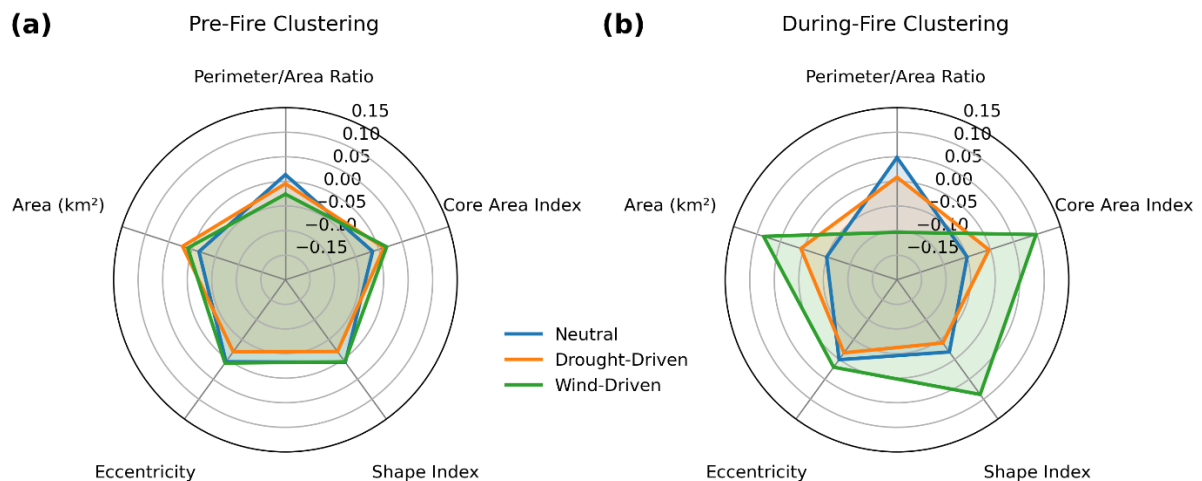
711 **Fig. 10.** Spatial distribution and frequency of pre- and during-fire meteorological clusters across the Gran Chaco (2001–2022). Panels (a) and
 712 (b) show the geographic location of fire patches classified into three Fire-Weather Types (FWTs)—Neutral (blue), Drought-Driven (orange),
 713 and Wind-Driven (green)—for the pre-fire and during-fire periods, respectively, overlaid on Chaco sub-region boundaries. Some patches
 714 overlap through the years and may partially or totally cover each other. Panels (c) and (d) display the total number of patches assigned to each
 715 FWT for pre-fire and during-fire clustering methods, respectively.
 716
 717

718 Neutral FWTs dominate both clustering groups, but their share decreases from 50.9 % to 45.3 % overall,
 719 while Drought-Driven rises from 26.6 % to 30.8 % and Wind-Driven from 22.4 % to 23.9 % (**Fig. 10c–
 720 d and Fig. S12**). This indicates that when fires are clustered according to the meteorology during the

721 fire rather than before ignition, a larger fraction falls into drought or wind related conditions and fewer
 722 remain neutral. In the Wet Chaco, Neutral FWTs drop from 49 % to 42 % with a marked increase in
 723 Drought-Driven; in the Dry Chaco, both non-neutral types grow moderately; in the Very Dry Chaco,
 724 Wind-Driven types increase sharply (from 15 % to 26 %), especially in the south where complex
 725 topography may strongly influence fire–atmosphere dynamics (see *Section 2.1*). These regional shifts
 726 suggest that dryness is particularly important in the Wet Chaco, while stronger winds become
 727 comparatively more relevant in the southern Very Dry Chaco.
 728



729
 730 **Fig. 11.** Mean daily anomalies of temperature (Temp.), relative humidity (RH), 10-meter wind speed, Drought Code (DC), and Duff Moisture
 731 Code (DMC) from 20 days before to 20 days after fire ignition, averaged over fire patches assigned to the Neutral, Drought-Driven, and Wind-
 732 Driven clusters for Pre-Fire (left) and During-Fire (right) clustering approaches.
 733



734

735 **Fig. 12.** Clusters mean morphology profiles for (a) Pre-Fire and (b) During-Fire clustering. Each axis represents a standardized morphology
736 variable (z-score), and each colored polygon shows the mean profile for one cluster. The radial extent indicates the relative value of each
737 variable within the dataset.

739 **Fig. 11** shows mean daily anomalies from 20 days before to 20 days after ignition for each FWT for
740 both clustering types. In the *Pre-Fire* FWT, we see that the Wind-Driven fires present a sharp rise in
741 wind speed and temperature in the days around ignition, coupled with a drop in RH, creating highly
742 flammable conditions. Drought-Driven fires exhibit a long build-up of dryness before ignition, with
743 persistently high DC and DMC values and low RH, indicating extended fuel curing. Neutral fires occur
744 under conditions close to climatology, with only small fluctuations in all variables.

745 The time series of the *During-Fire* FWTs show that the dry conditions characteristic of the Drought-
746 Driven cluster begin to develop before ignition and remain well differentiated during the fire, with very
747 low RH and high DC and DMC values. Wind speed anomalies are also elevated in this cluster, although
748 not as sharply as in the Wind-Driven cluster. This indicates that dryness and wind can co-occur in
749 Drought-Driven fires, whereas Wind-Driven fires are characterized by a clear and sustained peak in
750 wind speed combined with dry conditions, but without the prolonged build-up of drought observed in
751 the Drought-Driven cluster. The Neutral cluster remains close to climatology throughout, with only a
752 slight decrease in RH immediately prior to ignition, suggesting a minimum dryness threshold for fire
753 initiation across clusters.

754 When comparing FP morphology across clusters, *Pre-Fire* FWTs appear broadly similar (**Fig. 12, S13–**
755 **S14**), with comparable FP area, shape index (deviation from compactness), core-area index (interior
756 cohesion), eccentricity (elongation), and perimeter-to-area ratio (boundary complexity). In contrast,
757 *During-Fire* FWTs show clear differences: Wind-Driven fires tend to be larger, more elongated (higher
758 eccentricity), and more cohesive (higher core-area index and lower perimeter-to-area ratio) than
759 Drought-Driven fires, consistent with a directional spread under strong and sustained winds.

760 The combination of high eccentricity and low perimeter-to-area ratio reflects elongated but relatively
761 smooth fire perimeters produced by the rapid advancement of the fire under strong winds. In contrast,
762 Drought-Driven fires tend to generate more irregular boundaries for a given size, consistent with a
763 stronger dependence on the spatial distribution of cured fuels, which causes the fire to advance unevenly
764 across fuel patches and results in more complex and less smooth perimeter shapes.

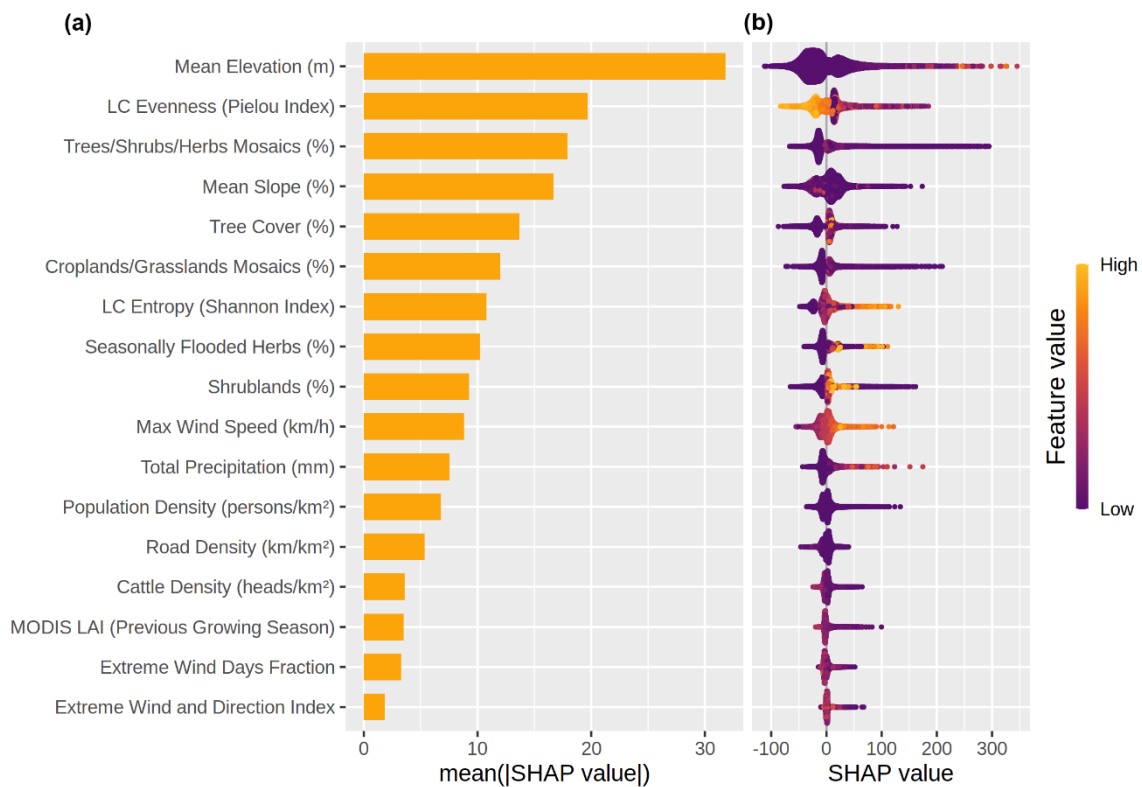
765 Overall, *Pre-Fire* FWTs capture the atmospheric conditions leading to ignition, whereas *During-Fire*
766 FWTs better reflect the conditions that shape the eventual size and geometry of the fire. These results
767 show that both clustering types capture different aspects of fire–weather interactions, but that the
768 *During-Fire* FWTs provides clearer separation in terms of final fire size and morphology.

769

770 **3.6 Fire size drivers**

771 Our RF analysis identified static topographic and vegetation structure variables as the dominant
 772 predictors of final fire size in the Gran Chaco (**Fig. 13a**). *Mean elevation* showed the highest mean
 773 SHAP value (17.4%), followed by *LC evenness* (10.8%), *tree/shrub/herbs mosaics* (9.79%) and *mean*
 774 *slope* (9.1%). These four variables consistently occupied the top positions across the global model and
 775 all twelve specific models (**Fig. 14**). LC fractions within the FPs, including cropland or flooded
 776 herbaceous cover, made moderate contributions, whereas meteorological and social variables such as
 777 maximum wind speed, precipitation, population density or cattle density ranked markedly lower in
 778 importance. **Fig. 14** demonstrates that this hierarchy is almost unchanged across regional, seasonal and
 779 fire-weather subsets, underscoring that the dominance of topography and vegetation structure is not an
 780 artefact of spatial domain or sample composition.

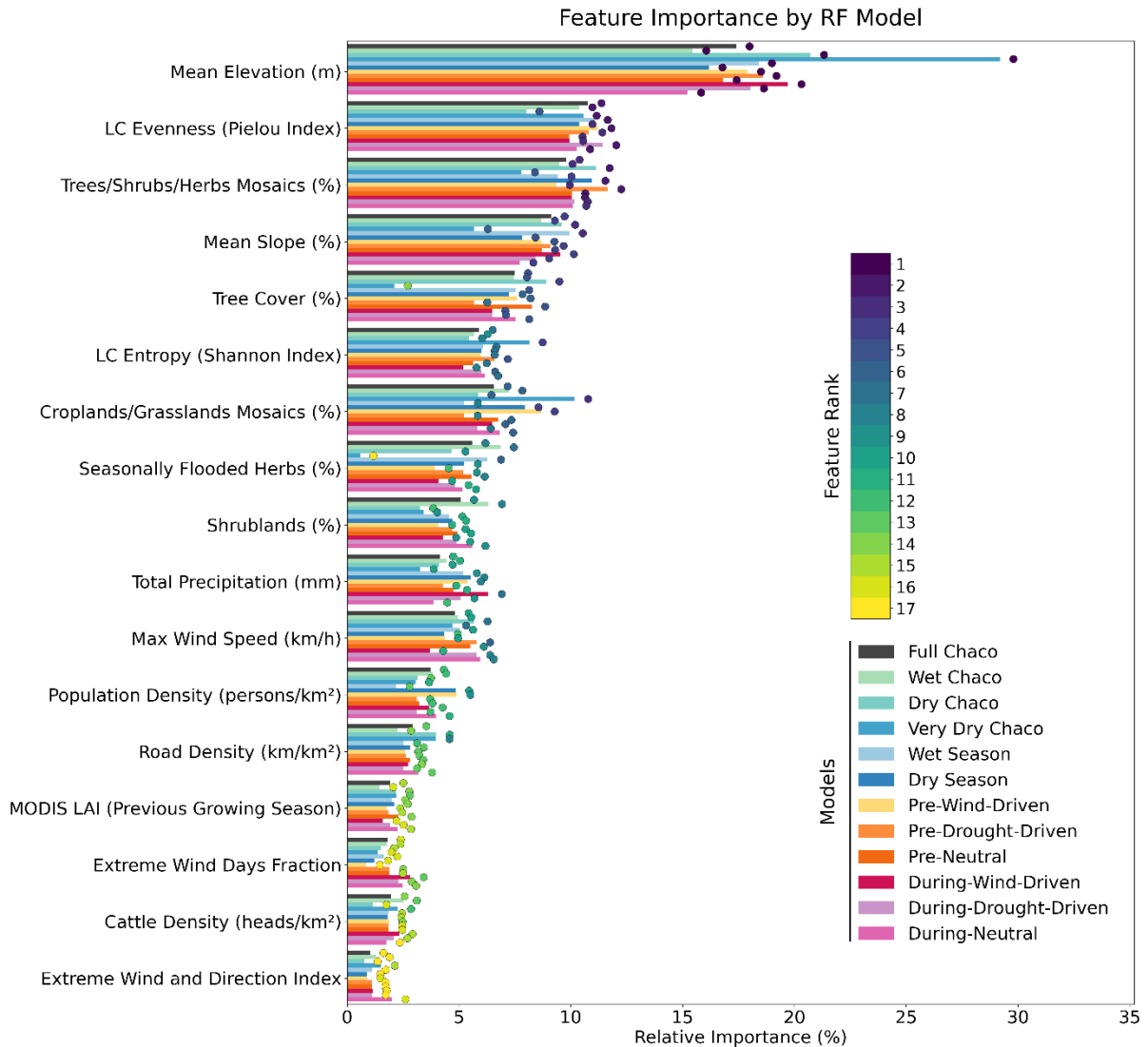
781



782 **Fig. 13.** Feature importance ranking for the Random Forest model predicting fire patch (FP) size across the entire Gran Chaco. (a) shows the
 783 average importance of each variable, expressed as the mean absolute SHAP value, which reflects how strongly each feature contributes to
 784 model predictions on average. (b) shows the SHAP values for all individual fire patches, indicating how low (purple) or high (yellow) feature
 785 values influence the prediction toward smaller or larger fires. SHAP values are used here to quantify feature importance consistently across
 786 the dataset.

787
 788
 789 Model performance was satisfactory, with the global RF achieving a correlation of 0.74 on the test set
 790 and a test RMSE of ~110 burned pixels, compared with 0.96 and ~54 pixels on the training set (**S14**).
 791 These values indicate limited overfitting and show that the model captures a substantial fraction of the
 792 variance in fire size despite the inherent noise and strong skewness of the response variable. Because

793 the target variable is the number of burned FRY pixels within each FP, RMSE values are interpreted
 794 directly in pixel units; with the 250 m FireCCI51 resolution, 110 pixels correspond to approximately 6.9
 795 km², less than 7 % of the 1–100 km² size range analyzed here. Comparable performance was obtained
 796 across all regional, seasonal and fire-weather configurations (**Table S3**).
 797



798
 799 **Fig. 14.** SHAP feature importance ranks across all trained Random Forest models used to predict fire patch size (n_{cell}) based on 17 explanatory
 800 variables. Colored dots at the end of bars shows the rank of a variable's importance (1 = most important, 17 = least important) for a given
 801 model.

802
 803 Predictor distributions were strongly skewed for many variables (e.g., LC fractions, anthropogenic
 804 densities), with high proportions of zeros and long upper tails, whereas elevation and slope varied mostly
 805 within narrow low-lying ranges with few high-elevation observations (**Table S2; Fig. S15**). These
 806 empirical distributions are critical for interpreting SHAP behavior in **Fig. 13** and **15**, as they define the
 807 domains within which the RF partitions landscape conditions.

808 The global SHAP distribution (**Fig. 13b**) shows that elevation exerts a consistently positive influence
809 on predicted fire size across most of its range, with the PDP in **Fig. 15** revealing a steep rise in SHAP
810 values between 0 and ~40–60 m, followed by a broad plateau. Large fires dominate this low to mid
811 elevation interval, while higher elevations generally host smaller events. This pattern indicates that
812 elevation is acting not as a physical driver but as a proxy for geomorphological and ecological gradients
813 that determine fuel structure and continuity. In the lowlands of the Chaco, shallow depressions, seasonal
814 marshes (“bañados”), and permanent wetlands (“esteros”) develop over silty clay soils with poor
815 infiltration and minimal slope, accumulating abundant herbaceous biomass that cures during dry periods
816 and supports extensive fire spread (Bravo et al., 2025). Slightly elevated terraces and woody islets
817 (“montes”, “albardones”) act instead as natural barriers. Because the RF does not encode these fine
818 spatial transitions explicitly, elevation functions as an integrative descriptor of landscape contexts
819 conducive to large fires. Regional PDPs (**Figs. S17–S19**) confirm and refine this interpretation. In the
820 Wet Chaco, SHAP values rise sharply from 0 to ~20–40 m and stabilize above that threshold, while in
821 the Dry Chaco the increase is concentrated in the 0–20 m band and flattens near 50–100 m, reflecting
822 transitions from floodplain matrices to agricultural or post-deforestation mosaics. In contrast, the Very
823 Dry Chaco exhibits a nearly linear positive gradient up to ~700 m, with large fires clearly associated
824 with higher elevation.

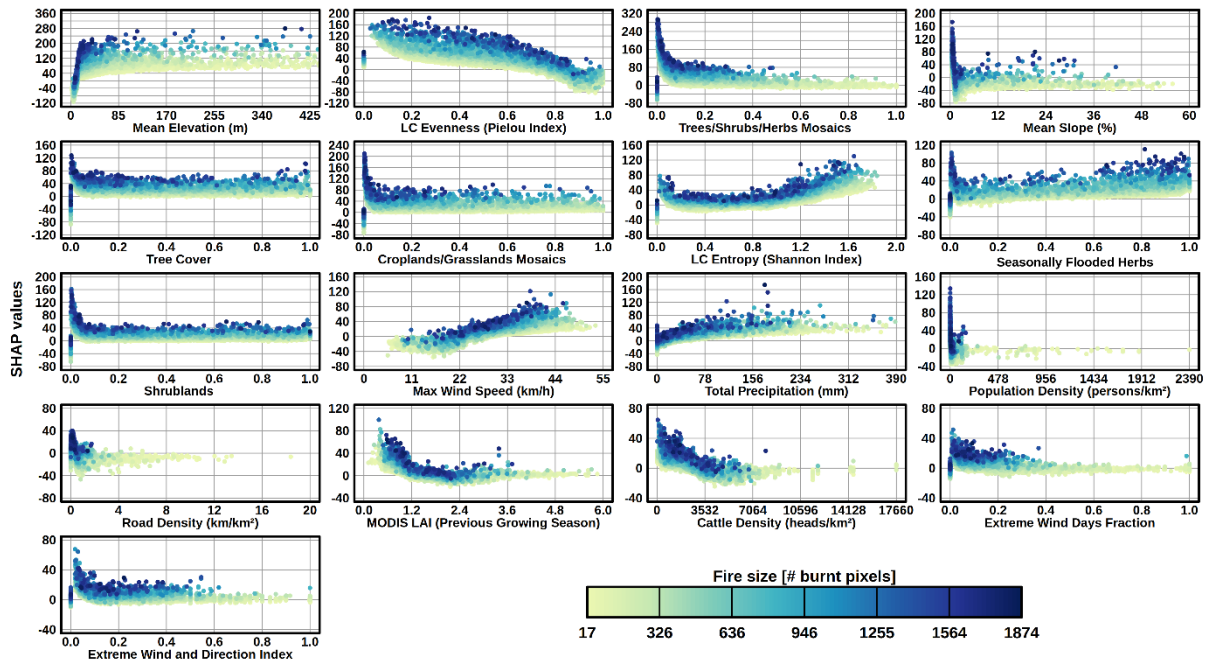
825 Mean slope refines this topographic signal. Although its global importance is slightly lower than
826 elevation, its SHAP dependence curve (**Fig. 15**) mirrors the elevation-driven distinction between flat
827 floodplain fuels and more fragmented uplands. SHAP values decline sharply between 0 and ~2–3 %
828 slopes, where the largest fires are concentrated, and then stabilize. Regional PDPs show the same
829 structure in the Wet and Dry Chaco, with large fires almost entirely confined to slopes below ~2–3 %,
830 whereas steeper terrain hosts only small fires. The Very Dry Chaco departs from this pattern, showing
831 a monotonic negative gradient with a small cluster of large fires at intermediate slopes (~20–30 %),
832 likely corresponding to large fire events in sierran landscapes. Together, elevation and slope provide
833 complementary, non-redundant information: elevation captures broad physiographic and hydrological
834 gradients that determine where continuous fuels develop, while slope distinguishes the flat or gently
835 inclined surfaces that permit lateral spread from rugged terrains that constrain it. Their combined
836 behavior explains why topography consistently emerges as the strongest predictor of fire size across all
837 RF configurations.

838 LC evenness and LC entropy display opposite but complementary patterns because they describe
839 different dimensions of landscape heterogeneity. Evenness decreases when one or two land-cover
840 classes dominate the patch, creating long continuous fuel runs that favor sustained spread, whereas
841 entropy increases with the number and diversity of cover types, even when their proportions are uneven.
842 Both indices are zero when only one class is present, creating a structural bias toward low values for
843 homogeneous patches typically associated with small or moderate fires. In the global SHAP summary
844 (**Figs. 13b and 15**), many of the largest fires occur where a dominant class (low evenness) coexists with

845 several secondary LC types (intermediate entropy), coherent with the idea of a continuous flammable
846 matrix with patches of secondary fuels, providing both continuity and diversity of burnable material.
847 The regional PDPs (Figs. S17–S19) confirm and refine these relationships. Evenness shows a
848 consistently negative SHAP gradient across the Wet, Dry and Very Dry Chaco, with the transition to
849 negative contributions near 0.6 in all regions, although small and large fires occur across the full range,
850 indicating modulation rather than strict control. Entropy exhibits a more complex U-shaped structure
851 regionally, with SHAP values decreasing up to ~0.2 and rising toward intermediate entropies, where
852 large fires concentrate, before declining again at high entropy values, where only small fires are
853 observed. These regional patterns reinforce the global interpretation: large fires are most likely to occur
854 in landscapes characterized by a dominant continuous fuel bed enriched by a limited variety of
855 secondary flammable types, whereas highly homogeneous or highly fragmented patches constrain fire
856 growth.

857 LC fractions modulate fire size through their control on fuel characteristics, continuity and structural
858 barriers, and their SHAP dependence patterns (Figs. 13b, 15, S17–S19) are consistent with the
859 heterogeneity indices described above. The tree–shrub–herb mosaic class shows a strong and monotonic
860 negative relationship with fire size across the entire Gran Chaco and in all three regions: high fractional
861 cover of mosaics systematically shifts SHAP values toward smaller fires, whereas the largest fires
862 appear at lower fractions of the mosaic class. Because mosaics are represented as a single categorical
863 class in CCI-MRLC, patches dominated by mosaics behave as homogeneous units in the evenness and
864 entropy indices because they count as a single LC class. Tree cover displays a broadly similar
865 negative trend in the global model and in the Wet Chaco, reflecting their role of barriers to lateral
866 propagation under a certain threshold of fire intensity. Regional PDPs refine this picture: in the Very
867 Dry Chaco the decline in SHAP values is nearly linear across the tree-cover gradient, whereas in the
868 Dry Chaco a secondary rise in SHAP values at high fractional tree cover suggests the presence of large
869 fires in recently deforested or thinly wooded areas still mapped as forest, where cured understory fuels
870 or active land-clearing may cause or enhance the fire spread.

871



872
 873 **Fig. 15.** SHAP dependence plots for the 17 explanatory variables used to predict fire patch size (n_{cell}) with the Random Forest model trained
 874 on fire patches between 1 km² and 100 km² in the entire Gran Chaco between 2001 and 2022. Each panel shows the SHAP value (y-axis) across
 875 the range between 0 and the 0.995 quantile of a given feature (x-axis), illustrating the marginal effect of that feature on the model's output.
 876 Dots are colored by fire size (number of burned pixels), with darker tones indicating larger fires. Land cover classes represented as fractions.

877
 878 Shrublands exhibit more heterogeneous behavior, underscoring their different ecological roles across
 879 the precipitation–aridity gradient. In the global model and in the Wet Chaco, shrub fractions show a
 880 steep negative exponential decay, with the largest fires concentrated at low shrub cover and exclusively
 881 small fires at high shrub dominance, consistent with shrublands forming natural barriers within
 882 floodplain matrices. The Dry Chaco shows the opposite pattern: SHAP values increase with shrub cover,
 883 indicating that flammable shrublands, which are common on higher, drier terraces, can support large
 884 fires when fuels are continuous and well cured. The Very Dry Chaco exhibits a distinct, strongly non-
 885 linear shape, with SHAP values stable at low and intermediate shrub fractions but increasing sharply
 886 around ~0.8-0.9, before declining at the extreme upper tail; this reflects the concentration of the largest
 887 fires in extensive shrub-dominated matrices typical of the western Chaco drylands.
 888 Flooded herbaceous vegetation shows a mixed response globally: SHAP values initially decrease
 889 between 0 and ~0.1 but become increasingly positive toward higher fractions, indicating that fires
 890 occurring in seasonally desiccated wetlands often reach large sizes. Regional PDPs confirm that this
 891 effect is strongest in the Wet Chaco, where dark points cluster at high flooded-herbaceous fractions, and
 892 absent in the Very Dry Chaco, where large fires occur only where flooded cover is ~0.
 893 Cropland/grassland mosaics mirror the global shrubland pattern, with a clear negative exponential
 894 relationship in all regions: large fires almost exclusively occur at low fractions, whereas patches
 895 dominated by these mosaics generate small fires. This behavior reflects both their intrinsically
 896 discontinuous fuel structure and the fact that agricultural and improved-pasture landscapes are heavily

897 subdivided by field boundaries, roads, and irrigation infrastructure that limit lateral spread. In addition,
898 active fire suppression, systematic fuel removal, and prescribed burning practices in productive cropland
899 and grazing areas further reduce the likelihood that fires in these mosaics evolve into large, contiguous
900 events.

901 The influence of pre-fire biomass accumulation, represented by previous-season LAI, is modest in
902 global importance but shows consistent region-specific patterns that reflect its role as a broad proxy for
903 vegetation productivity (**Fig. 15; Figs. S17–S19**). At the scale of the entire Gran Chaco, SHAP values
904 decrease strongly from low to moderate LAI, with the largest fires concentrated at LAI < 1–1.5,
905 consistent with highly open herbaceous or sparsely wooded systems where fine, continuous fuels
906 dominate. Higher LAI values correspond to increasingly negative SHAP contributions across all
907 regions, indicating vegetation types with greater structural complexity or woody dominance that
908 constrain lateral spread. Regional PDPs refine this interpretation: in the Wet Chaco, increases in LAI
909 coincide with vegetation types that tend to reduce spread regardless of their biomass; in the Very Dry
910 Chaco, the compressed LAI range reflects lower overall productivity (0-4 vs 0-6 in the other regions),
911 and large fires remain associated with the lowest values; in the Dry Chaco, a weak secondary rise in
912 SHAP values at intermediate LAI, forming a U-shape curve, likely reflects biomass accumulation in
913 flammable shrubland systems where moderate productivity enhances fuel availability. Overall, LAI
914 emerges not as a universal driver of fire size but as a vegetation-structure proxy whose meaning shifts
915 along the Gran Chaco's precipitation–aridity gradient.

916 Meteorological predictors show consistent but secondary influences relative to topography and
917 vegetation structure (**Figs. 13b, 15, S17–S19**). Maximum wind speed exhibits the clearest signal: SHAP
918 values increase steadily with maximum wind speed up to roughly 40–45 km/h, beyond which they form
919 a plateau. In all regions, large fires cluster toward the upper half of the wind-speed distribution, with a
920 shallow positive slope that reflects the well-known effect of stronger winds enhancing the forward
921 spread of fire fronts. In the FWT-specific RF models, this effect becomes more prominent in Drought-
922 Driven configurations, where maximum wind speed attains higher SHAP-based importance ranks and
923 larger absolute SHAP amplitudes than in Neutral or Wind-Driven FWTs (**Fig. 14**). This pattern indicates
924 that strong winds have greater leverage on fire size when fuels are already cured and moisture is low,
925 while under more benign or mixed weather conditions their influence remains positive but more muted.
926 The similarity of the response among the Wet, Dry and Very Dry Chaco indicates that this relationship
927 is robust across contrasting fuel types and landscape configurations.

928 In contrast, the two extreme-wind metrics (extreme wind days fraction and extreme wind-and-direction
929 index) display weak negative or near-flat SHAP responses. SHAP values decline from slightly positive
930 to near-zero between fractions of 0 and ~0.2, after which only small fires occur in all regions. The Very
931 Dry Chaco shows a shallow positive segment at very low fractions but converges toward the same
932 pattern. These tendencies likely arise because the extreme-wind variables summarize the frequency of
933 extreme conditions rather than the instantaneous wind state during fire growth, and because extreme-

934 wind events are typically rare and dispersed, producing SHAP structures dominated by the large mass
935 of low-fraction observations. Their behavior therefore does not contradict the positive effect of
936 maximum wind speed but instead reflects the different statistical role of occurrence-based indices in the
937 RF model.

938 Total precipitation shows uniformly weak contributions across regions. Although the global SHAP
939 curve appears moderately positive at low to intermediate precipitation totals, large fires are clearly
940 concentrated at low rainfall values in all regional PDPs, and small fires dominate wetter intervals. The
941 apparent positive SHAP slope between 0 and ~150 mm results from the construction of the variable
942 itself: precipitation represents the fire-duration-integrated rainfall, which is confounded with event
943 duration. Larger, longer-lasting fires have more opportunity to accumulate rainfall even if spread
944 occurred primarily under dry conditions. This duration bias explains why some large fires appear at
945 relatively high precipitation totals despite the overall negative association between wet conditions and
946 fire growth. Thus, precipitation contributes only marginally to the RF predictions once static fuel and
947 topographic structure are accounted for.

948 Human-pressure variables (road density, population density, cattle density) have consistently low mean
949 SHAP importance across all RF models (**Fig. 13a**), indicating that they explain only a minor portion of
950 the variance in fire size once topography and vegetation structure are accounted for. Nevertheless, their
951 marginal SHAP responses (**Figs. 15, S17–S19**) reveal systematic gradients that are interpretable in a
952 fire-management context.

953 Cattle density shows the clearest pattern: SHAP values decline almost monotonically with increasing
954 cattle density, and the largest fires are concentrated at low to moderate densities. At high densities,
955 SHAP values are strongly negative and large fires are absent. This trend is constant across all regions.
956 The most plausible interpretation is indirect: highly stocked ranching systems typically involve intensive
957 fuel management, pasture renewal, and active fire control, reducing the likelihood that ignitions develop
958 into large, contiguous fire patches. However, this mechanism cannot be tested directly with the available
959 data and should be regarded as a behavioral correlation rather than a causal inference.

960 Road density and population density exhibit parallel patterns. SHAP values are positive at low densities
961 and become increasingly negative as infrastructure or settlement density increases. Large fires occur
962 almost exclusively where road and population density are low, whereas high-density areas are dominated
963 by small fires. These gradients hold in each region, though they are most pronounced in the Wet and
964 Dry Chaco and slightly attenuated in the Very Dry Chaco, where human populations and infrastructure
965 are sparser overall. The interpretation is consistent with broad-scale patterns of fire management: remote
966 areas with limited access generally allow fires to grow larger, whereas areas with more roads, people,
967 and managed landscapes tend to suppress or fragment fires earlier.

968 Despite these coherent marginal trends, the overall contribution of human-pressure variables remains
969 secondary. Their effects are largely overshadowed by static topographic structure and LC composition,
970 and their marginal signals do not alter the dominance hierarchy observed in **Fig. 14**. Taken together,

971 these results indicate that anthropogenic influences on fire size operate mainly through long-term land-
972 use changes embedded within topographic and vegetation-structure variables, rather than through direct
973 effects captured by density proxies alone.

974

975 **3.7 Sensitivity experiments**

976 To assess the robustness of the models and the sources of explanatory power, we performed two targeted
977 sensitivity experiments: (i) training a RF without topographic variables, and (ii) replacing the baseline
978 road density product for another with more road detections.

979 In the No-Topography experiment, the most important observation is that the overall ordering of non-
980 topographic predictors remained stable (**Fig. S20**): vegetation-structure metrics (LC evenness, mosaic
981 cover, tree cover, LC entropy) continued to dominate, while human-pressure and weather variables
982 remained secondary. Despite this stability in feature hierarchy, removing topography resulted in a
983 marked decline in predictive performance (test COR decreasing from ~0.74 to ~0.67; test RMSE
984 increasing from ~110 to ~119 pixels; **Table S3**). SHAP rankings also became less coherent, with several
985 land-cover variables inflating artefactually in importance to compensate for the absence of structural
986 information. These changes confirm that elevation and slope do not act as direct physical drivers but
987 capture slow-varying ecological gradients that distinguish floodplain herbaceous systems from slightly
988 elevated woody landscapes, which strongly condition the potential for large fire growth.

989 Before evaluating the effect of substituting OSM with MS road density in the RF models, we quantified
990 how the two datasets differ across the landscape. OSM, being community-curated, captures paved and
991 unpaved major roads reliably but tends to underrepresent informal, secondary, and seasonal tracks,
992 particularly in remote ranching landscapes and sparsely populated areas of the western Dry and Very
993 Dry Chaco. In our dataset, OSM identified 1.12 million km of linear features, whereas MS mapped 1.95
994 million km, an increase of roughly 74 % in total detected road length. By contrast, the MS product,
995 generated through automated detection from high-resolution imagery, identifies a much larger set of
996 linear features: about 45–60 % of MS segments have no corresponding OSM segment within 50 m, and
997 a large fraction consist of faint, narrow dirt tracks, fencing lines, internal ranch access paths, and grid-
998 aligned extraction routes. These additional features increase the apparent density of minor routes in areas
999 where OSM shows little or no coverage. As a consequence, MS tends to expand the low-to-moderate
1000 density classes (0.1–2 km km⁻²) by 30–50 % in frequency, while suppressing the long extreme tail of
1001 OSM, generating a smoother and more homogeneous density surface.

1002 These differences are not spatially uniform. In the Wet Chaco, where agriculture, fragmentation, and
1003 population density are higher, the two datasets converge strongly, with Pearson correlations of 0.85–
1004 0.90, mean absolute differences of 0.12–0.18 km km⁻², and only modest discrepancies in the upper tail.
1005 In the Dry Chaco, the correlation drops to 0.80–0.83, as MS detects 40–65 % more low-density tracks
1006 than OSM, especially in cattle-ranching corridors and logging frontiers. The Very Dry Chaco shows the

1007 largest divergence, with correlations of 0.65–0.72: MS maps a more continuous network of faint tracks
1008 and straight-line property boundaries, whereas OSM retains extensive areas of near-zero density but
1009 captures some mountainous trail systems that MS misses. Consequently, MS compresses the density
1010 distribution (IQR: 0.05–0.45 km km⁻²) and produces a quasi-normal shape, while OSM remains highly
1011 skewed with a dominant zero-density mode and occasional extreme values exceeding 5 km km⁻².
1012 Nonetheless, median density values remain comparable (OSM: 0.21 km km⁻²; MS: 0.27 km km⁻²), and
1013 both datasets reproduce the broad east–west gradient in accessibility.

1014 Because road density interacts strongly with landscape structure, we also compared differences across
1015 LC contexts and heterogeneity indices. OSM-based density is highest in mosaic-dominated landscapes
1016 and cropland–grassland transitions, where road networks are well established and frequently used,
1017 reaching median values of 0.8–1.2 km km⁻². MS broadens this association by detecting a widespread
1018 network of faint tracks within shrublands and semi-open dry forests, raising densities in those classes
1019 by 0.1–0.3 km km⁻² and reducing the contrast between mosaic-rich areas and large, relatively
1020 homogeneous herbaceous or woody expanses. When cross-referenced with LC evenness and Shannon
1021 entropy, OSM systematically highlights high-density pockets in highly heterogeneous areas ($E > 0.7$, H
1022 > 1.2), while MS produces weaker gradients and spreads low-to-moderate values more widely across
1023 structural classes. These differences suggest that OSM reinforces the tight connectivity between road
1024 density and heterogeneity in mixed landscapes, whereas MS dilutes it by mapping a more pervasive set
1025 of minor linear features.

1026 Despite these large structural differences, substituting OSM with MS in the RF models produced
1027 negligible changes in predictive performance and no change in feature rankings. Test COR remained at
1028 0.74 for both datasets and test RMSE shifted only marginally from 110.4 to 111.2 pixels (**Table S3**).
1029 Road density retained a similarly low mean absolute SHAP value (2–3 % of total importance), and the
1030 SHAP dependence curves were nearly identical, showing positive contributions at very low densities
1031 (< 0.3 km km⁻²) and increasingly negative contributions as accessibility increases. This indicates that the
1032 additional detail captured by MS—particularly the dense network of faint tracks in remote dry areas—
1033 does not provide additional explanatory power.

1034 Taken together, these findings support the same conclusions drawn from the original sensitivity
1035 experiment: (i) road density is strongly collinear with land-cover composition and landscape
1036 heterogeneity; (ii) patch-level aggregation of road metrics reduces the discriminating power of fine-
1037 scale differences between datasets; (iii) roads exert only a modest direct influence on final fire size at
1038 this regional scale, with most anthropogenic effects being mediated by geography, vegetation structure
1039 and long-term land-use patterns.

1040 As a result, neither OSM nor MS provides independent explanatory power beyond what is already
1041 captured by topography and LC, and the RF hierarchy of predictors remains stable across both
1042 configurations.

1043 **4 DISCUSSION**

1044 Building on event-level fire patches (FPs), we examine how meteorology, landscape structure, and
1045 human pressures shape fire size and morphology across the Wet, Dry, and Very Dry Chaco.

1046 **4.1 Fire regime and extreme events**

1047 FP data reveal a strongly skewed size distribution: many small fires (<5 km²) and a few very large events
1048 that dominate burned area (BA), consistent with global patterns (Archibald et al., 2009; Hantson et al.,
1049 2015, 2017; García et al., 2022; Haas et al., 2022). Megafires (>100 km²) are most frequent in the Wet
1050 Chaco, where continuous herbaceous fuels in savannas and seasonally flooded vegetation support
1051 spread. Gigafires (>1000 km²), although rare, occur predominantly in the Dry Chaco and are often
1052 concentrated in remote areas where suppression access may be limited, and where seasonally cured fuels
1053 and low humidity can favor sustained spread.

1054 In the Gran Chaco, most ignitions are human-caused and fire use remains widespread across rural
1055 activities (Bravo et al., 2010, 2025), so the spatial and temporal distribution of fire occurrence largely
1056 reflects anthropogenic pressure. However, once a fire is ignited, its final size depends more strongly on
1057 fuel continuity, landscape structure and fire-weather conditions than on ignition source. Human
1058 pressures and their proxies are discussed in *Section 4.5*.

1059 Feron et al. (2024) show that the Gran Chaco region in South America has experienced an increase in
1060 the frequency of warm, dry and flammable days, together with a rise in compound warm-dry anomalies
1061 over recent decades. Although these diagnostics do not quantify fire behavior, they indicate a
1062 background shift toward more frequent atmospheric conditions conducive to high flammability. In our
1063 record, 2019–2022 coincides with strongly positive FWI anomalies and multiple large fire years,
1064 particularly in the Wet Chaco. Despite the overall decline in BA between 2001 and the mid-2010s, the
1065 clustering of extreme years at the end of the time series is consistent with increasing exposure to periods
1066 of elevated fire weather under recurrent drought and large-scale climate variability (e.g. intensified La
1067 Niña conditions), while noting that the satellite era remains short for robust trend detection.

1068 Extreme fire periods, such as the 2019–2022 season, illustrate this sensitivity. In our record, a handful
1069 of very large fires contributed a substantial share of total BA across the three subregions. This pattern
1070 aligns with reconstructions of twentieth-century fire activity showing that the Gran Chaco woodlands
1071 experience relatively frequent but generally low-to-moderate severity fires, with large fire seasons
1072 emerging when fuel accumulation coincides with prolonged dry periods (Bravo et al., 2021, 2025; San
1073 Martín et al., 2023; Vidal-Riveros et al., 2023). During 2019–2022, multi-year drought affected large
1074 parts of the La Plata basin, including the Gran Chaco, reducing river discharge, soil moisture and
1075 wetland extent (Naumann et al., 2023). Consistent with this hydroclimatic context, we observe
1076 widespread positive BA anomalies and high FWI, particularly during 2020–2021 and especially in the
1077 Wet Chaco, where rivers and floodplains typically constrain lateral spread.

1078 Additionally, as discussed in the Introduction, the COVID-19 pandemic altered mobility, enforcement
1079 and on-the-ground fire management across South America, with contrasted effects on fire activity
1080 depending on whether restrictions reduced ignitions or weakened surveillance and suppression (Garcia
1081 et al., 2021; Eklund et al., 2022; Kumar et al., 2022; Naval Fernández et al., 2023). In the Gran Chaco,
1082 mobility declined during peak fire months, yet suppression capacity remained relatively stable due to
1083 the continued availability of volunteer brigades, while agrarian expansion and land-clearing dynamics,
1084 including deforestation burns and infrastructure projects, continued during lockdown (Castilla, 2021;
1085 Naval Fernández et al., 2023; Schmidt and Castilla, 2023). Together, these observations indicate that
1086 the persistence of extreme fire seasons during 2020–2022 cannot be explained solely by pandemic-
1087 related changes in human activity, and that concurrent drought and elevated fire weather likely played
1088 a central role in enabling large fire spread.

1089 We therefore examined how short-term fire weather relates to BA across subregions and found strong
1090 spatial contrasts consistent with a fuel-limited to moisture-limited continuum across the Gran Chaco. In
1091 the Wet Chaco, high FWI is consistently associated with large BA, confirming moisture limitation and
1092 strong sensitivity to atmospheric conditions, in line with earlier BA-based analyses (San Martín et al.,
1093 2023) and with varying-constraint frameworks across resource gradients (Krawchuk and Moritz, 2011).
1094 In the Dry and Very Dry Chaco, correlations are weaker and more heterogeneous, indicating partial
1095 decoupling between short-term fire weather and final size, with FWI effects mediated by antecedent fuel
1096 conditions and landscape continuity, consistent with evidence that wildfire activity peaks at intermediate
1097 rainfall and productivity levels in semiarid Chaco landscapes, where fuel loads are sufficient but
1098 seasonal curing remains pronounced (Bravo et al., 2010; Argañaraz et al., 2015; San Martín et al., 2023).
1099 Lagged relationships reinforce this contrast: in drier areas, positive rainfall and vegetation productivity
1100 4–6 months before fire are followed by higher BA once fuels cure, supporting the fire–productivity
1101 hypothesis (Pausas and Bradstock, 2007) and matching wet-to-dry sequences linked to widespread burns
1102 in western and central Chaco forests (Bravo et al., 2010; Argañaraz et al., 2015; San Martín et al., 2023),
1103 whereas in wetter areas short dry spells immediately prior to fire are more predictive of activity because
1104 fuels are rarely limiting (Krawchuk and Moritz, 2011).

1105

1106 **4.2 Fire-weather types across the Chaco region**

1107 To assess how daily fire weather influences fire size, we built on the framework of Hernandez et al.
1108 (2015) and Ruffault et al. (2016, 2020), who classified Mediterranean wildfires into Fire-Weather Types
1109 (FWTs) based on pre-fire meteorological anomalies (heat, drought, wind) and found that Hot-Drought
1110 and Wind-Driven types were strongly linked to large events. Applying a similar pre-fire clustering in
1111 the Gran Chaco (Neutral, Drought-Driven, Wind-Driven) captured ignition contexts but explained little
1112 variation in final size or shape. This limited explanatory power is consistent with flat, fuel-rich systems

1113 where pre-fire anomalies modulate the probability of fire occurrence but do not reliably predict how far
1114 fires will spread once ignited.

1115 In contrast, clustering based on during-fire variables (maximum wind speed, total precipitation, drought
1116 indices, and the Extreme Wind Directionality Index developed in this study) clearly separated groups
1117 with significant differences in size and morphology. Dry, windy days during the fire, favored rapid and
1118 large expansion.

1119 Our findings contrast with Ruffault et al. (2016, 2020) and Belhadj-Kheder et al. (2020), who found pre-
1120 fire or near-ignition anomalies predictive in Mediterranean and North African settings, respectively,
1121 with the latter highlighting anomaly duration in low-suppression contexts. The stronger size–weather
1122 link for during-fire meteorology that we found likely reflects Chaco-specific traits such as a relatively
1123 flat terrain, continuous fuels, and permissive fire conditions (Bucher, 1982; Vidal-Riveros et al., 2023),
1124 which make wind and humidity more decisive than pre-fire anomalies. In the Mediterranean, fragmented
1125 fuels, complex topography, and strong suppression (Ruffault and Mouillot, 2015, 2017), translate into
1126 ignition-day extremes mattering more. A similar modulation by suppression capacity occurs in western
1127 U.S. forests (Higuera et al., 2015).

1128 In semiarid mountain landscapes of the Very Dry Chaco, Argañaraz et al. (2015) showed that climatic
1129 gradients and productivity govern where fires tend to occur, while topography and land-use mosaics
1130 constrain their spatial extent. Although their study addressed fire frequency rather than fire size, the
1131 distinction reinforces that the drivers of fire occurrence and the drivers of fire spread are related but not
1132 identical, and that landscape context mediates how daily fire weather translates into final fire extent.

1133 Our clustering extends fire-weather typologies to a tropical dry forest context and complements recent
1134 Gran Chaco regime classifications (Vidal-Riveros et al., 2024; Naval-Fernández et al., 2025) that
1135 omitted meteorological variables, highlighting the key role of fire-active weather in shaping fire
1136 morphology.

1137 These fire-weather patterns operate within a landscape where ignitions are predominantly
1138 anthropogenic, meaning that, aside from the few lightning-ignited events, human activities largely
1139 determine when and where fires start. The eventual size of these events, however, depends more strongly
1140 on daily meteorological conditions and fuel continuity, in a context where fire suppression capacity is
1141 uneven and often limited in remote areas. This contrasts with Mediterranean systems, where highly
1142 effective suppression can dampen the influence of during-fire weather on final fire size.

1143

1144 **4.3 Topography and landscape structure as primary controls of fire size**

1145 Random Forest (RF) models identified topographic, land cover (LC) and landscape-structure variables
1146 as the dominant predictors of final fire size in the Gran Chaco, with mean elevation, LC evenness, the
1147 tree–shrub–herb mosaic LC class and mean slope consistently ranking at the top of the SHAP-based
1148 hierarchy across all regional, seasonal and fire-weather configurations. The ordering remained stable in

1149 sensitivity experiments, and model performance declined when elevation and slope were removed (**Fig.**
1150 **S20, Table S3**), confirming that topography acts as an integrative proxy for geomorphological,
1151 hydrological and ecological gradients that shape the spatial context in which fires propagate. A
1152 mechanistic interpretation of vegetation effects in terms of fuel continuity and fuel moisture is developed
1153 in *Section 4.4*; here we focus on how elevation and slope structure the physical template of fire growth
1154 and why they dominate RF-based fire size prediction.

1155 Elevation captures the major physiographic contrasts that structure fuel continuity across the Gran
1156 Chaco. In the Wet Chaco, extensive low-lying floodplains and seasonal wetlands generally limit fire
1157 spread but can become highly flammable during the dry season, especially following multi-year
1158 droughts when herbaceous biomass cures over broad, continuous surfaces. The marked increase in
1159 SHAP values below approximately 20–40 m reflects these drought-prone floodplain and marsh systems,
1160 where cured grasses form highly connected fuel beds that facilitate large fire growth. In contrast, slightly
1161 elevated terraces and woody islets (“montes” or “albardones”) interrupt fuel continuity and act as natural
1162 barriers that constrain lateral fire propagation. Spatial patterns in representative Wet Chaco landscapes
1163 (**Figs. S21–S22**) support this interpretation, with large fire patches consistently associated with drought-
1164 exposed, low-elevation herbaceous systems.

1165 In the Dry Chaco, elevation contrasts distinguish floodplain matrices from agricultural mosaics and post-
1166 deforestation surfaces that break continuity. Here, the largest fires tend to occur on flat to gently elevated
1167 terrain where broad, relatively homogeneous landscape units maintain sufficiently connected fine fuels
1168 to support lateral fire growth. These tendencies align with landscape-level analyses in semi-arid central
1169 Argentina, where shrub-dominated fuel beds and topographically channeled winds promote the
1170 expansion of fire fronts (Fischer et al., 2012). In deforested landscapes, the spatial configuration of fuels
1171 is strongly shaped by clearing patterns rather than by geomorphological gradients. As a result, BA within
1172 highly fragmented agricultural or recently cleared regions (**Fig. S23**) often exhibit weaker visual
1173 correspondence with elevation contrasts, since fuel continuity arises from land-use structure rather than
1174 from topographic controls.

1175 In the Very Dry Chaco, rising elevation leads into sierran landscapes where open shrublands and xeric
1176 woodlands dominate. We found a near-linear positive association between fires and elevation up to
1177 several hundred meters, consistent with the concentration of large fires in shrub-dominated belts with
1178 continuous cured fuels along the mountains. Local examples from the Sierras de Córdoba (**Fig. S23**)
1179 demonstrate how topographic position aligns with vegetation structure. Similar relationships between
1180 physiographic position, shrub cover and extensive fire spread have been documented in other semi-arid
1181 regions of central Argentina (Fischer et al., 2012), underscoring that topography often serves as an
1182 effective proxy for the spatial organization of continuous fuels.

1183 Slope provides complementary information to elevation. The largest fires overwhelmingly occur on
1184 surfaces with slopes below approximately 2–3 %, where lateral propagation is mostly unrestricted and
1185 drainage patterns do not fragment fuels. Steeper terrain consistently hosts smaller fires across the Wet

1186 and Dry Chaco, reflecting natural fuel discontinuities. In the Very Dry Chaco, most large fires also occur
1187 at low slopes, although some events exploit elongated ridge–valley structures at intermediate slopes,
1188 particularly in the sierran environments (Fig. S23). The combined behavior of elevation and slope
1189 explains why removing both variables in the sensitivity experiment substantially reduced model skill
1190 (Fig. S20).

1191 Overall, these results indicate that topography structures the physical template within which fire growth
1192 unfolds, summarizing geomorphological and hydrological contrasts that influence where large, spatially
1193 connected burning conditions can develop. Although ignitions and land management are predominantly
1194 human-driven in the Gran Chaco, event-scale human-pressure proxies add limited incremental
1195 explanatory power once topography and landscape structure are accounted for; implications for fire use
1196 and land-use driven fuel restructuring are developed in *Section 4.5*.

1197 **4.4 Vegetation structure, fuel continuity and fuel moisture**

1198 Vegetation structure exerts a central influence on fire behavior in the Gran Chaco by shaping fuel
1199 continuity and the potential for lateral spread. Across the precipitation gradient, the largest fires occur
1200 in herbaceous and shrub-dominated systems where fine fuels can become continuous and seasonally
1201 flammable, whereas woody vegetation and heterogeneous mosaics constrain propagation (San Martín
1202 et al., 2023). These patterns align with long-standing ecological characterizations of Chaco fire regimes,
1203 in which open woodlands, grass–shrub mixtures and seasonally flooded herbaceous vegetation burn
1204 more extensively and more frequently than denser forest formations (Bravo et al., 2010, 2025; Naval-
1205 Fernández et al., 2025; San Martín et al., 2023; Vidal-Riveros et al., 2023). As discussed in *Section 4.3*,
1206 these vegetation effects operate within a topographic template, but they control fire growth primarily
1207 through the composition and spatial continuity of burnable fuels.

1208 A key mechanism emerging from our results is the role of fuel continuity rather than fuel abundance per
1209 se. Herbaceous floodplain systems in the Wet Chaco and shrub-dominated systems in the Dry and Very
1210 Dry Chaco can provide highly connected fuel matrices during drought years, while woody islets, post-
1211 deforestation mosaics, cropland–grassland interfaces and other managed landscapes introduce sharp
1212 discontinuities that restrict spread. This mechanism is directly reflected in the strong importance of land
1213 cover evenness: low evenness (dominance by a single flammable class) is associated with large fires,
1214 whereas high evenness or high entropy corresponds to smaller events due to fragmentation. Similarly,
1215 the tree–shrub–herb mosaic class shows a strong negative influence, consistent with mixed woody
1216 patches acting as barriers and breaking connectivity.

1217 These structure effects are also coherent with broader evidence that increasing tree cover often reduces
1218 burned area by limiting fine-fuel continuity and increasing shade and moisture retention (Bistinas et al.,
1219 2014; Haas et al., 2022). However, exceptions are well documented where particular forest types can be
1220 more flammable than native broadleaf formations, including introduced pine plantations in some regions
1221 (Barros and Pereira, 2014; Paritsis et al., 2018; Vidal-Riveros et al., 2023). In the Chaco context, this

1222 underscores that “woody cover” is not a single fire-behavior category: the relevant control is how
1223 vegetation structure translates into horizontal continuity of ignitable fuels and seasonal drying.

1224 A second dimension is fuel moisture seasonality, which varies markedly among growth forms.
1225 Experimental and remote-sensing work in the Southern Gran Chaco indicates that shrubs and grasses
1226 reach low live fuel moisture thresholds earlier in the dry season and maintain these conditions longer
1227 than tree species (Bianchi et al., 2014; Argañaraz et al., 2016, 2018). Differences in live fuel moisture
1228 among growth forms provide a mechanistic basis for the contrasting role of shrublands along the
1229 gradient, with shrub patches often limiting spread in wetter floodplain landscapes but promoting larger
1230 fires in drier regions where shrub matrices cure rapidly and sustain combustion over large areas. This is
1231 consistent with the broader finding that shrubs and grasses can reach lower moisture contents during the
1232 dry season than tree species (Yebra et al., 2019). Flooded herbaceous vegetation likewise can function
1233 either as a barrier or as a flammable matrix depending on hydrological conditions, becoming a major
1234 driver of large burns when multi-year droughts desiccate wetlands.

1235 Productivity effects on fire behavior also emerge at broader temporal scales. We showed that vegetation
1236 greenness anomalies (EVI) respond tightly to antecedent rainfall and covary with FWI during the fire
1237 season, highlighting a classic fuel–productivity pathway: wet periods promote biomass accumulation,
1238 followed by curing during dry spells that increases flammability. This mechanism is widely documented
1239 in semi-arid Chaco systems (Bravo et al., 2010; Argañaraz et al., 2015; San Martín et al., 2023). In
1240 contrast, previous-season LAI, used here as a coarse proxy for accumulated biomass, played a
1241 comparatively minor role. LAI integrates total canopy foliage, including woody components, and
1242 therefore does not isolate the herbaceous and shrub layers most critical for fire spread. This likely
1243 explains its weak association with fire size in our models and reinforces the importance of considering
1244 fuel type and structure, rather than total leaf area, when interpreting vegetation controls on fire behavior
1245 in the Chaco.

1246 Taken together, these results show that vegetation structure mediates fire size in the Gran Chaco through
1247 three complementary mechanisms: (i) the fuel type and its degree of continuity across the landscape,
1248 which determines how far fires can propagate; (ii) the seasonal and interannual dynamics of fuel
1249 moisture, which vary among plant growth forms and strongly influence the timing and intensity of
1250 burning; and (iii) the productivity–curing sequence that links antecedent rainfall, herbaceous biomass
1251 accumulation and subsequent desiccation. These mechanisms operate differently along the
1252 precipitation–aridity gradient, producing distinct spatial fire regimes but a consistent overall pattern:
1253 large fires emerge primarily in continuous, fine-fuel systems that undergo strong seasonal drying, while
1254 fragmented or woody-dominated landscapes constrain spread regardless of weather conditions.

1255

1256 **4.5 Human pressures and fire use in the Gran Chaco**

1257 Fire regimes worldwide are tightly linked to human activity: most ignitions are anthropogenic, and both
1258 land-use change and active suppression have reshaped BA patterns in many regions (Bowman et al.,
1259 2009, 2011; Archibald et al., 2013; Andela and van der Werf, 2014; Andela et al., 2017). The Gran
1260 Chaco fits within this global picture. It is a human-dominated dry forest and savanna system where fire
1261 is at once a natural ecological process and a widespread management tool, particularly in rangelands
1262 and agricultural frontiers (Bucher, 1982; Kunst and Bravo, 2003; Bravo et al., 2010, 2025).

1263 Within the Gran Chaco, fire use is deeply embedded in pastoral and agricultural practices. Historical
1264 and ethnographic accounts document the use of fire by indigenous and rural communities in the Chaco
1265 and neighboring ecoregions for hunting, communication, warfare and the management of plant resources
1266 (Arenas, 2003; Junk and Nunes da Cunha, 2012; Sugiyama et al., 2025). As in other tropical dry regions,
1267 most events are human-ignited and intentional, associated with land clearing, slash-and-burn
1268 deforestation or the disposal of residues, with a smaller fraction being accidental or natural (Baumann
1269 et al., 2018; De Marzo et al., 2023; Gasparri and Baldi, 2013; Gürtler, 2009). Modern land users
1270 routinely burn grasslands and savannas at the end of the dry season to stimulate grass regrowth and
1271 improve forage quality, often under informal or weakly regulated conditions (Kunst and Bravo, 2003;
1272 Kunst et al., 2016; Coronel et al., 2021; San Martín et al., 2023; Bravo et al., 2025). Many fires start in
1273 managed or unmanaged grasslands, savannas or croplands and subsequently spread into neighboring
1274 forests and shrublands (Bravo et al., 2010; Tálamo et al., 2013; Loto and Bravo, 2020; Giorgis et al.,
1275 2021; De Marzo et al., 2022). In this context, exotic grasses have been shown to enhance fuel continuity
1276 and fire intensity in several dryland systems (D'Antonio and Vitousek, 1992; Kunst et al., 2016; Bravo
1277 et al., 2025), but their spatial extent and dominance within the Gran Chaco remain heterogeneous and
1278 poorly constrained at regional scales. They should therefore be regarded as one of several possible
1279 mechanisms influencing fuel structure, rather than as a pervasive or dominant driver of large fires.

1280 A further anthropogenic dimension concerns deforestation fires and the diverse forms of land-clearing
1281 burns that accompany agricultural expansion. In the Gran Chaco, the agricultural frontier has advanced
1282 rapidly over the past decades, and fire is routinely used to remove woody debris and prepare newly
1283 cleared fields, often as part of slash-and-burn cycles (Baumann et al., 2018, 2022; Boletta et al., 2006;
1284 De Marzo et al., 2023; Gasparri and Baldi, 2013; Gürtler, 2009). These fires can be extensive, but their
1285 spatial footprint depends strongly on how clearing interacts with fuel continuity, woody debris loads
1286 and local weather (San Martín et al., 2023).

1287 A similar challenge applies to prescribed and semi-prescribed burns, which are widespread in rangeland
1288 management but rarely conducted under formal prescriptions or systematic monitoring frameworks
1289 (Bravo et al., 2025; Coria et al., 2021, p.202; Kunst et al., 2016; Kunst and Bravo, 2003). Many burns
1290 are intended to be low-intensity pasture treatments undertaken in late winter or early spring, yet under
1291 drought or wind anomalies they may escape control and evolve into landscape-scale events, as

1292 documented in multiple regions of the Chaco. Although global inventories of prescribed fire exist (Hsu
1293 et al., 2025), they do not cover the Gran Chaco, underscoring the need for regional efforts to differentiate
1294 intentional, escaped and accidental fires. The lack of this information helps explain why our human-
1295 pressure variables account for little variance in final fire size: the signal of fire use is embedded within
1296 vegetation structure, fuel loads and land-cover mosaics, rather than through independent demographic
1297 metrics or ignition proxies that lack temporal and operational detail.

1298 In this context, our finding that human-pressure variables play a secondary role in predicting final fire
1299 size does not imply that humans are unimportant for the fire regime, but rather that their influence is
1300 mediated primarily through long-term land-use change and fuel restructuring. FRY v2.0 and related
1301 satellite products cannot distinguish between wildfires, escaped prescribed burns, deforestation fires or
1302 routine pasture burns, and thus the anthropogenic component enters the analysis mainly through its
1303 imprint on vegetation structure, land-cover mosaics and fuel continuity. As discussed in *Sections 4.1*
1304 and *4.4*, the extreme fire seasons of 2019–2022 occurred during a prolonged La Niña episode that
1305 produced exceptional drought across the La Plata basin (Naumann et al., 2023; San Martín, 2024; Bravo
1306 et al., 2025). Despite changes in mobility and surveillance during the COVID-19 pandemic, large fires
1307 remained concentrated in fuel-rich, drought-stressed landscapes, indicating that climatic anomalies and
1308 fuel structure set the upper bound for fire size, while humans primarily determine ignition timing and
1309 location.

1310 Livestock production offers a clear example of how human pressures modulate fire regimes indirectly.
1311 Grazing can interrupt the positive feedback between grasses and fire by reducing fine fuels, altering
1312 vegetation composition and promoting woody encroachment (Adámoli et al., 1990; Cingolani et al.,
1313 2013; Coria et al., 2021; Bravo et al., 2025). A global analysis showed that higher livestock densities in
1314 tropical rangelands are associated with lower fire frequency and increased shrub and dwarf tree cover
1315 (Bernardi et al., 2019), and regional syntheses for the Gran Chaco report that grazing interferes with
1316 fire–grass feedbacks and contributes to shrub expansion (Alessio et al., 2008; Alinari et al., 2015; Vidal-
1317 Riveros et al., 2023). The SHAP gradients we obtained for cattle density mirror these findings: large
1318 fires are concentrated at low to moderate densities, while high-density ranching landscapes are
1319 dominated by small events, consistent with a scenario where heavy grazing reduces continuous fine
1320 fuels and increases woody cover, thereby limiting maximum fire size even if fire weather remains
1321 conducive.

1322 Road density and accessibility show a similar, albeit more complex, relationship. Numerous studies
1323 indicate that road expansion can both increase ignitions and fragment landscapes, thereby reducing the
1324 maximum size of individual fires (Andela and van der Werf, 2014; Bowring et al., 2024). In our analysis,
1325 both OpenStreetMap and Microsoft road detections density exhibited the same marginal pattern: large
1326 fires occur predominantly in areas with low road density, whereas regions with high road density are
1327 dominated by small fires. The sensitivity experiment substituting OSM with Microsoft roads confirmed
1328 that this pattern is robust and that differences in road datasets have negligible impact on predictive

1329 performance when medium to high resolution topography and LC mapping are included. The low overall
1330 importance of road density likely reflects two structural issues. First, road networks are strongly
1331 collinear with geography, LC composition and landscape heterogeneity, so much of their influence on
1332 fragmentation and suppression potential is already encoded by those variables. Second, averaging road
1333 density at the FP scale erases the spatial configuration of roads relative to ignition points and spread
1334 pathways, which is critical for understanding how roads constrain or redirect fire fronts.
1335 Population density exhibits a comparable gradient, with sparse human presence associated with larger
1336 fires and densely populated areas dominated by smaller events, consistent with more active suppression,
1337 earlier detection and greater fuel management in productive landscapes. However, remotely sensed data
1338 and coarse demographic layers cannot capture the full social dimension of fire, including local
1339 perceptions, traditional burning practices and informal suppression. Recent reviews emphasize that the
1340 perspectives and knowledge of local communities are rarely incorporated into peer-reviewed fire
1341 research in the Gran Chaco, despite being widely discussed in grey literature and the media (McDaniel
1342 et al., 2005; Devisscher et al., 2016, 2019; Coronel et al., 2021; Vidal-Riveros et al., 2023). San Martín
1343 et al. (2023) and Bravo et al. (2025) explicitly call for interdisciplinary approaches that combine
1344 environmental and social sciences to better understand human–fire interactions in this region.
1345 Overall, our results suggest that anthropogenic influences on fire size in the Gran Chaco operate mainly
1346 through their cumulative effects on vegetation structure, fuel continuity and landscape fragmentation,
1347 rather than through direct, independently measurable controls at the event scale. Ignitions are
1348 overwhelmingly human-driven, but the final size of fires is governed by the interaction between this
1349 ignition pressure, long-term land-use trajectories and the windows of opportunity created by drought
1350 and fire-conducive weather. Future work that integrates spatially explicit ignition records, fine-scale fuel
1351 management data, and socio-cultural information on fire use would allow a more complete
1352 quantification of the human contribution to fire size distributions in this rapidly changing dry forest
1353 biome. One good example of the potential of such interactions is presented in Hernández et al. (2022),
1354 who show that climate-related risks in rural Chaco communities can only be understood through
1355 frameworks that combine environmental diagnostics with local practices, knowledge systems and power
1356 relations. Their coproduction process demonstrates that the way people perceive, monitor and respond
1357 to climatic hazards fundamentally shapes exposure and outcomes. A comparable socio-environmental
1358 approach applied to fire research could reveal how decisions about land clearing, burning, suppression
1359 and access interact with drought and fuel conditions to determine whether an ignition remains small or
1360 develops into a large fire.

1361

1362 **4.6 Limitations and perspectives**

1363 Several limitations of this study stem from the nature of the available datasets and from methodological
1364 constraints. First, the meteorological information used to characterize fire weather, which relies on

1365 ERA5-Land at 0.1° resolution and cannot resolve local wind acceleration, channeled flows, shading, or
1366 fine-scale thermal gradients that influence fire spread in heterogeneous terrains. Although maximum
1367 wind speed and directional persistence emerged as meaningful predictors, the coarse resolution likely
1368 under-represents sub-kilometer variability in fire-atmosphere coupling, particularly in sierran
1369 environments. In addition, ERA5-Land precipitation is not bias-corrected, and its known tendency to
1370 smooth short-lived convective events at sub-daily scales may influence variables derived from it, such
1371 as total precipitation during the fire, potentially dampening the detection of sharp wetting or drying
1372 transitions within the time window of fire growth. Advances in downscaling techniques for wind
1373 (Dujardin and Lehning, 2022), solar radiation (Druel et al., 2025), and temperature (Kusch and Davy,
1374 2022) may improve the spatial realism of these variables in future fire regime analyses, especially in
1375 complex landscapes. However, these approaches were not applied here.

1376 Second, the FRY v2.0 dataset inherits all structural uncertainties of FireCCI51, including omission of
1377 small or low-intensity burns, overestimation in heterogeneous pixels, and potential inconsistencies in
1378 early MODIS years (Lizundia-Loiola et al., 2020; Pettinari et al., 2021). The reconstruction of FPs also
1379 depends on temporal grouping parameters that merge or split neighboring pixel clusters (Oom et al.,
1380 2016; Moreno et al., 2021). These issues constrain our ability to resolve very small events, the fine-scale
1381 geometry of scars, and rapid-fire spread fronts. The development of higher-resolution BA products has
1382 been repeatedly requested by the fire science community (Mouillot et al., 2014), and regional examples,
1383 such as the FireCCISFD20 product at 20 m for Africa (Chuvieco et al., 2022), have already demonstrated
1384 large gains in BA detection. Such advances will be essential to quantify fire size distributions and fire
1385 spread processes more accurately across the Gran Chaco.

1386 Third, the satellite BA products used here do not provide information on fire type and therefore cannot
1387 distinguish among wildfires, escaped prescribed burns, deforestation fires, and routine rangeland burns.
1388 This restricts our capacity to attribute human-driven fire dynamics directly, since the anthropogenic
1389 signal enters the models primarily through long-term structural changes in vegetation composition,
1390 fragmentation and fuel continuity rather than through explicit information on ignition sources or
1391 operational decisions. The absence of spatially explicit ignition datasets, suppression records and fine-
1392 scale fuel management layers further limits our ability to separate environmental controls from
1393 management outcomes.

1394 In the absence of direct information on fire type or ignition mechanism, human-pressure variables such
1395 as road density, population density or cattle density are used as indirect proxies for socio-environmental
1396 processes. Their weak importance in the RF models should therefore not be interpreted as evidence that
1397 human influence is negligible, but rather as a reflection of the limited thematic precision, spatial
1398 resolution and temporal representativeness of the available demographic and infrastructure datasets.
1399 These proxies capture only broad accessibility and land-use patterns, and they cannot represent
1400 operational decisions, intentional fire use or suppression capacity. As a result, landscape and LC
1401 variables at the scale of our analysis absorb much of the anthropogenic signal in our models.

1402 Fourth, additional limitations arise from the interaction between the RF framework and the structure of
1403 the predictor datasets. Tree-based ensembles and SHAP-based rankings can be sensitive to differences
1404 in data quality, spatial support and collinearity among predictors. These conditions are better met by
1405 high-quality satellite-derived predictors such as elevation and annual land-cover layers than by
1406 demographic or infrastructure datasets, which are often coarser, noisier or less spatially complete. As a
1407 result, part of the dominant SHAP importance of topography and vegetation likely reflects both genuine
1408 structural controls on fuel continuity and the statistical advantages associated with these higher-quality
1409 predictors, rather than their purely mechanistic influence. The sensitivity experiment without
1410 topography confirms that elevation and slope summarize multiple unobserved gradients, partly
1411 compensating for limitations in other predictors. Although cross-validation diagnostics suggest limited
1412 overfitting, the RF remains bound to the chosen feature set and to the aggregation scale of fire patches.
1413 Future work could evaluate machine-learning architectures that operate directly on high-resolution
1414 imagery or spatial neighborhoods, for example through convolutional or graph-based neural networks
1415 combined with richer socio-economic layers, to test whether the predictor hierarchy found here is robust.
1416 Fifth, several environmental variables used in this study should be interpreted as proxies rather than
1417 mechanistic drivers. Elevation and slope summarize hydrological, geomorphological and ecological
1418 gradients rather than exerting direct effects on combustion. Similarly, the previous-season LAI
1419 integrates productivity and vegetation structure but does not explicitly represent live fuel moisture or
1420 curing dynamics. Incorporating finer-resolution fuel moisture content datasets, daily vegetation optical
1421 depth or in situ biomass measurements (Argañaraz et al., 2016, 2018) would strengthen mechanistic
1422 interpretations.

1423 Finally, our statistical models do not capture feedbacks between fire behavior and atmospheric
1424 processes, nor do they represent dynamic suppression, diurnal cycles of wind and humidity, or sub-daily
1425 fire-growth stages. Mechanistic fire-spread models and hybrid statistical–physical approaches could
1426 help resolve these processes and offer a complementary perspective.

1427 Despite these limitations, our results provide a consistent regional picture: static landscape structure,
1428 summarized by topography and vegetation composition, dominates fire-size outcomes, while
1429 meteorology governs the windows of opportunity for rapid spread. Future work that combines high-
1430 resolution BA mapping, improved fire-weather fields, ignition and management records, and socio-
1431 cultural dimensions of fire use would allow a more comprehensive understanding of the evolving fire
1432 regime of the Gran Chaco.

1433 5 CONCLUSIONS

1434 This study advances understanding of fire regimes across the Wet, Dry, and Very Dry Chaco through a
1435 spatially explicit analysis of fire events from 2001–2022. We document strong regional contrasts in fire
1436 size, seasonality and morphology, and show that these patterns arise from the combined effects of fuel
1437 structure, fire weather and long-term land use change.

1438 Fire patch (FP) sizes were highly skewed: over 80% of detected fires were <5 km², yet large events
1439 dominated total burned area (BA). Megafires (>100 km²) occurred in all subregions, with the Wet Chaco
1440 recording the most. Gigafires (>1000 km²) were rare but concentrated in the Dry Chaco, where some
1441 single events exceeded 50% of annual BA. The Wet Chaco burned most extensively ($\sim 2\times$ the Dry
1442 Chaco), with the highest fire frequency and ignition density, reflecting greater biomass productivity and
1443 continuous fuels. The Very Dry Chaco, although it contributes the smallest share of total BA, is
1444 characterized by sporadic large, mega and gigafires that produce abrupt interannual peaks, consistent
1445 with a more stochastic fire regime where a few extreme events dominate variability.

1446 The Fire Weather Index (FWI) displayed its strongest and most coherent relationship with BA and fire
1447 counts in the Wet Chaco, where most pixels (93%) showed positive correlations between monthly FWI
1448 and BA anomalies (R up to 0.7), confirming a moisture limited regime. In the Dry and Very Dry Chaco,
1449 correlations were weaker and more heterogeneous, indicating that short term fire weather alone cannot
1450 explain spatial and interannual variability in BA. The extreme fire seasons of 2019–2022 coincided with
1451 a prolonged La Niña event and widespread positive FWI anomalies, especially in the Wet, yet some
1452 years with extensive burning occurred without exceptional FWI, underscoring the additional roles of
1453 fuel continuity, antecedent conditions and ignition patterns.

1454 Lagged analyses revealed a fuel productivity mechanism in drier areas and a short-term drying control
1455 in wetter ones. In the Dry and Very Dry Chaco, positive rainfall and greenness anomalies several months
1456 before the fire season were followed by higher BA once fuels cured, consistent with a productivity–
1457 curing sequence where wet periods build biomass that later dries and burns. In wetter sectors of the
1458 Chaco, shorter dry spells immediately before the fire season were more closely associated with BA
1459 peaks, reflecting conditions where fuels are rarely limiting and fire activity responds primarily to
1460 transient moisture deficits. La Niña phases strengthened fire potential across the region through reduced
1461 rainfall and elevated fire weather, and the clustering of extreme fire years at the end of the record
1462 suggests increasing exposure to such windows of opportunity.

1463 Fire weather types (FWT) provided additional insight into how daily meteorology shapes fire outcomes.
1464 Pre-fire clustering captured ignition contexts but showed limited discrimination in final size or shape,
1465 consistent with a system where ignitions are predominantly anthropogenic and occur under broadly
1466 permissive conditions. In contrast, clustering based on during-fire meteorology separated neutral,
1467 drought-driven and wind-driven fires with clear differences in size and morphology. Wind-driven events
1468 were larger, more elongated and more cohesive than drought-driven fires, highlighting fire patch

1469 morphology as a signature of strong, persistent winds that could be used to benchmark process-based
1470 fire models and emerging machine learning approaches for fire behavior prediction.

1471 Random Forest models showed that static landscape structure dominates fire size outcomes. Mean
1472 elevation, land cover evenness, a tree–shrub–herb mosaic land cover class and mean slope consistently
1473 ranked highest in SHAP based importance across regions, seasons and FWTs, ahead of meteorologic al
1474 and human pressure variables. With regional variations, large fires mostly concentrated in flat, low lying
1475 or gently elevated areas that host continuous herbaceous or shrub fuels, while steeper slopes and higher
1476 tree cover limited spread. Shrublands and flooded herbaceous vegetation played contrasted roles along
1477 the precipitation gradient, inhibiting spread in wetter, fragmented floodplains and supporting large fires
1478 in drier, shrub dominated matrices.

1479 Human pressures in the Gran Chaco are essential for ignition but emerged as secondary for explaining
1480 the variation in final fire size once landscape structure is accounted for. Cattle, road, and population
1481 density all showed interpretable SHAP gradients, with larger fires occurring in remote, sparsely
1482 populated landscapes with low accessibility and low to moderate grazing pressure, and smaller fires in
1483 heavily managed areas with high road density or high stocking levels. However, their overall importance
1484 in the models was low, reflecting that most anthropogenic effects on fire size operate indirectly through
1485 long term transformations of vegetation structure, fuel continuity and fragmentation, or that they are
1486 hard to account for through remote sensing. Deforestation and land clearing fires contributed to BA,
1487 particularly in expanding agricultural frontiers, but the largest megafires and gigafires arose when
1488 continuous fine fuels, drought and wind aligned in ways that exceeded available suppression capacity.

1489 By combining medium resolution FP data, reanalysis-based weather metrics, machine learning and
1490 landscape analysis, we identify key biophysical, climatic and anthropogenic determinants of fire size
1491 and shape in a major South American ecoregion, the Gran Chaco. Our results emphasize that topography
1492 and vegetation structure set the primary template for fire spread, that during-fire meteorology governs
1493 when ignited fires evolve into large, elongated events, and that human activities shape fire size mainly
1494 through their cumulative imprint on fuels and landscape configuration rather than through simple
1495 demographic gradients. These findings inform fire risk assessment and management under ongoing land
1496 use intensification and climate variability in the Gran Chaco, and highlight the need for high resolution
1497 BA products, improved fire weather fields, explicit ignition and management records and stronger
1498 integration of socio-cultural dimensions of fire use in order to anticipate how this fire regime will
1499 respond to future environmental and societal change.

1500

1501 **6 AUTHOR CONTRIBUTION**

1502

1503 RSM collected and processed the data, analyzed the results, and drafted the manuscript. CO and AS
1504 conceived the idea and led the project. PVA contributed to data analysis, specifically by performing
1505 Random Forest modeling. All co-authors discussed the results, provided critical feedback, and reviewed
1506 the manuscript.

1507

1508 **7 COMPETING INTERESTS**

1509 The authors declare that they have no conflict of interest.

1510

1511 **8 ACKNOWLEDGEMENTS**

1512 The authors thank all the researchers and institutions involved in providing open-access datasets,
1513 including ESA CCI, ERA5-Land, and the Copernicus Climate Data Store (CDS). We acknowledge the
1514 computational infrastructure and support provided by the Laboratoire des Sciences du Climat et de
1515 l'Environnement (LSCE/IPSL). We also express our gratitude to Dr. Sandra Bravo for her important
1516 collaboration and contributions to our understanding of the fire regime in the region, as well as
1517 colleagues from CONICET for their valuable insights into Chaco ecology. The authors also
1518 acknowledge the use of AI-based tools to assist with text editing, code debugging, and figure scripting
1519 throughout the preparation of the manuscript.

1520

1521 **9 FINANCIAL SUPPORT**

1522 This research was partially funded by the European Space Agency through the Climate Change Initiative
1523 programme, under contract numbers ESA/No. 4000126564 (Land_Cover_cci) and ESA ESRIN/No.
1524 4000125259/18/I-NB. A. Sörensson acknowledges support from the Agencia Nacional de Promoción
1525 Científica y Tecnológica (ANPCyT, Argentina) via project PICT 2018-02511, and from the Consejo
1526 Nacional de Investigaciones Científicas y Técnicas (CONICET, Argentina) through grant PIP
1527 11220200102141CO. R. San Martin received doctoral funding from the Environmental Science
1528 Doctoral School of Île-de-France (DS 129).

1529

1530 **10 REFERENCES**

1531

1532 Adámoli, J., Sennhauser, E., Acero, J. M., and Rescia, A.: Stress and Disturbance: Vegetation
1533 Dynamics in the Dry Chaco Region of Argentina, *Journal of Biogeography*, 17, 491–500,
1534 <https://doi.org/10.2307/2845381>, 1990.

1535 Alencar, A. A., Brando, P. M., Asner, G. P., and Putz, F. E.: Landscape fragmentation, severe
1536 drought, and the new Amazon forest fire regime, *Ecological Applications*, 25, 1493–1505,
1537 <https://doi.org/10.1890/14-1528.1>, 2015.

1538 Alessio, G. A., Peñuelas, J., Llusà, J., Ogaya, R., Estiarte, M., and De Lillis, M.: Influence of
1539 water and terpenes on flammability in some dominant Mediterranean species, *Int J Wildland*
1540 *Fire*, 17, 274–286, <https://doi.org/10.1071/WF07038>, 2008.

1541 Alinari, J., Muller, A. von, and Renison, D.: The contribution of fire damage to restricting high
1542 mountain *Polylepis australis* forests to ravines: Insights from an un-replicated comparison,
1543 *Ecología Austral*, 25, 11–18, <https://doi.org/10.25260/EA.15.25.1.0.53>, 2015.

1544 Andela, N. and van der Werf, G. R.: Recent trends in African fires driven by cropland expansion
1545 and El Niño to La Niña transition, *Nature Clim Change*, 4, 791–795,
1546 <https://doi.org/10.1038/nclimate2313>, 2014.

1547 Andela, N., Morton, D. C., Giglio, L., Chen, Y., van der Werf, G. R., Kasibhatla, P. S., DeFries,
1548 R. S., Collatz, G. J., Hantson, S., Kloster, S., Bachelet, D., Forrest, M., Lasslop, G., Li, F.,
1549 Mangeon, S., Melton, J. R., Yue, C., and Randerson, J. T.: A human-driven decline in global
1550 burned area, *Science*, 356, 1356–1362, <https://doi.org/10.1126/science.aal4108>, 2017.

1551 Andela, N., Morton, D. C., Giglio, L., Paugam, R., Chen, Y., and Hantson, S.: The Global Fire
1552 Atlas of individual fire size, duration, speed and direction, 2019.

1553 Archibald, S., Roy, D. P., Van WILGEN, B. W., and Scholes, R. J.: What limits fire? An
1554 examination of drivers of burnt area in Southern Africa, *Global Change Biology*, 15, 613–630,
1555 <https://doi.org/10.1111/j.1365-2486.2008.01754.x>, 2009.

1556 Archibald, S., Lehmann, C. E. R., Gómez-Dans, J. L., and Bradstock, R. A.: Defining pyromes
1557 and global syndromes of fire regimes, *Proceedings of the National Academy of Sciences*, 110,
1558 6442–6447, <https://doi.org/10.1073/pnas.1211466110>, 2013.

1559 Archibald, S., Lehmann, C. E. R., Belcher, C. M., Bond, W. J., Bradstock, R. A., Daniau, A.-
1560 L., Dexter, K. G., Forrester, E. J., Greve, M., He, T., Higgins, S. I., Hoffmann, W. A., Lamont,
1561 B. B., McGlenn, D. J., Moncrieff, G. R., Osborne, C. P., Pausas, J. G., Price, O., Ripley, B. S.,
1562 Rogers, B. M., Schwilk, D. W., Simon, M. F., Turetsky, M. R., Van der Werf, G. R., and Zanne,
1563 A. E.: Biological and geophysical feedbacks with fire in the Earth system, *Environ. Res. Lett.*,
1564 13, 033003, <https://doi.org/10.1088/1748-9326/aa9ead>, 2018.

1565 Arenas, P.: ARENAS, Pastor. 2003. Etnografía y alimentación entre los toba-ñachilamole#ek
1566 y wichí-lhuku'tas del Chaco Central (Argentina). Buenos Aires, Edición del autor, 562 p. 24x17
1567 cm. ISBN 987-43-6483-1., Book, 2003.

- 1568 Argañaraz, Pizarro, G. G., Zak, M., Landi, M. A., and Bellis, L. M.: Human and biophysical
 1569 drivers of fires in Semiarid Chaco mountains of Central Argentina, *Science of the Total*
 1570 *Environment*, 520, 1–12, 2015.
- 1571 Argañaraz, Landi, M. A., Bravo, S. J., Gavier-Pizarro, G. I., Scavuzzo, C. M., and Bellis, L.
 1572 M.: Estimation of Live Fuel Moisture Content From MODIS Images for Fire Danger
 1573 Assessment in Southern Gran Chaco, *IEEE Journal of Selected Topics in Applied Earth*
 1574 *Observations and Remote Sensing*, 9, 5339–5349,
 1575 <https://doi.org/10.1109/JSTARS.2016.2575366>, 2016.
- 1576 Argañaraz, Landi, M. A., Scavuzzo, C. M., and Bellis, L. M.: Determining fuel moisture
 1577 thresholds to assess wildfire hazard: A contribution to an operational early warning system,
 1578 *PLoS ONE*, 13, e0204889, <https://doi.org/10.1371/journal.pone.0204889>, 2018.
- 1579 Arias, P. A., Rivera, J. A., Sörensson, A. A., Zachariah, M., Barnes, C., Philip, S., Kew, S.,
 1580 Vautard, R., Koren, G., Pinto, I., Vahlberg, M., Singh, R., Raju, E., Li, S., Yang, W., Vecchi,
 1581 G. A., and Otto, F. E. L.: Interplay between climate change and climate variability: the 2022
 1582 drought in Central South America, *Climatic Change*, 177, 6, [https://doi.org/10.1007/s10584-](https://doi.org/10.1007/s10584-023-03664-4)
 1583 [023-03664-4](https://doi.org/10.1007/s10584-023-03664-4), 2024.
- 1584 Barros, A. M. G. and Pereira, J. M. C.: Wildfire Selectivity for Land Cover Type: Does Size
 1585 Matter?, *PLOS ONE*, 9, e84760, <https://doi.org/10.1371/journal.pone.0084760>, 2014.
- 1586 Baumann, M., Levers, C., Macchi, L., Bluhm, H., Waske, B., Gasparri, N. I., and Kuemmerle,
 1587 T.: Mapping continuous fields of tree and shrub cover across the Gran Chaco using Landsat 8
 1588 and Sentinel-1 data, *Remote Sensing of Environment*, 216, 201–211,
 1589 <https://doi.org/10.1016/j.rse.2018.06.044>, 2018.
- 1590 Baumann, M., Gasparri, I., Buchadas, A., Oeser, J., Meyfroidt, P., Levers, C., Romero-Muñoz,
 1591 A., le Polain de Waroux, Y., Müller, D., and Kuemmerle, T.: Frontier metrics for a process-
 1592 based understanding of deforestation dynamics, *Environ. Res. Lett.*, 17, 095010,
 1593 <https://doi.org/10.1088/1748-9326/ac8b9a>, 2022.
- 1594 Belhadj-Khedher, C., El-Melki, T., and Mouillot, F.: Saharan Hot and Dry Sirocco Winds Drive
 1595 Extreme Fire Events in Mediterranean Tunisia (North Africa), *Atmosphere*, 11, 590,
 1596 <https://doi.org/10.3390/atmos11060590>, 2020.
- 1597 Bernardi, R. E., Staal, A., Xu, C., Scheffer, M., and Holmgren, M.: Livestock Herbivory Shapes
 1598 Fire Regimes and Vegetation Structure Across the Global Tropics, *Ecosystems*, 22, 1457–1465,
 1599 <https://doi.org/10.1007/s10021-019-00349-x>, 2019.
- 1600 Bianchi, L., Defossé, G., Dentoni, M., Kunst, C., Ledesma, R., and Bravo, S.: Dynamics of fuel
 1601 moisture and its relation to the ecology and management of fire in the western Chaco region
 1602 (Argentina) I: basic concepts., 2014.
- 1603 Bistinas, I., Harrison, S. P., Prentice, I. C., and Pereira, J. M. C.: Causal relationships versus
 1604 emergent patterns in the global controls of fire frequency, *Biogeosciences*, 11, 5087–5101,
 1605 <https://doi.org/10.5194/bg-11-5087-2014>, 2014.
- 1606 Boletta, P. E., Ravelo, A. C., Planchuelo, A. M., and Grilli, M.: Assessing deforestation in the
 1607 Argentine Chaco, *Forest Ecology and Management*, 228, 108–114,
 1608 <https://doi.org/10.1016/j.foreco.2006.02.045>, 2006.

- 1609 Bowman, Balch, J., Artaxo, P., Bond, W. J., Cochrane, M. A., D’Antonio, C. M., DeFries, R.,
 1610 Johnston, F. H., Keeley, J. E., Krawchuk, M. A., Kull, C. A., Mack, M., Moritz, M. A., Pyne,
 1611 S., Roos, C. I., Scott, A. C., Sodhi, N. S., and Swetnam, T. W.: The human dimension of fire
 1612 regimes on Earth: The human dimension of fire regimes on Earth, *Journal of Biogeography*, 38,
 1613 2223–2236, <https://doi.org/10.1111/j.1365-2699.2011.02595.x>, 2011.
- 1614 Bowman, D. M. J. S., Balch, J. K., Artaxo, P., Bond, W. J., Carlson, J. M., Cochrane, M. A.,
 1615 D’Antonio, C. M., DeFries, R. S., Doyle, J. C., Harrison, S. P., Johnston, F. H., Keeley, J. E.,
 1616 Krawchuk, M. A., Kull, C. A., Marston, J. B., Moritz, M. A., Prentice, I. C., Roos, C. I., Scott,
 1617 A. C., Swetnam, T. W., van der Werf, G. R., and Pyne, S. J.: Fire in the Earth System, *Science*,
 1618 324, 481–484, <https://doi.org/10.1126/science.1163886>, 2009.
- 1619 Bowring, S. P. K., Li, W., Mouillot, F., Rosan, T. M., and Ciais, P.: Road fragment edges
 1620 enhance wildfire incidence and intensity, while suppressing global burned area, *Nat Commun*,
 1621 15, 9176, <https://doi.org/10.1038/s41467-024-53460-6>, 2024.
- 1622 Bravo, S., Kunst, C., Grau, R., and Aráoz, E.: Fire–rainfall relationships in Argentine Chaco
 1623 savannas, *Journal of Arid Environments*, 74, 1319–1323,
 1624 <https://doi.org/10.1016/j.jaridenv.2010.04.010>, 2010.
- 1625 Bravo, S., Kunst, C., Leiva, M., and Ledesma, R.: Response of hardwood tree regeneration to
 1626 surface fires, western Chaco region, Argentina, *Forest Ecology and Management*, 326, 36–45,
 1627 <https://doi.org/10.1016/j.foreco.2014.04.009>, 2014.
- 1628 Bravo, S., Bogino, S., Leiva, M., Lepiscopo, M., Cendoya, M., Kunst, C., and Biurrun, F.:
 1629 Wood anatomy, fire wounds and dendrochronological potential of *Prosopis pugionata* Burkart
 1630 (Fabaceae) in arid Argentine Chaco, *IAWA journal / International Association of Wood*
 1631 *Anatomists*, 42, 1–10, <https://doi.org/10.1163/22941932-bja10056>, 2021.
- 1632 Bravo, S., Ledesma, R., Coria, D., and Loto, D.: Fire in the Chaco Region: Ecological Aspects
 1633 and Land Management, in: *Fire in the South American Ecosystems*, edited by: Fidelis, A. and
 1634 Pivello, V. R., Springer Nature Switzerland, Cham, 213–241, https://doi.org/10.1007/978-3-031-89372-8_8, 2025.
- 1636 Bucher, E. H.: Chaco and Caatinga — South American Arid Savannas, Woodlands and
 1637 Thickets, in: *Ecology of Tropical Savannas*, vol. 42, edited by: Huntley, B. J. and Walker, B.
 1638 H., Springer Berlin Heidelberg, Berlin, Heidelberg, 48–79, https://doi.org/10.1007/978-3-642-68786-0_4, 1982.
- 1640 Bucher, E. H. and Huszar, P. C.: Sustainable management of the Gran Chaco of South America:
 1641 Ecological promise and economic constraints, *Journal of Environmental Management*, 57, 99–
 1642 108, <https://doi.org/10.1006/jema.1999.0290>, 1999.
- 1643 Castilla, M.: “Ahora tenemos este virus, pero cuando tenés tantos problemas en la zona nada
 1644 alcanza”: Extractivismo, segregación y pandemia en la provincia del Chaco, 2021.
- 1645 Center For International Earth Science Information Network-CIESIN-Columbia University:
 1646 Gridded Population of the World, Version 4 (GPWv4): Population Density, Revision 11,
 1647 <https://doi.org/10.7927/H49C6VHW>, 2017.

- 1648 Chuvieco, E., Aguado, I., Salas, J., García, M., Yebra, M., and Oliva, P.: Satellite Remote
1649 Sensing Contributions to Wildland Fire Science and Management, *Curr Forestry Rep*, 6, 81–
1650 96, <https://doi.org/10.1007/s40725-020-00116-5>, 2020.
- 1651 Chuvieco, E., Roteta, E., Sali, M., Stroppiana, D., Boettcher, M., Kirches, G., Storm, T.,
1652 Khairoun, A., Pettinari, M. L., Franquesa, M., and Albergel, C.: Building a small fire database
1653 for Sub-Saharan Africa from Sentinel-2 high-resolution images, *Science of The Total*
1654 *Environment*, 845, 157139, <https://doi.org/10.1016/j.scitotenv.2022.157139>, 2022.
- 1655 Cingolani, A. M., Vaieretti, M. V., Giorgis, M. A., La Torre, N., Whitworth-Hulse, J. I., and
1656 Renison, D.: Can livestock and fires convert the sub-tropical mountain rangelands of central
1657 Argentina into a rocky desert?, *Rangel J*, 35, 285–297, <https://doi.org/10.1071/RJ12095>, 2013.
- 1658 Coria, R. D., Kunst, C. R., and Bravo, S. J.: A contribution to the understanding of the woody
1659 encroachment in grasslands/savannas from the South American Semiarid Chaco., 2021.
- 1660 Coronel, G., Pastén, M., Breuer, N., Celeste, A., Rejalaga, L., Domecq, F. M., and Nagy, G. J.:
1661 Wildfires in Paraguay: Environmental and Human Impacts, in: *Sustainability in Natural*
1662 *Resources Management and Land Planning*, edited by: Leal Filho, W., Azeiteiro, U. M., and
1663 Setti, A. F. F., Springer International Publishing, Cham, 429–444, [https://doi.org/10.1007/978-](https://doi.org/10.1007/978-3-030-76624-5_25)
1664 [3-030-76624-5_25](https://doi.org/10.1007/978-3-030-76624-5_25), 2021.
- 1665 D’Antonio, C. M. and Vitousek, P. M.: Biological Invasions by Exotic Grasses, the Grass/Fire
1666 Cycle, and Global Change, *Annual Review of Ecology and Systematics*, 23, 63–87, 1992.
- 1667 De Marzo, T., Pflugmacher, D., Baumann, M., Lambin, E. F., Gasparri, I., and Kuemmerle, T.:
1668 Characterizing forest disturbances across the Argentine Dry Chaco based on Landsat time
1669 series, *International Journal of Applied Earth Observation and Geoinformation*, 98, 102310,
1670 <https://doi.org/10.1016/j.jag.2021.102310>, 2021.
- 1671 De Marzo, T., Gasparri, N. I., Lambin, E. F., and Kuemmerle, T.: Agents of Forest Disturbance
1672 in the Argentine Dry Chaco, *Remote Sensing*, 14, 1758, <https://doi.org/10.3390/rs14071758>,
1673 2022.
- 1674 De Marzo, T., Pratzer, M., Baumann, M., Gasparri, N. I., Pötzschner, F., and Kuemmerle, T.:
1675 Linking disturbance history to current forest structure to assess the impact of disturbances in
1676 tropical dry forests, *Forest Ecology and Management*, 539, 120989,
1677 <https://doi.org/10.1016/j.foreco.2023.120989>, 2023.
- 1678 Defourny, P., Lamarche, C., Brockmann, C., Boettcher, M., Bontemps, S., Maet, T., Duveiller,
1679 G. L. H., K., H. A., Kirches, G., Moreau, I., Peylin, P., Ottlé, C., J., R., Bogaert, E., Ramoino,
1680 F., Albergel, C., and Arino, O.: Observed annual global land-use change from 1992 to 2020
1681 three times more dynamic than reported by inventory-based statistics, in preparation, 2023.
- 1682 Devisscher, T., Boyd, E., and Malhi, Y.: Anticipating future risk in social-ecological systems
1683 using fuzzy cognitive mapping: the case of wildfire in the Chiquitania, Bolivia, *Ecology and*
1684 *Society*, 21, <https://doi.org/10.5751/ES-08599-210418>, 2016.
- 1685 Devisscher, T., Malhi, Y., and Boyd, E.: Deliberation for wildfire risk management: Addressing
1686 conflicting views in the Chiquitania, Bolivia, *The Geographical Journal*, 185, 38–54,
1687 <https://doi.org/10.1111/geoj.12261>, 2019.

- 1688 Doblas-Reyes, F. J., Sorensson, A. A., Almazroui, M., Dosio, A., Gutowski, W. J., Haarsma,
1689 R., Hamdi, R., Hewitson, B., Kwon, W.-T., Lamptey, B. L., Maraun, D., Stephenson, T. S.,
1690 Takayabu, I., Terray, L., Turner, A., and Zuo, Z.: Linking global to regional climate change,
1691 edited by: Masson-Delmotte, V., Zhai, P., Pirani, A., Connors, S. L., Pean, C., Berger, S., Caud,
1692 N., Chen, Y., Goldfarb, L., Gomis, M. I., Huang, M., Leitzell, K., Lonnoy, E., Matthews, J. B.
1693 R., Maycock, T. K., Waterfield, T., Yelekci, O., Yu, R., and Zhou, B., Cambridge University
1694 Press, 2021.
- 1695 Druel, A., Ruffault, J., Davi, H., Chanzy, A., Marloie, O., De Cáceres, M., Oliosio, A., Mouillot,
1696 F., François, C., Soudani, K., and Martin-StPaul, N. K.: Enhancing environmental models with
1697 a new downscaling method for global radiation in complex terrain, *Biogeosciences*, 22, 1–18,
1698 <https://doi.org/10.5194/bg-22-1-2025>, 2025.
- 1699 Dujardin, J. and Lehning, M.: Wind-Topo: Downscaling near-surface wind fields to high-
1700 resolution topography in highly complex terrain with deep learning, *Quarterly Journal of the*
1701 *Royal Meteorological Society*, 148, 1368–1388, <https://doi.org/10.1002/qj.4265>, 2022.
- 1702 Eklund, J., Jones, J. P. G., Räsänen, M., Geldmann, J., Jokinen, A.-P., Pellegrini, A., Rakotobe,
1703 D., Rakotonarivo, O. S., Toivonen, T., and Balmford, A.: Elevated fires during COVID-19
1704 lockdown and the vulnerability of protected areas, *Nat Sustain*, 5, 603–609,
1705 <https://doi.org/10.1038/s41893-022-00884-x>, 2022.
- 1706 Feron, S., Cordero, R. R., Damiani, A., MacDonell, S., Pizarro, J., Goubanova, K., Valenzuela,
1707 R., Wang, C., Rester, L., and Beaulieu, A.: South America is becoming warmer, drier, and more
1708 flammable, *Communications Earth & Environment*, 5, [https://doi.org/10.1038/s43247-024-](https://doi.org/10.1038/s43247-024-01654-7)
1709 01654-7, 2024.
- 1710 Fischer, M. A., Di Bella, C. M., and Jobbágy, E. G.: Fire patterns in central semiarid Argentina,
1711 *Journal of Arid Environments*, 78, 161–168, <https://doi.org/10.1016/j.jaridenv.2011.11.009>,
1712 2012.
- 1713 Garcia, L. C., Szabo, J. K., de Oliveira Roque, F., de Matos Martins Pereira, A., Nunes da
1714 Cunha, C., Damasceno-Júnior, G. A., Morato, R. G., Tomas, W. M., Libonati, R., and Ribeiro,
1715 D. B.: Record-breaking wildfires in the world’s largest continuous tropical wetland: Integrative
1716 fire management is urgently needed for both biodiversity and humans, *Journal of*
1717 *Environmental Management*, 293, 112870, <https://doi.org/10.1016/j.jenvman.2021.112870>,
1718 2021.
- 1719 García, M., Pettinari, M. L., Chuvieco, E., Salas, J., Mouillot, F., Chen, W., and Aguado, I.:
1720 Characterizing Global Fire Regimes from Satellite-Derived Products, *Forests*, 13, 699,
1721 <https://doi.org/10.3390/f13050699>, 2022.
- 1722 Gasparri, N. I. and Baldi, G.: Regional patterns and controls of biomass in semiarid woodlands:
1723 lessons from the Northern Argentina Dry Chaco, *Reg Environ Change*, 13, 1131–1144,
1724 <https://doi.org/10.1007/s10113-013-0422-x>, 2013.
- 1725 Gasparri, N. I., Grau, H. R., and Manghi, E.: Carbon Pools and Emissions from Deforestation
1726 in Extra-Tropical Forests of Northern Argentina Between 1900 and 2005, *Ecosystems*, 11,
1727 1247–1261, <https://doi.org/10.1007/s10021-008-9190-8>, 2008.
- 1728 Ginzburg, R., Adámoli, J., Herrera, P., and Torrella, S.: Los Humedales del Chaco:
1729 clasificación, inventario y mapeo a escala regional, *Miscelánea*, 14, 121–138, 2005.

- 1730 Giorgis, M. A., Zeballos, S. R., Carbone, L., Zimmermann, H., von Wehrden, H., Aguilar, R.,
1731 Ferreras, A. E., Tecco, P. A., Kowaljow, E., Barri, F., Gurvich, D. E., Villagra, P., and
1732 Jaureguiberry, P.: A review of fire effects across South American ecosystems: the role of
1733 climate and time since fire, *fire ecol*, 17, 11, <https://doi.org/10.1186/s42408-021-00100-9>,
1734 2021.
- 1735 Gürtler, R. E.: Sustainability of vector control strategies in the Gran Chaco Region: current
1736 challenges and possible approaches, *Memórias do Instituto Oswaldo Cruz*, 104, 52–59, 2009.
- 1737 Haas, O., Prentice, I. C., and Harrison, S. P.: Global environmental controls on wildfire burnt
1738 area, size, and intensity, *Environ. Res. Lett.*, 17, 065004, [https://doi.org/10.1088/1748-](https://doi.org/10.1088/1748-9326/ac6a69)
1739 9326/ac6a69, 2022.
- 1740 Hantson, S., Pueyo, S., and Chuvieco, E.: Global fire size distribution is driven by human
1741 impact and climate, *Global Ecology and Biogeography*, 24, 77–86,
1742 <https://doi.org/10.1111/geb.12246>, 2015.
- 1743 Hantson, S., Scheffer, M., Pueyo, S., Xu, C., Lasslop, G., Nes, E. H., and Mendelsohn, J.: Rare,
1744 Intense, Big fires dominate the global tropics under drier conditions, *Scientific reports*, 7, 1–5,
1745 2017.
- 1746 Harper, K. L., Lamarche, C., Hartley, A., Peylin, P., Ottlé, C., Bastrikov, V., San Martín, R.,
1747 Bohnenstengel, S. I., Kirches, G., Boettcher, M., Shevchuk, R., Brockmann, C., and Defourny,
1748 P.: A 29-year time series of annual 300 m resolution plant-functional-type maps for climate
1749 models, *Earth Syst. Sci. Data*, 15, 1465–1499, <https://doi.org/10.5194/essd-15-1465-2023>,
1750 2023.
- 1751 Hernandez, C., Drobinski, P., and Turquety, S.: How much does weather control fire size and
1752 intensity in the Mediterranean region?, *Annales Geophysicae*, 33, 931–939,
1753 <https://doi.org/10.5194/angeo-33-931-2015>, 2015.
- 1754 Hernández, V., Florencia Fossa Riglos, M., and Vera, C.: Addressing climate services in
1755 SouthAmerican Chaco region through a knowledge coproduction process, *Global*
1756 *Environmental Change*, 72, 102443, <https://doi.org/10.1016/j.gloenvcha.2021.102443>, 2022.
- 1757 Higuera, P. E., Abatzoglou, J. T., Littell, J. S., and Morgan, P.: The Changing Strength and
1758 Nature of Fire-Climate Relationships in the Northern Rocky Mountains, U.S.A., 1902-2008,
1759 *PLOS ONE*, 10, e0127563, <https://doi.org/10.1371/journal.pone.0127563>, 2015.
- 1760 Horn, B. K. P.: Hill shading and the reflectance map, *Proceedings of the IEEE*, 69, 14–47,
1761 <https://doi.org/10.1109/PROC.1981.11918>, 1981.
- 1762 Hsu, A., Jones, M. W., Thurgood, J. R., Smith, A. J. P., Carmenta, R., Abatzoglou, J. T.,
1763 Anderson, L. O., Clarke, H., Doerr, S. H., Fernandes, P. M., Kolden, C. A., Santín, C., Strydom,
1764 T., Le Quééré, C., Ascoli, D., Castellnou, M., Goldammer, J. G., Guiomar, N. R. G. N.,
1765 Kukavskaya, E. A., Rigolot, E., Tanpipat, V., Varner, M., Yamashita, Y., Baard, J., Barreto, R.,
1766 Becerra, J., Brunn, E., Bergius, N., Carlsson, J., Cheney, C., Druce, D., Elliot, A., Evans, J., De
1767 Moraes Falleiro, R., Prat-Guitart, N., Hiers, J. K., Kaiser, J. W., Macher, L., Morris, D., Park,
1768 J., Robles, C., Román-Cuesta, R. M., Rücker, G., Senra, F., Steil, L., Valverde, J. A. L., and
1769 Zerr, E.: A global assemblage of regional prescribed burn records — GlobalRx, *Sci Data*, 12,
1770 1083, <https://doi.org/10.1038/s41597-025-04941-w>, 2025.

- 1771 Jones, Abatzoglou, J. T., Veraverbeke, S., Andela, N., Lasslop, G., and Forkel, M.: Global and
1772 regional trends and drivers of fire under climate change, *Reviews of Geophysics*, 60, 2020
1773 000726, <https://doi.org/10.1029/2020RG000726>, 2022.
- 1774 Junk, W. J. and Nunes da Cunha, C.: Pasture clearing from invasive woody plants in the
1775 Pantanal: a tool for sustainable management or environmental destruction?, *Wetlands Ecol*
1776 *Manage*, 20, 111–122, <https://doi.org/10.1007/s11273-011-9246-y>, 2012.
- 1777 Kelley, D. I., Bistinas, I., Whitley, R., Burton, C., Marthews, T. R., and Dong, N.: How
1778 contemporary bioclimatic and human controls change global fire regimes, *Nat. Clim. Chang.*,
1779 9, 690–696, <https://doi.org/10.1038/s41558-019-0540-7>, 2019.
- 1780 Krawchuk, M. A. and Moritz, M. A.: Constraints on global fire activity vary across a resource
1781 gradient, *Ecology*, 92, 121–132, <https://doi.org/10.1890/09-1843.1>, 2011.
- 1782 Kumar, S., Getirana, A., Libonati, R., Hain, C., Mahanama, S., and Andela, N.: Changes in land
1783 use enhance the sensitivity of tropical ecosystems to fire-climate extremes, *Sci Rep*, 12, 964,
1784 <https://doi.org/10.1038/s41598-022-05130-0>, 2022.
- 1785 Kunst, C. and Bravo, S.: Ecología y régimen de fuego en la región chaqueña argentina, in:
1786 Fuego en los ecosistemas Argentinos, 47–59, 2003.
- 1787 Kunst, C., Bravo, S., Monti, E., Cornacchione, M., and Godoy, J.: El fuego y el manejo de
1788 pasturas naturales y cultivadas de la región chaqueña, *Fuego en los Ecosistemas Argentinos*.
1789 Ediciones INTA, 21, 239–247, 2003.
- 1790 Kunst, C., Navall, M., Ledesma, R., Silberman, J., Anríquez, A., Coria, D., Bravo, S., Gómez,
1791 A., Albanesi, A., Grasso, D., Nuñez, J. A. D., González, A., Tomsic, P., and Godoy, J.:
1792 Silvopastoral Systems in the Western Chaco Region, Argentina, in: *Silvopastoral Systems in*
1793 *Southern South America*, edited by: Peri, P. L., Dube, F., and Varella, A., Springer International
1794 Publishing, Cham, 63–87, https://doi.org/10.1007/978-3-319-24109-8_4, 2016.
- 1795 Kusch, E. and Davy, R.: KrigR – A tool for downloading and statistically downscaling climate
1796 reanalysis data, *Environmental Research Letters*, 17, [https://doi.org/10.1088/1748-](https://doi.org/10.1088/1748-9326/ac48b3)
1797 [9326/ac48b3](https://doi.org/10.1088/1748-9326/ac48b3), 2022.
- 1798 Laurent, P., Mouillot, F., Yue, C., Ciais, P., Moreno, M. V., and Nogueira, J. M. P.: FRY, a
1799 global database of fire patch functional traits derived from space-borne burned area products,
1800 *Sci Data*, 5, 180132, <https://doi.org/10.1038/sdata.2018.132>, 2018.
- 1801 Levers, C., Piquer-Rodríguez, M., Gollnow, F., Baumann, M., Camino, M., Gasparri, N. I.,
1802 Gavier-Pizarro, G. I., le Polain de Waroux, Y., Müller, D., Nori, J., Pötzschner, F., Romero-
1803 Muñoz, A., and Kuemmerle, T.: What is still at stake in the Gran Chaco? Social-ecological
1804 impacts of alternative land-system futures in a global deforestation hotspot, *Environ. Res. Lett.*,
1805 19, 064003, <https://doi.org/10.1088/1748-9326/ad44b6>, 2024.
- 1806 Linley, G. D., Jolly, C. J., Doherty, T. S., Geary, W. L., Armenteras, D., Belcher, C. M., Bliege
1807 Bird, R., Duane, A., Fletcher, M., Giorgis, M. A., Haslem, A., Jones, G. M., Kelly, L. T., Lee,
1808 C. K. F., Nolan, R. H., Parr, C. L., Pausas, J. G., Price, J. N., Regos, A., Ritchie, E. G., Ruffault,
1809 J., Williamson, G. J., Wu, Q., and Nimmo, D. G.: What do you mean, ‘megafire’?, *Global Ecol*
1810 *Biogeogr*, 31, 1906–1922, <https://doi.org/10.1111/geb.13499>, 2022.

- 1811 Lizundia-Loiola, J., Otón, G., Ramo, R., and Chuvieco, E.: A spatio-temporal active-fire
 1812 clustering approach for global burned area mapping at 250 m from MODIS data, *Remote*
 1813 *Sensing of Environment*, 236, 111493, <https://doi.org/10.1016/j.rse.2019.111493>, 2020.
- 1814 Loto, D. and Bravo, S.: Species composition, structure, and functional traits in Argentine Chaco
 1815 forests under two different disturbance histories, *Ecological Indicators*, 113, 106232,
 1816 <https://doi.org/10.1016/j.ecolind.2020.106232>, 2020.
- 1817 MacQueen, J.: Some methods for classification and analysis of multivariate observations, in:
 1818 *Proceedings of the Fifth Berkeley Symposium on Mathematical Statistics and Probability*,
 1819 *Volume 1: Statistics*, 281–298, 1967.
- 1820 Marengo, J., Martinez, R., Tapia, B., Allen, T., Basantes, R., Hernandez-Espinoza, K.,
 1821 Alvarado, L., Baddour, O., Ransom, C., Silva, Á., Báez, J., Gomez, F., Costa, F., Avalos, G.,
 1822 Estella, J., and Kennedy, J.: State of the Climate in Latin America and the Caribbean 2021
 1823 (WMO-No. 1295), 2022.
- 1824 McDaniel, J., Kennard, D., and Fuentes, A.: Smokey the Tapir: Traditional Fire Knowledge
 1825 and Fire Prevention Campaigns in Lowland Bolivia, *Society & Natural Resources*, 18, 921–
 1826 931, <https://doi.org/10.1080/08941920500248921>, 2005.
- 1827 Meinshausen, N.: Quantile Regression Forests, *Journal of Machine Learning Research*, 7, 983–
 1828 999, 2006.
- 1829 Morello, J. H. and Adámoli, J. M.: Las grandes unidades de vegetación y ambiente del Chaco
 1830 argentino, 1968.
- 1831 Moreno, M. V., Laurent, P., and Mouillot, F.: Global intercomparison of functional
 1832 pyrodiversity from two satellite sensors, *International Journal of Remote Sensing*, 42, 9523–
 1833 9541, <https://doi.org/10.1080/01431161.2021.1999529>, 2021.
- 1834 Mouillot, F., Schultz, M. G., Yue, C., Cadule, P., Tansey, K., Ciais, P., and Chuvieco, E.: Ten
 1835 years of global burned area products from spaceborne remote sensing—A review: Analysis of
 1836 user needs and recommendations for future developments, *International Journal of Applied*
 1837 *Earth Observation and Geoinformation*, 26, 64–79, <https://doi.org/10.1016/j.jag.2013.05.014>,
 1838 2014.
- 1839 Mouillot, F., Chen, W., Campagnolo, M., and Ciais, P.: FRYv2.0: a global fire patch
 1840 morphology database from FireCCI51 and MCD64A1, *Copernicus Meetings*,
 1841 <https://doi.org/10.5194/egusphere-egu23-9575>, 2023.
- 1842 Muñoz-Sabater, J., Dutra, E., Agustí-Panareda, A., Albergel, C., Arduini, G., Balsamo, G.,
 1843 Boussetta, S., Choulga, M., Harrigan, S., Hersbach, H., Martens, B., Miralles, D. G., Piles, M.,
 1844 Rodríguez-Fernández, N. J., Zsoter, E., Buontempo, C., and Thépaut, J.-N.: ERA5-Land: a
 1845 state-of-the-art global reanalysis dataset for land applications, *Earth System Science Data*, 13,
 1846 4349–4383, <https://doi.org/10.5194/essd-13-4349-2021>, 2021.
- 1847 Musser, K.: Río de la Plata, Wikipedia, 2024.
- 1848 Naumann, G., Podesta, G., Marengo, J., Luterbacher, J., Bavera, D., Acosta, N. J., Arias-
 1849 Muñoz, C., Barbosa, P., Cammalleri, C., Cuartas, L. A., De, E. M., De, F. M., De, J. A., Escobar,
 1850 C., Fioravanti, G., Giordano, L., Hrast, E. A., Hidalgo, C., Leal, D. M. O. L., Maetens, W.,

- 1851 Magni, D., Masante, D., Mazzeschi, M., Osman, M., Rossi, L., Seluchi, M., De, L. M. S. M.,
 1852 Spennemann, P., Spinoni, J., Toreti, A., and Vera, C.: Extreme and long-term drought in the La
 1853 Plata Basin: event evolution and impact assessment until September 2022,
 1854 <https://doi.org/10.2760/62557>, 2023.
- 1855 Naval Fernández, Albornoz, J., Bellis, L. M., Baldini, C., Arcamone, J., Silvetti, L., Álvarez,
 1856 M. P., and Argañaraz, J. P.: Megaincendios 2020 en Córdoba: Incidencia del fuego en áreas de
 1857 valor ecológico y socioeconómico, *Ecol. Austral*, 33, 136–151,
 1858 <https://doi.org/10.25260/EA.23.33.1.0.2120>, 2023.
- 1859 Naval-Fernández, M. C., Elia, M., Giannico, V., Bellis, L. M., Bravo, S. J., and Argañaraz, J.
 1860 P.: The Pyrogeography of the Gran Chaco's Dry Forest: A Comparison of Clustering
 1861 Algorithms and the Scale of Analysis, *Forests*, 16, 1114, <https://doi.org/10.3390/fl6071114>,
 1862 2025.
- 1863 Nori, J., Torres, R., Lescano, J. N., Cordier, J. M., Periago, M. E., and Baldo, D.: Protected
 1864 areas and spatial conservation priorities for endemic vertebrates of the Gran Chaco, one of the
 1865 most threatened ecoregions of the world, *Diversity and Distributions*, 22, 1212–1219,
 1866 <https://doi.org/10.1111/ddi.12497>, 2016.
- 1867 Olson, D. M., Dinerstein, E., Wikramanayake, E. D., Burgess, N. D., Powell, G. V.,
 1868 Underwood, E. C., and Kassem, K. R.: Terrestrial Ecoregions of the World: A New Map of
 1869 Life on Earth A new global map of terrestrial ecoregions provides an innovative tool for
 1870 conserving biodiversity, *BioScience*, 51, 933–938, 2001.
- 1871 Oom, D., Silva, P. C., Bistinas, I., and Pereira, J. M. C.: Highlighting Biome-Specific
 1872 Sensitivity of Fire Size Distributions to Time-Gap Parameter Using a New Algorithm for Fire
 1873 Event Individuation, *Remote Sensing*, 8, 663, <https://doi.org/10.3390/rs8080663>, 2016.
- 1874 Paritsis, J., Landesmann, J. B., Kitzberger, T., Tiribelli, F., Sasal, Y., Quintero, C., Dimarco, R.
 1875 D., Barrios-García, M. N., Iglesias, A. L., Diez, J. P., Sarasola, M., and Nuñez, M. A.: Pine
 1876 Plantations and Invasion Alter Fuel Structure and Potential Fire Behavior in a Patagonian
 1877 Forest-Steppe Ecotone, *Forests*, 9, 117, <https://doi.org/10.3390/f9030117>, 2018.
- 1878 Paudel, J.: Short-run environmental effects of COVID-19: Evidence from forest fires, *World*
 1879 *Development*, 137, 105120, <https://doi.org/10.1016/j.worlddev.2020.105120>, 2021.
- 1880 Pausas, J. G. and Bradstock, R. A.: Fire persistence traits of plants along a productivity and
 1881 disturbance gradient in mediterranean shrublands of south-east Australia, *Global Ecol*
 1882 *Biogeography*, 16, 330–340, <https://doi.org/10.1111/j.1466-8238.2006.00283.x>, 2007.
- 1883 Pettinari, M. L., Lizundia-Loiola, J., and Chuvieco, E.: ESA CCIECV fire disturbance: D4. 2.1
 1884 product user guide—MODIS, version 1.1, 2021.
- 1885 Pielou, E. C.: The measurement of diversity in different types of biological collections, *Journal*
 1886 *of Theoretical Biology*, 13, 131–144, [https://doi.org/10.1016/0022-5193\(66\)90013-0](https://doi.org/10.1016/0022-5193(66)90013-0), 1966.
- 1887 Poulter, B., Freeborn, P., Jolly, W., and Varner, J.: COVID-19 lockdowns drive decline in
 1888 active fires in southeastern United States, *Proceedings of the National Academy of Sciences*,
 1889 118, e2105666118, <https://doi.org/10.1073/pnas.2105666118>, 2021.

- 1890 Redford, K. H., Taber, A., and Simonetti, J. A.: There is More to Biodiversity than the Tropical
1891 Rain Forests, *Conservation Biology*, 4, 328–330, 1990.
- 1892 Ruffault, J. and Mouillot, F.: How a new fire-suppression policy can abruptly reshape the fire-
1893 weather relationship, *Ecosphere*, 6, art199, <https://doi.org/10.1890/ES15-00182.1>, 2015.
- 1894 Ruffault, J. and Mouillot, F.: Contribution of human and biophysical factors to the spatial
1895 distribution of forest fire ignitions and large wildfires in a French Mediterranean region, *Int. J.*
1896 *Wildland Fire*, 26, 498–508, <https://doi.org/10.1071/WF16181>, 2017.
- 1897 Ruffault, J., Moron, V., Trigo, R. M., and Curt, T.: Objective identification of multiple large
1898 fire climatologies: an application to a Mediterranean ecosystem, *Environ. Res. Lett.*, 11,
1899 075006, <https://doi.org/10.1088/1748-9326/11/7/075006>, 2016.
- 1900 Ruffault, J., Curt, T., Moron, V., Trigo, R. M., Mouillot, F., Koutsias, N., Pimont, F., Martin-
1901 StPaul, N., Barbero, R., Dupuy, J.-L., Russo, A., and Belhadj-Khedher, C.: Increased likelihood
1902 of heat-induced large wildfires in the Mediterranean Basin, *Sci Rep*, 10, 13790,
1903 <https://doi.org/10.1038/s41598-020-70069-z>, 2020.
- 1904 San Martín, R.: Fires, land use, and forest loss in the South American Chaco: understanding
1905 the links between fires, climate, ecosystems, and human activity through remote sensing, PhD
1906 Thesis, Université Paris-Saclay, 2024.
- 1907 San Martín, R., Otlé, C., and Sörensson, A.: Fires in the South American Chaco, from dry
1908 forests to wetlands: response to climate depends on land cover, *fire ecol*, 19, 57,
1909 <https://doi.org/10.1186/s42408-023-00212-4>, 2023.
- 1910 Saucedo, G. I. and Kurtz, D. B.: Seasonality and post fire recovery in a wetland dominated
1911 region: Insights from satellite data analysis in northern Argentina, *Remote Sensing*
1912 *Applications: Society and Environment*, 37, 101480,
1913 <https://doi.org/10.1016/j.rsase.2025.101480>, 2025.
- 1914 Schmidt, M. A. and Castilla, M.: La emergencia del fuego en un territorio hidrosocial: incendios
1915 en las provincias de Salta y Chaco, I Encuentro Territorios Hidrosociales en Disputa (ETHIS)
1916 (Chaco, 25 y 26 de agosto de 2022), 2023.
- 1917 Shannon, C. E.: A Mathematical Theory of Communication, *Bell System Technical Journal*,
1918 27, 379–423, <https://doi.org/10.1002/j.1538-7305.1948.tb01338.x>, 1948.
- 1919 Sugiyama, M. S., Mendoza, M., and Carpio, M. B.: Resilience and Recovery in the Dry Chaco:
1920 Ecological Knowledge Encoded in Forager Wildfire Narratives, *Journal of Ethnobiology*, 45,
1921 76–94, <https://doi.org/10.1177/02780771241303896>, 2025.
- 1922 Takacs, S., Schulte to Bühne, H., and Pettorelli, N.: What shapes fire size and spread in African
1923 savannahs?, *Remote Sensing in Ecology and Conservation*, 7, 610–620,
1924 <https://doi.org/10.1002/rse2.212>, 2021.
- 1925 Tálamo, A., Lopez De Casenave, J., Núñez-Regueiro, M., and Caziani, S. M.: Regeneración de
1926 plantas leñosas en el Chaco semiárido argentino: relación con factores bióticos y abióticos en
1927 micrositios creados por el aprovechamiento forestal, *Bosque (Valdivia)*, 34, 13–14,
1928 <https://doi.org/10.4067/S0717-92002013000100007>, 2013.

- 1929 Torrella, S. A. and Adámoli, J.: Situación ambiental de la ecorregión del Chaco Seco, La
 1930 situación ambiental Argentina, 75–82, 2005.
- 1931 Van Wagner, C. E.: Development and structure of the Canadian Forest Fire Weather Index
 1932 System, Minister of Supply and Services Canada, Ottawa, 37 pp., 1987.
- 1933 Vidal-Riveros, C., Souza-Alonso, P., Bravo, S., Laino, R., and Ngo Bieng, M. A.: A review of
 1934 wildfires effects across the Gran Chaco region, *Forest Ecology and Management*, 549, 121432,
 1935 <https://doi.org/10.1016/j.foreco.2023.121432>, 2023.
- 1936 Vidal-Riveros, C., Watler Reyes, W. J., Ngo Bieng, M. A., and Souza-Alonso, P.: Assessing
 1937 Fire Regimes in the Paraguayan Chaco: Implications for Ecological and Fire Management, *Fire*,
 1938 7, 347, <https://doi.org/10.3390/fire7100347>, 2024.
- 1939 Vitolo, C., Di Giuseppe, F., Barnard, C., Coughlan, R., San-Miguel-Ayanz, J., Libertá, G., and
 1940 Krzeminski, B.: ERA5-based global meteorological wildfire danger maps, *Sci Data*, 7, 216,
 1941 <https://doi.org/10.1038/s41597-020-0554-z>, 2020.
- 1942 Wright, M. N. and Ziegler, A.: ranger: A Fast Implementation of Random Forests for High
 1943 Dimensional Data in C++ and R, *Journal of Statistical Software*, 77, 1–17,
 1944 <https://doi.org/10.18637/jss.v077.i01>, 2017.
- 1945 Yebra, M., Scortechini, G., Badi, A., Beget, M. E., Boer, M. M., Bradstock, R., Chuvieco, E.,
 1946 Danson, F. M., Dennison, P., Resco de Dios, V., Di Bella, C. M., Forsyth, G., Frost, P., Garcia,
 1947 M., Hamdi, A., He, B., Jolly, M., Kraaij, T., Martín, M. P., Mouillot, F., Newnham, G., Nolan,
 1948 R. H., Pellizzaro, G., Qi, Y., Quan, X., Riaño, D., Roberts, D., Sow, M., and Ustin, S.: Globe-
 1949 LFMC, a global plant water status database for vegetation ecophysiology and wildfire
 1950 applications, *Sci Data*, 6, 155, <https://doi.org/10.1038/s41597-019-0164-9>, 2019.
- 1951